WAPD-TM-1606
DOE RESEARCH AND
DEVELOPMENT REPORT

END-OF-LIFE DESTRUCTIVE EXAMINATION OF LIGHT WATER BREEDER REACTOR FUEL RODS

(LWBR Development Program)

OCTOBER 1987

CONTRACT DE-AC11-76PN00014

BETTIS ATOMIC POWER LABORATORY
WEST MIFFLIN, PENNSYLVANIA 15122-0079
Operated for the U. S. Department of Energy by
WESTINGHOUSE ELECTRIC CORPORATION

DISCLAIMER

WAPD-TM--1606

DE88 006586

WAPD-TM-1606
Distribution Category UC-78

END-OF-LIFE DESTRUCTIVE EXAMINATION OF LIGHT WATER BREEDER REACTOR FUEL RODS

(LWBR Development Program)

K. D. Richardson

Contributors: W. R. Campbell
J. C. Clayton
B. C. Smith

Contract No. DE-AC11-76PN00014

October 1987

Printed in the United States of America
Available from the
National Technical Information Service
5285 Port Royal Road
Springfield, Virginia 22161

NOTE

This document is an interim memorandum prepared primarily for internal reference and does not represent a final expression of the opinion of Westinghouse. When this memorandum is distributed externally, it is with the express understanding that Westinghouse makes no representation as to completeness, accuracy, or usability of information contained therein.

BETTIS ATOMIC POWER LABORATORY WEST MIFFLIN, PENNSYLVANIA 15122-0079

Operated for the U.S. Department of Energy by
WESTINGHOUSE ELECTRIC CORPORATION

NOTICE

FOREWORD

The Shippingport Atomic Power Station located in Shippingport, Pennsylvania was the first large-scale, central-station nuclear power plant in the United States and the first plant of such size in the world operated solely to produce electric power. This program was started in 1953 to confirm the practical application of nuclear power for large-scale electric power generation. It has provided much of the technology being used for design and operation of the commercial, central-station nuclear power plants now in use.

Subsequent to development and successful operation of the Pressurized Water Reactor in the Atomic Energy Commission (now Department of Energy, DOE) owned reactor plant at the Shippingport Atomic Power Station, the Atomic Energy Commission in 1965 undertook a research and development program to design and build a Light Water Breeder Reactor (LWBR) core for operation in the Shippingport Station.

The objective of the Light Water Breeder Reactor program has been to develop a technology that would significantly improve the utilization of the nation's nuclear fuel resources employing the well-established water reactor technology. To achieve this objective, work has been directed toward analysis, design, component tests, and fabrication of a water-cooled, thorium oxide-uranium oxide fuel cycle breeder reactor for installation and operation at the Shippingport Station. The LWBR core started operation in the Shippingport Station in the Fall of 1977 and finished routine power operation on October 1, 1982. After end-of-life core testing, the core was removed and the spent fuel shipped to the Naval Reactors Expended Core Facility for detailed examination to verify core performance including an evaluation of breeding characteristics.

In 1976, with fabrication of the Shippingport LWBR core nearing completion, the Energy Research and Development Administration, now DOE, established the Advanced Water Breeder Applications (AWBA) program to develop and disseminate technical information which would assist U.S. industry in evaluating the LWBR concept for commercial-scale applications. The AWBA program, which was concluded in September, 1982, explored some of the problems that would be faced by industry in adopting technology confirmed in the LWBR program. Information developed includes concepts for commercial-scale prebreeder cores which would produce uranium-233 for light water breeder cores while producing electric power, improvements for breeder cores based on the technology developed to fabricate and operate the Shippingport LWBR core, and other information and technology to aid in evaluating commercial-scale application of the LWBR concept.

All three development programs (Pressurized Water Reactor, Light Water Breeder Reactor, and Advanced Water Breeder Applications) have been conducted under the technical direction of the Office of the Deputy Assistant Secretary for Naval Reactors of DOE.

Technical information developed under the Shippingport, LWBR, and AWBA programs has been and will continue to be published in technical memoranda, one of which is this present report.

TABLE OF CONTENTS

TABLE OF CONTENTS (Cont)

LIST OF FIGURES

LIST OF FIGURES (Cont)

LIST OF FIGURES (Cont)

LIST OF FIGURES (Cont)

LIST OF FIGURES (Cont)

LIST OF TABLES

Destructive examination of 12 representative Light Water Breeder Reactor fuel rods was performed following successful operation in the Shippingport Atomic Power Station for 29,047 effective full power hours, about five years. Light Water Breeder Reactor fuel rods were unique in that the thorium oxide and uranium-233 oxide fuel was contained within Zircaloy-4 cladding. Destructive examinations included analysis of released fission gas; chemical analysis of the fuel to determine depletion, iodine, and cesium levels; chemical analysis of the cladding to determine hydrogen, iodine, and cesium levels; metallographic examination of the cladding, fuel, and other rod components to determine microstructural features and cladding corrosion features; and tensile testing of the irradiated cladding to determine mechanical strength. The examinations confirmed that Light Water Breeder Reactor fuel rod performance was excellent. No evidence of fuel rod failure was observed, and the fuel operating temperature was low (below 2580°F at which an increased percentage of fission gas is released).

END-OF-LIFE DESTRUCTIVE EXAMINATION OF LIGHT WATER BREEDER REACTOR FUEL RODS

(LWBR Development Program)

SECTION 1 - INTRODUCTION

The Light Water Breeder Reactor (LWBR) was designed and operated to confirm that breeding can be achieved in a light water reactor system using the thorium oxide and uranium-233 oxide fuel system. The fuel system was based on generating energy by depleting uranium-233 while producing more fissile uranium-233 from thorium, a relatively abundant, naturally-occurring fertile material. Figure 1 presents a schematic of the breeding process showing thorium-232 conversion to uranium. A neutron absorption in thorium-232 produces thorium-233, which β-decays to protactinium-233. Protactinium-233 β-decays with a 27-day half-life to produce uranium-233.

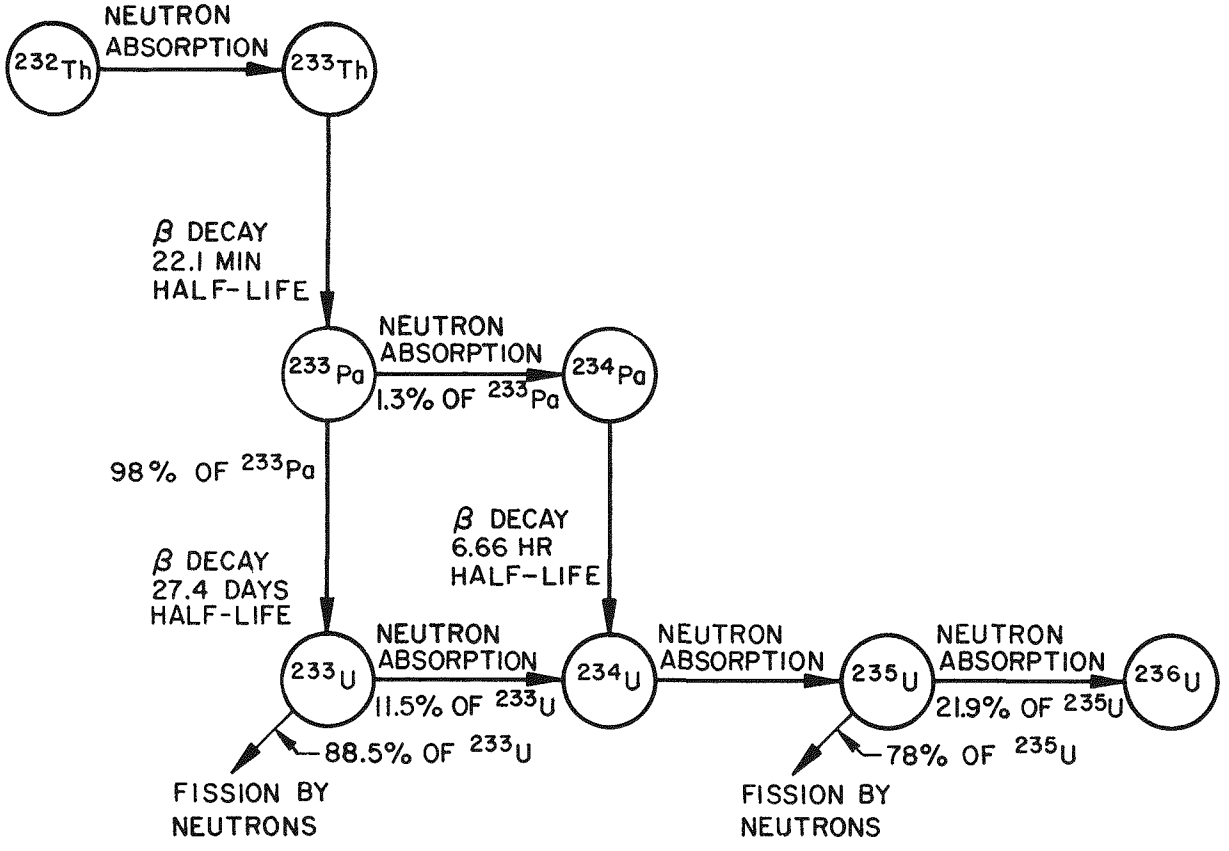

Figure 1. Thorium-232 to Uranium Breeding Process

The final phase of the LWBR program was examination of the breeder reactor following operation to confirm that design objectives were met. In addition to confirming the principal design objective of proof of breeding, examinations were conducted to confirm acceptable performance of the Zircaloy-clad thorium-based oxide fuel rod elements used in the LWBR.

Examination of LWBR fuel rod elements was performed at the Naval Reactors Expended Core Facility (ECF) in Idaho Falls, Idaho, following shipment of the spent fuel bundles, called modules, from the Shippingport Atomic Power Station in Shippingport, Pennsylvania. Fuel modules were examined first for visual appearance and module bow. Fuel rods were then removed from several of the fuel modules and examined. Proof that LWBR was a breeder reactor was confirmed by the nondestructive assaying of 524 fuel rods in the Production Irradiated Fuel Assay Gage (PIFAG) and destructively assaying 17 of these rods chemically at Argonne National Laboratory. The assay results determined that the Fissile Inventory Ratio (FIR) (the ratio of the fissile inventory at end of life relative to the fissile inventory at beginning of life) was greater than unity, namely, 1.0139. Nineteen fuel rods were examined nondestructively in the Rod Examination (REX) station to determine general appearance and such attributes as length, diameter, oxide thickness, ovality, free-hanging bow, cladding integrity and wear. Results from these end-of-life examinations are reported in References (1) through (3). Finally, 12 fuel rods were selected for destructive examination.

This report describes the results of destructive examination of 12 LWBR fuel rods at end of life. The general appearance of the rods and their microstructural and chemical condition following core operation to 29,047 effective full power hours (EFPH) was characterized. The effect of core operation on Zircaloy-4 cladding corrosion, hydriding, and iodine and cesium content was evaluated. Similarly, fuel microstructure (including grain size and porosity changes), iodine and cesium content, and in some cases depletion were assessed. The examinations confirmed that the thermal, mechanical, and chemical performance of the Zircaloy-clad thoria-urania fuel elements used in LWBR was excellent.

(Intentionally Blank)

SECTION 2 - BACKGROUND

2.1 - GENERAL CORE DESIGN

The Light Water Breeder Reactor (LWBR) was a small (236.6 Mw thermal, 72 Mw gross electrical) light water cooled, thorium cycle reactor installed and operated in the Department of Energy-owned pressurized water reactor plant at the Shippingport Atomic Power Station in Shippingport, Pennsylvania. A cutaway view of the reactor is shown in Figure 2. For this four-loop, single-pass reactor, coolant flow entered through four bottom inlet nozzles and was distributed through a flow baffle plate (only two inlet and two outlet nozzles are shown in Figure 2). The coolant, passing through the core in a single pass, was heated and exited the reactor vessel through four outlet nozzles.

Figure 3 shows a cross section of the LWBR core. Twelve hexagonally-shaped fuel module combinations were arrayed symmetrically and were surrounded by 15 reflector fuel modules of pentagonal or trapezoidal shapes. Each of the hexagonal module combinations contained a central movable seed fuel module within a stationary blanket fuel module. The seed and reflector modules were contained within Zircaloy shells for structural support and coolant flow control. Each annular blanket module had a Zircaloy guide tube at its inner boundary to serve as a guide path for the movable seed module. The different types of LWBR fuel modules are shown in Figures 4 through 7.

Fuel elements in the seed and blanket modules contained a solid state solution of ThO_2 and $^{233}UO_2$ binary fuel. In the reflector modules and in sections at the top and bottom of the seed and blanket modules, the fuel elements contained only ThO_2 fuel. The purpose of the thoria fuel regions was to minimize loss of neutrons needed for breeding by capturing them in the fertile thorium.

The seed and blanket modules were designated as Types I, II, or III, and the reflector modules as Types IV or V, depending on their shape and position in the core. All seed modules were identical but were given designations coinciding with their corresponding blanket module type. The three central

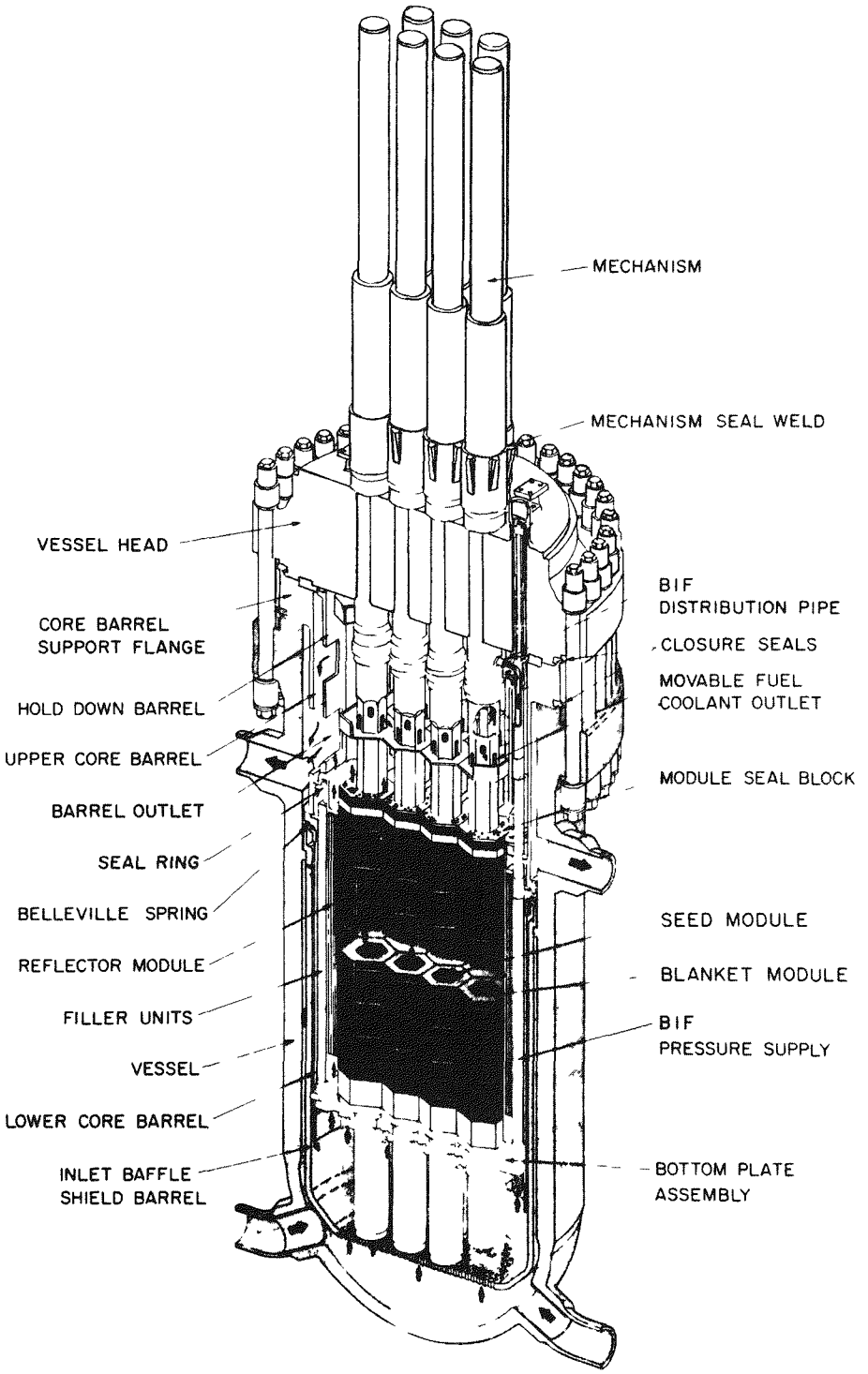

Figure 2. LWBR Core in Shippingport Reactor Vessel

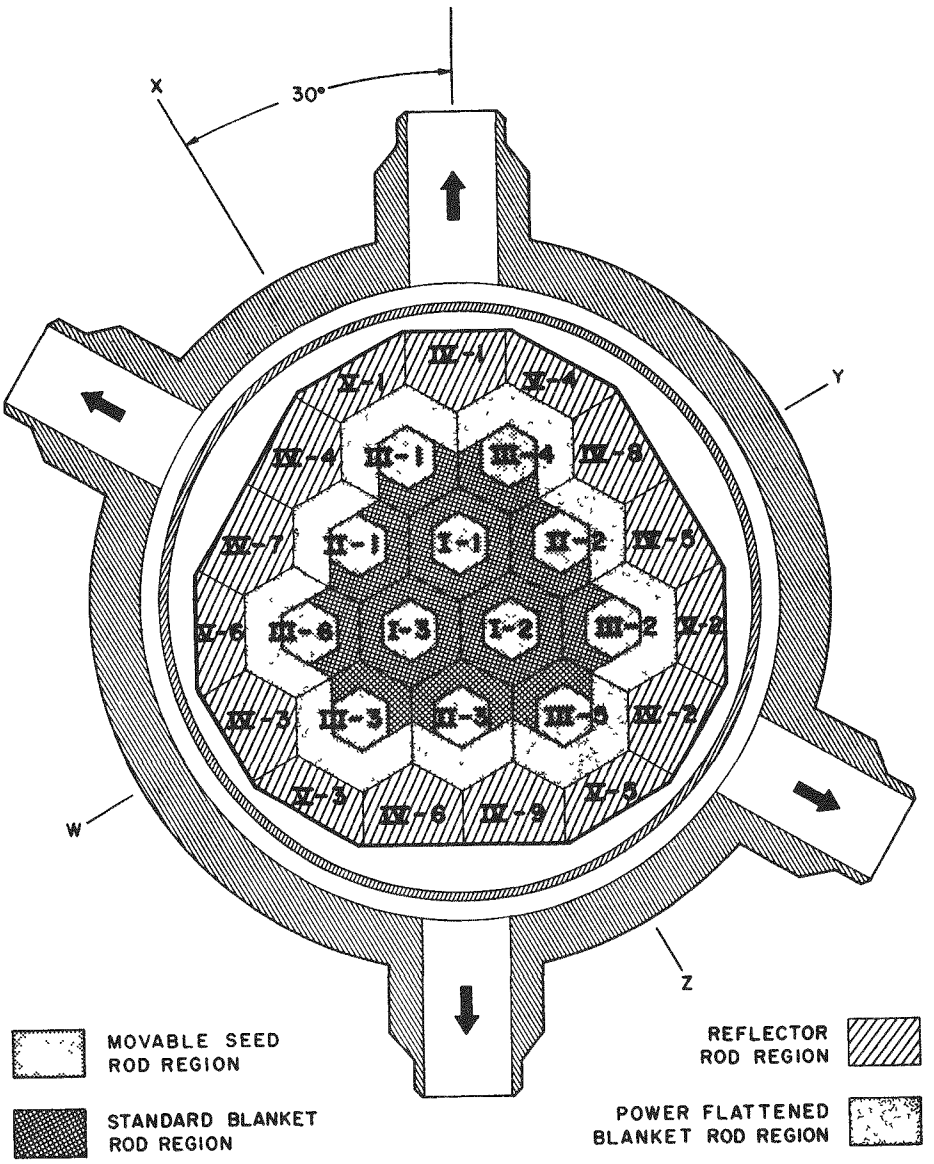

Figure 3. LWBR Core Cross Section with Module Identification

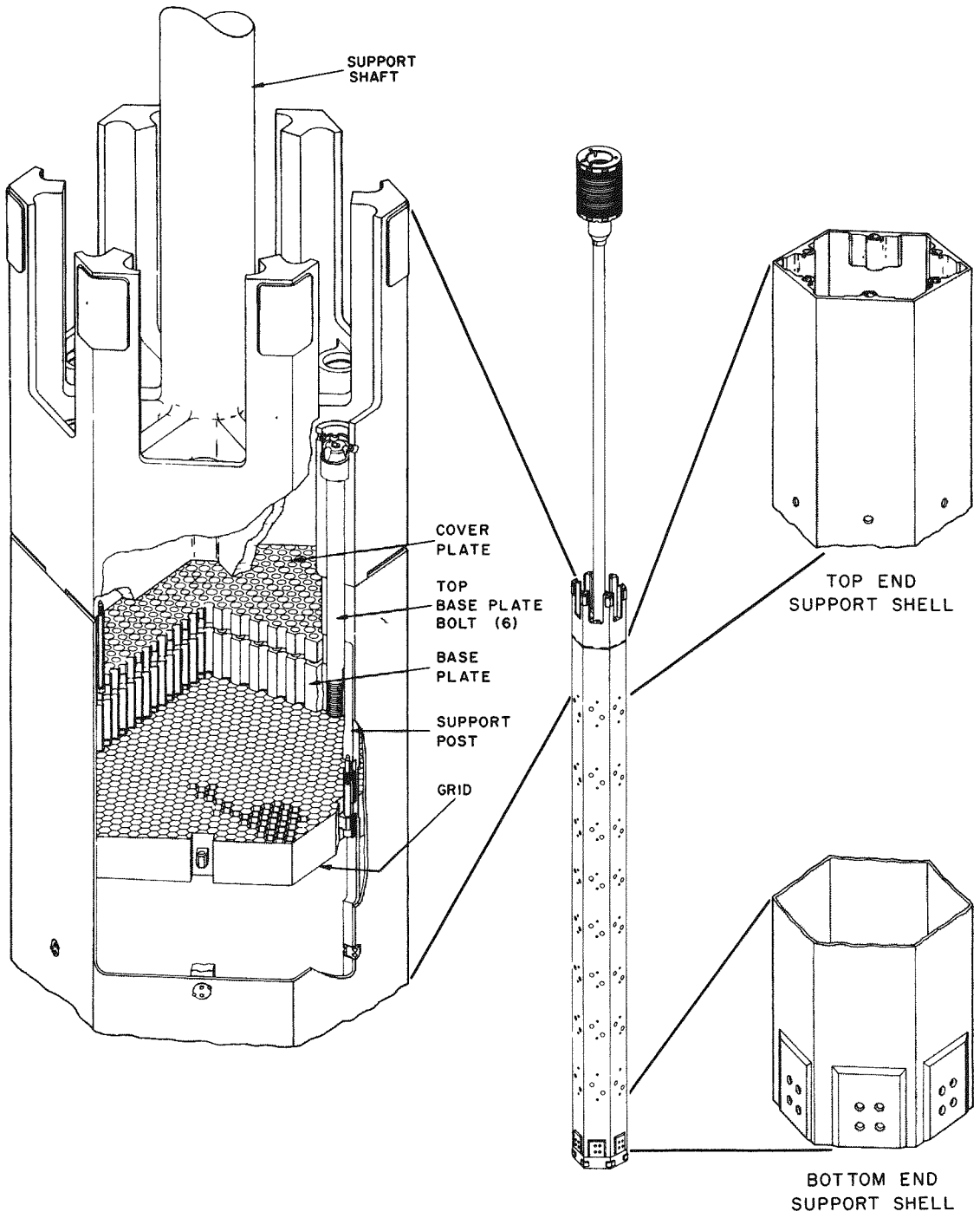

Figure 4. LWBR Movable Seed Fuel Module

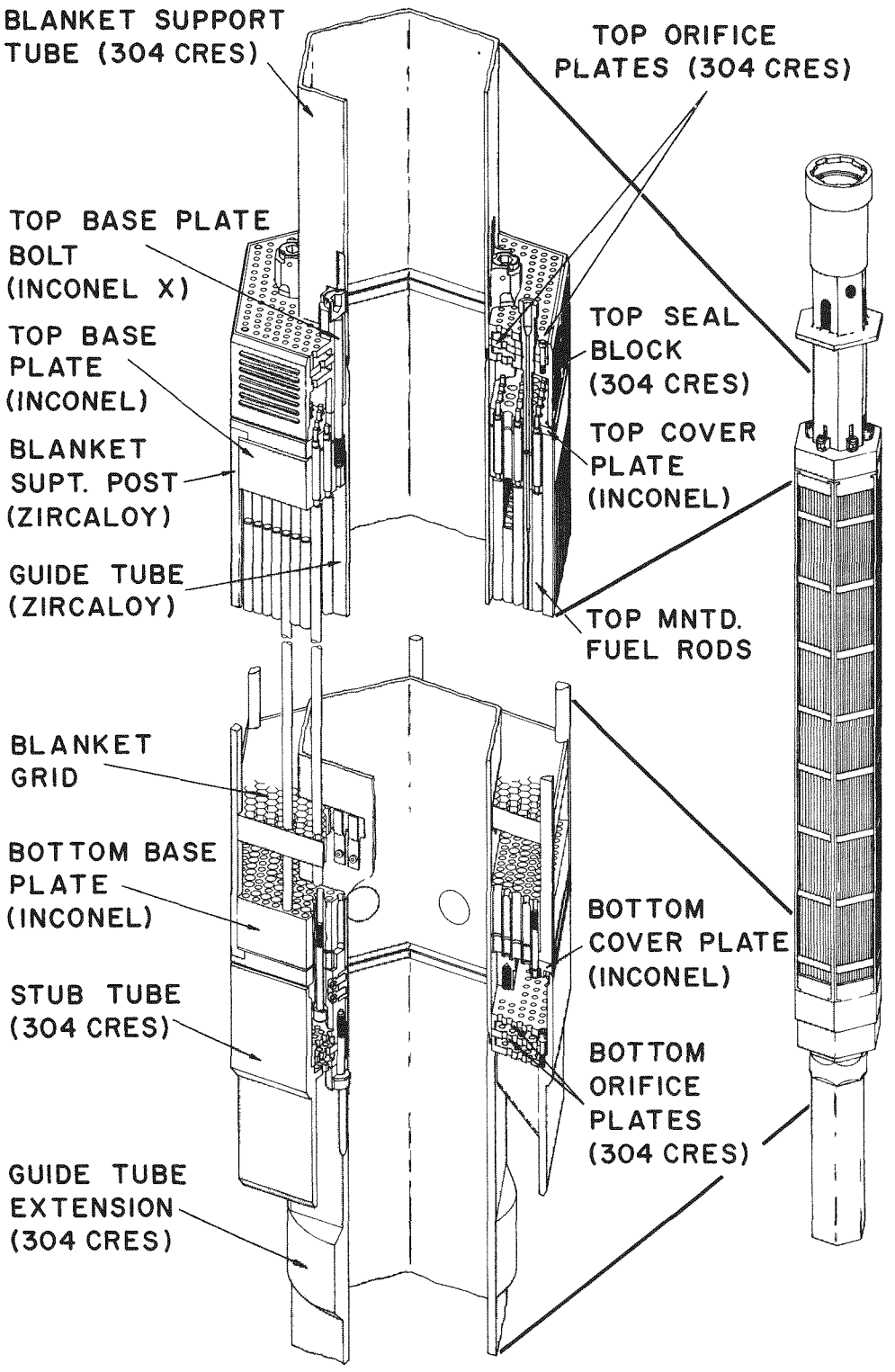

Figure 5. LWBR Type I Blanket Fuel Module

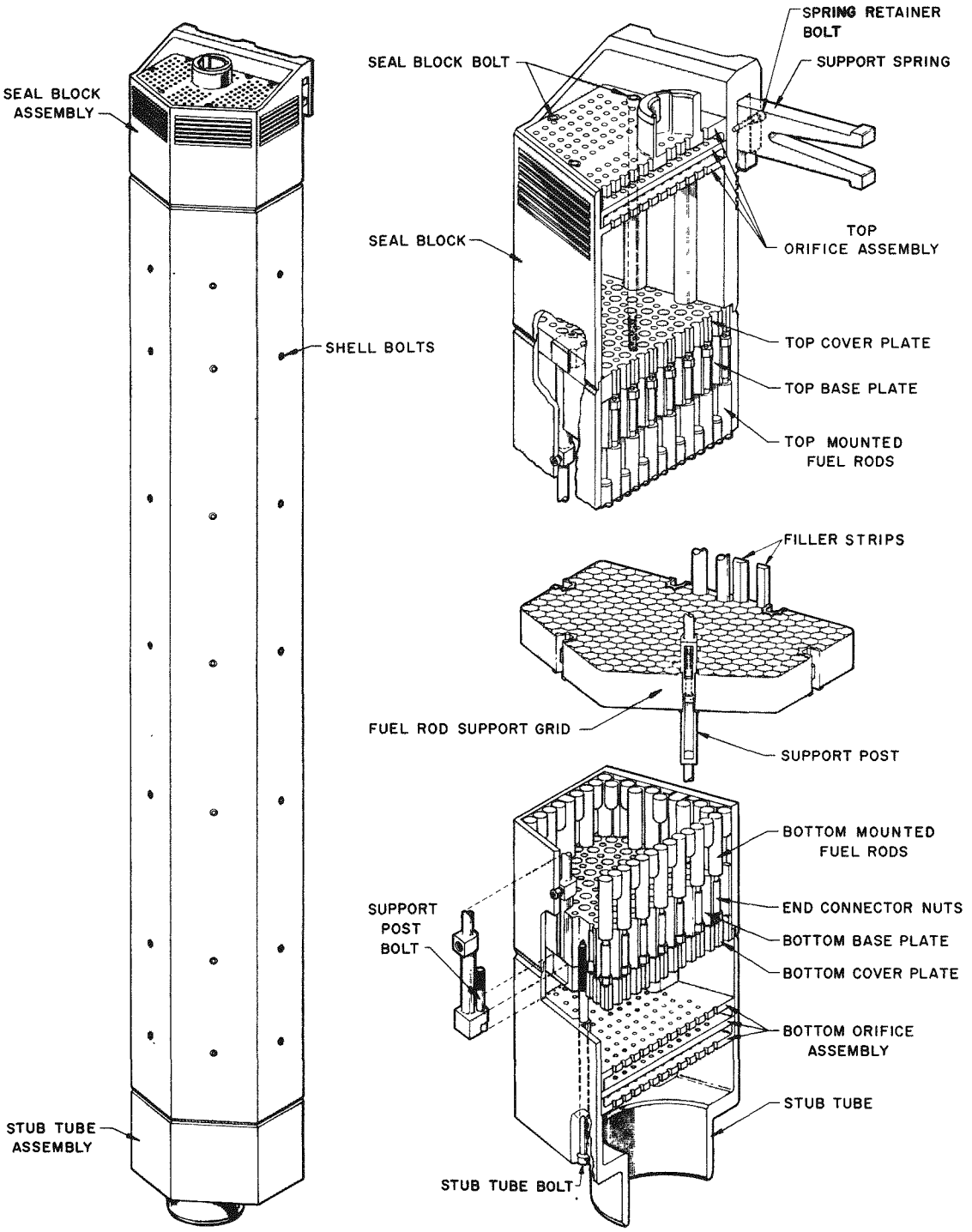

Figure 6. LWBR Type IV Reflector Fuel Module

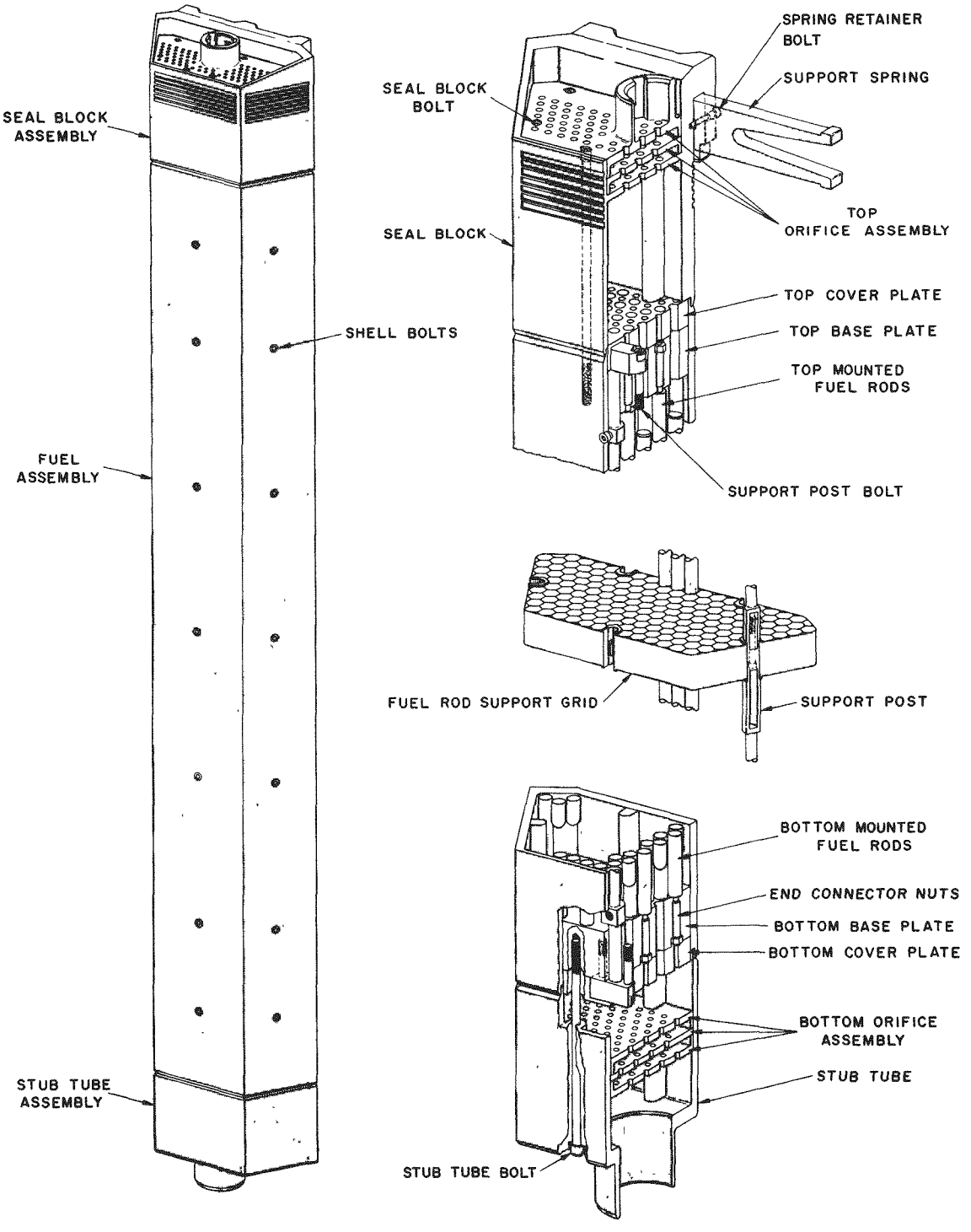

Figure 7. LWBR Type V Reflector Fuel Module

blanket modules (Type I, shown in Figure 5) were identical and symmetrical. The nine blanket modules surrounding these central modules (Types II and III) had a larger outer blanket region. This outer blanket region had a somewhat higher uranium-233 content and smaller rod diameter than the blanket regions of the inner modules. Use of this higher loaded, lower metal to water ratio blanket region produced a relatively uniform power distribution within the interior of the core and better simulated the low neutron leakage environment of a large (1000 Mw(e)) core. This power flattening region would be much smaller and possibly unnecessary in a large breeder core.

Reactivity control in LWBR was accomplished by varying the axial position of the movable seed fuel modules relative to their surrounding stationary blanket fuel modules. This design eliminated the need for conventional neutron-absorbing poison control rods, thereby making breeding possible. Further description of the LWBR core design is given in Reference (4).

2.2 - GENERAL FUEL ELEMENT DESIGN

The LWBR fuel elements were long rods composed of Zircaloy-4 tubes filled with oxide fuel pellets. The rods are depicted schematically in Figures 8 through 10. The tubes, approximately 10 feet long, were welded at both ends to solid Zircaloy-4 end connectors. A plenum space at the top of each rod contained a helical spring of Inconel X-750 material. The purpose of the spring was to prevent the development of axial gaps between the pellets stacked in the fuel rods. Such gaps could develop during handling or because of differential thermal expansion and shock loading during core operation. A special pellet, the spring bearing pellet, transmitted the axial load of the plenum spring to the fuel stack. A support sleeve of Type 348 stainless steel was placed in the plenum region of the blanket and reflector fuel rods between the cladding and the spring. All fuel rods were filled with helium at one atmosphere of pressure.

A threaded stem on one end of each rod was used with a Zircaloy-4 nut to secure the fuel rod to a structural baseplate of Inconel-600 at either the top or the bottom of the module. Approximately half the rods were secured, or mounted, to the top baseplate and half were mounted to the bottom baseplate to

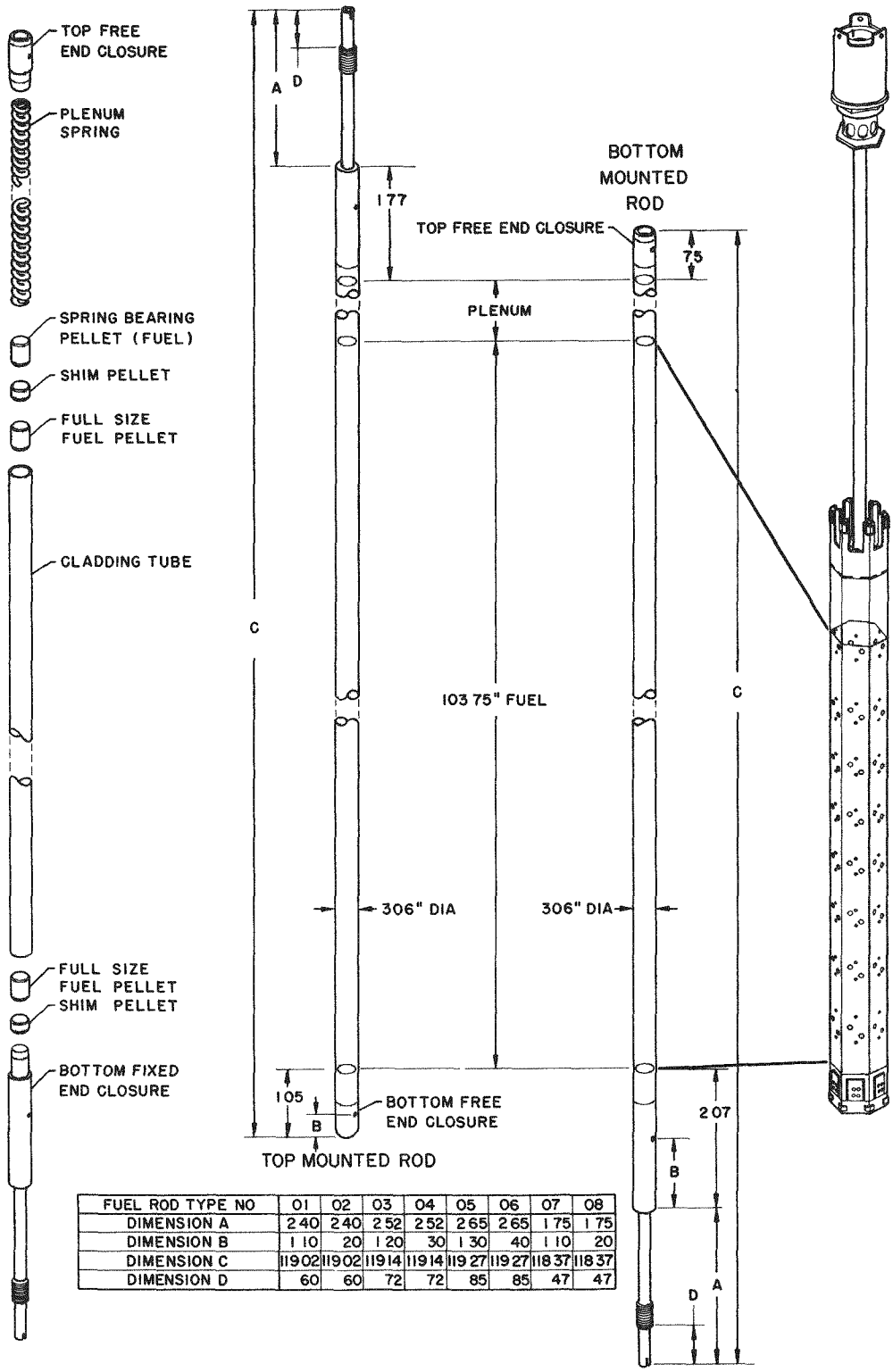

FUEL ROD TYPE NO	01	02	03	04	05	06	07	08
DIMENSION A	240	240	252	252	265	265	175	175
DIMENSION B	110	20	120	30	130	40	110	20
DIMENSION C	119 02	119 02	119 14	119 14	119 27	119 27	118 37	118 37
DIMENSION D	60	60	72	72	85	85	47	47

Figure 8. LWBR Seed Region Fuel Rods

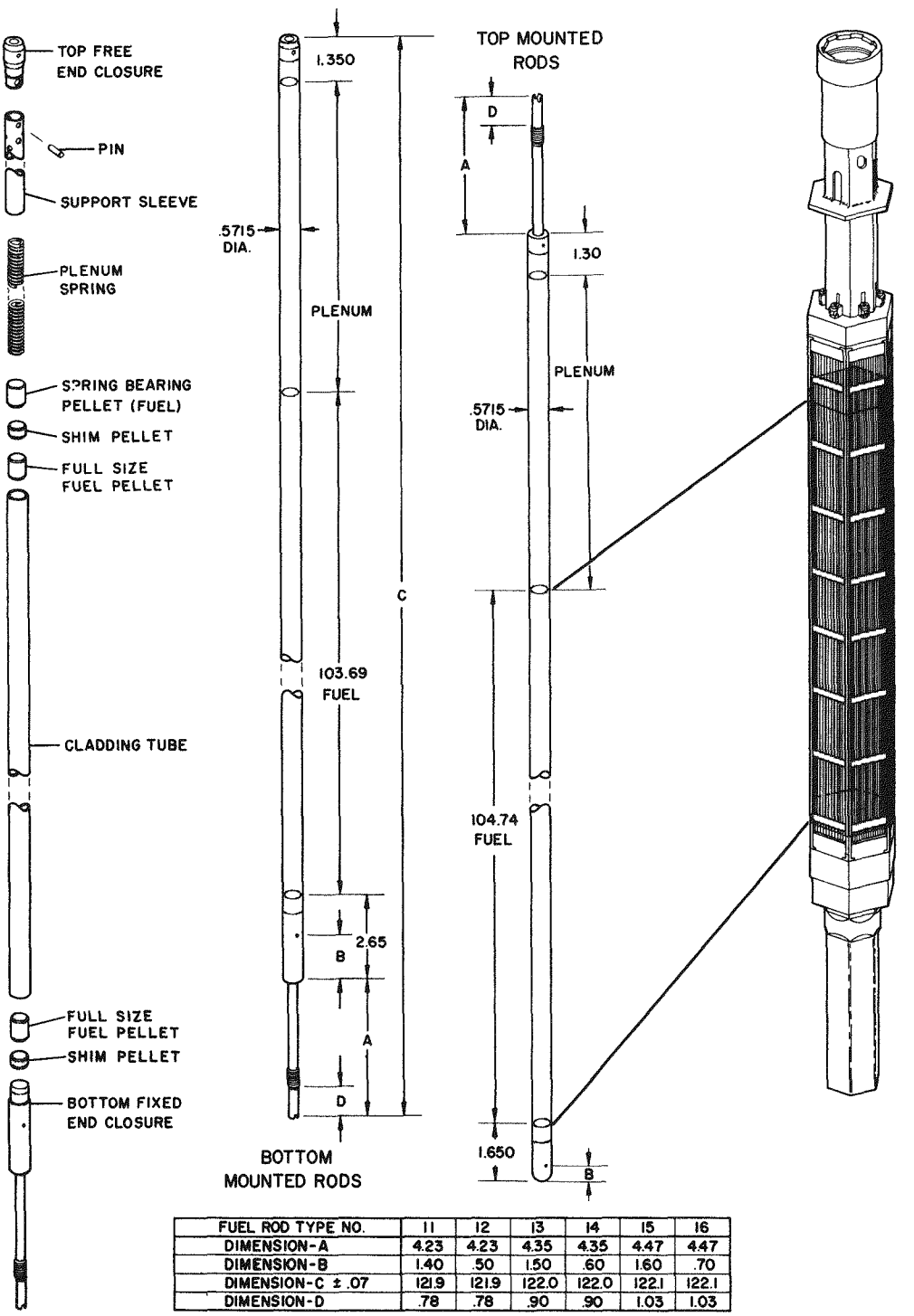

FUEL ROD TYPE NO.	11	12	13	14	15	16
DIMENSION-A	4.23	4.23	4.35	4.35	4.47	4.47
DIMENSION-B	1.40	.50	1.50	.60	1.60	.70
DIMENSION-C ± .07	121.9	121.9	122.0	122.0	122.1	122.1
DIMENSION-D	.78	.78	.90	.90	1.03	1.03

Figure 9. LWBR Blanket Region Fuel Rods

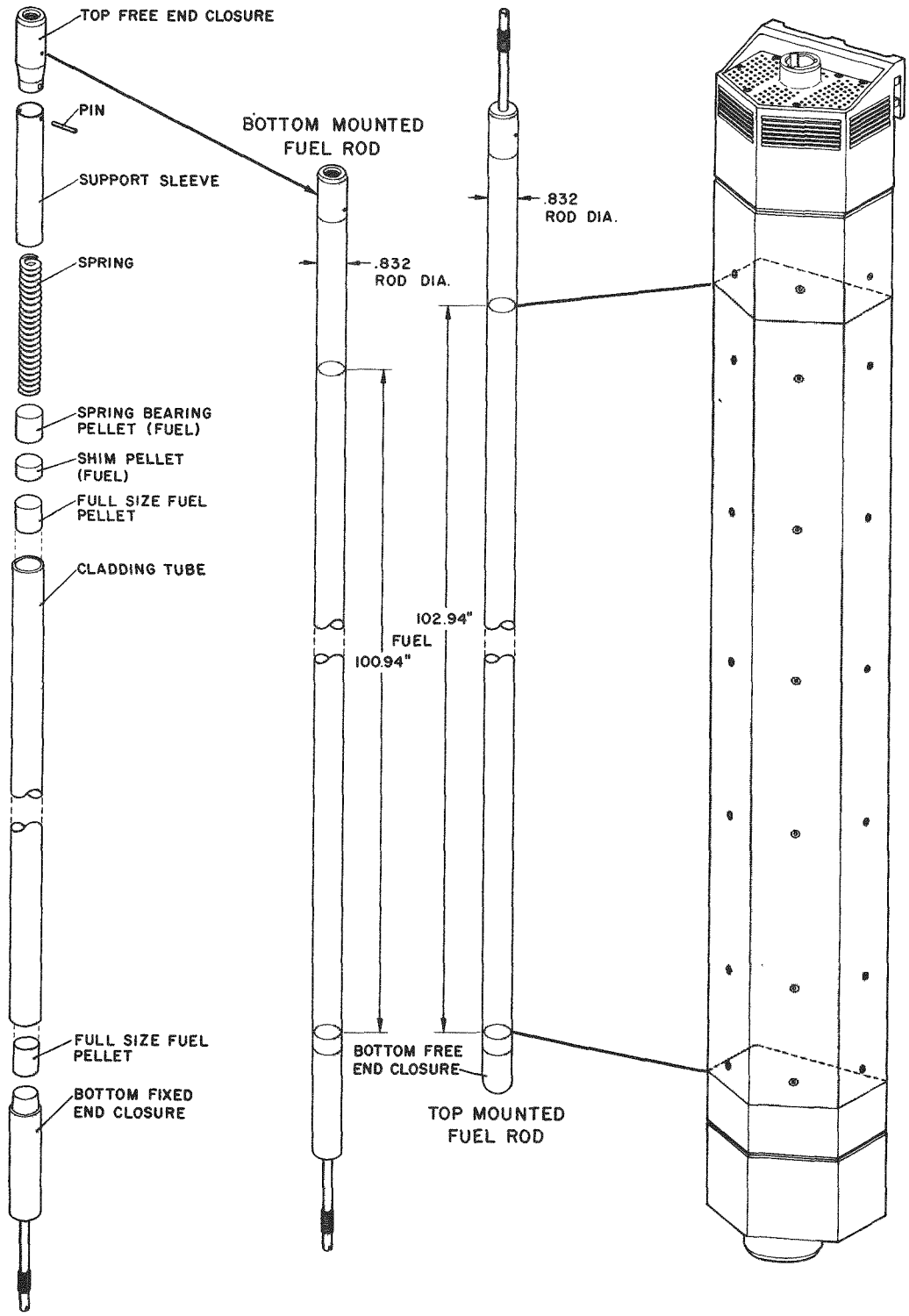

Figure 10. LWBR Reflector Region Fuel Rods

equalize axial thrust forces on the module support structures resulting from axial growth of the fuel rods.

Four fuel rod diameters were used in the LWBR core. These four rod types were designed for the seed, standard blanket, power flattening blanket, and reflector regions of the core. The fuel rods in the seed modules were the smallest in diameter, 0.306 inch, and were arranged on a triangular pitch of 0.369 inch. The gap between seed fuel rods was nominally 0.063 inch.

Fuel rods in the blanket modules were of two sizes: the standard blanket fuel rods were 0.5715 inch in diameter on a triangular pitch of 0.630 inch and a rod-to-rod gap of 0.058 inch; the power flattening blanket fuel rods were 0.5275 inch in diameter, also on a triangular pitch of 0.630 inch, resulting in a larger rod-to-rod gap of 0.102 inch.

Fuel rods in the reflector modules were of one size. The rods were nominally 0.832 inch in diameter on a triangular pitch of 0.901 inch. The rod-to-rod gap was 0.069 inch.

Fuel rod spacing was established by support grids of AM-350 precipitation-hardening stainless steel. The honeycomb-shaped support grids used a combination of dimples and a spring to center the rod within each grid cell. Arrangements of seed rods and blanket rods within their respective support grids are shown in Figures 11 and 12. This general arrangement is typical of grids used in light water reactors (LWRs) except that the LWBR cell pitch is triangular instead of square and the dimples and spring are at 120 degrees to each other within the hexagonal-shaped cells instead of at 90 degrees. A triangular pitch was used to provide the high metal-to-water ratio necessary to achieve breeding in light water. The seed fuel rods were supported by nine levels of grids, the blanket fuel rods by eight levels of grids, and the reflector fuel rods by six levels of grids. The number of grid supports needed to control fuel rod bow differed among the regions because the fuel rod diameters (and hence rod stiffnesses) and the environmental conditions (power and neutron flux) differed for each type module.

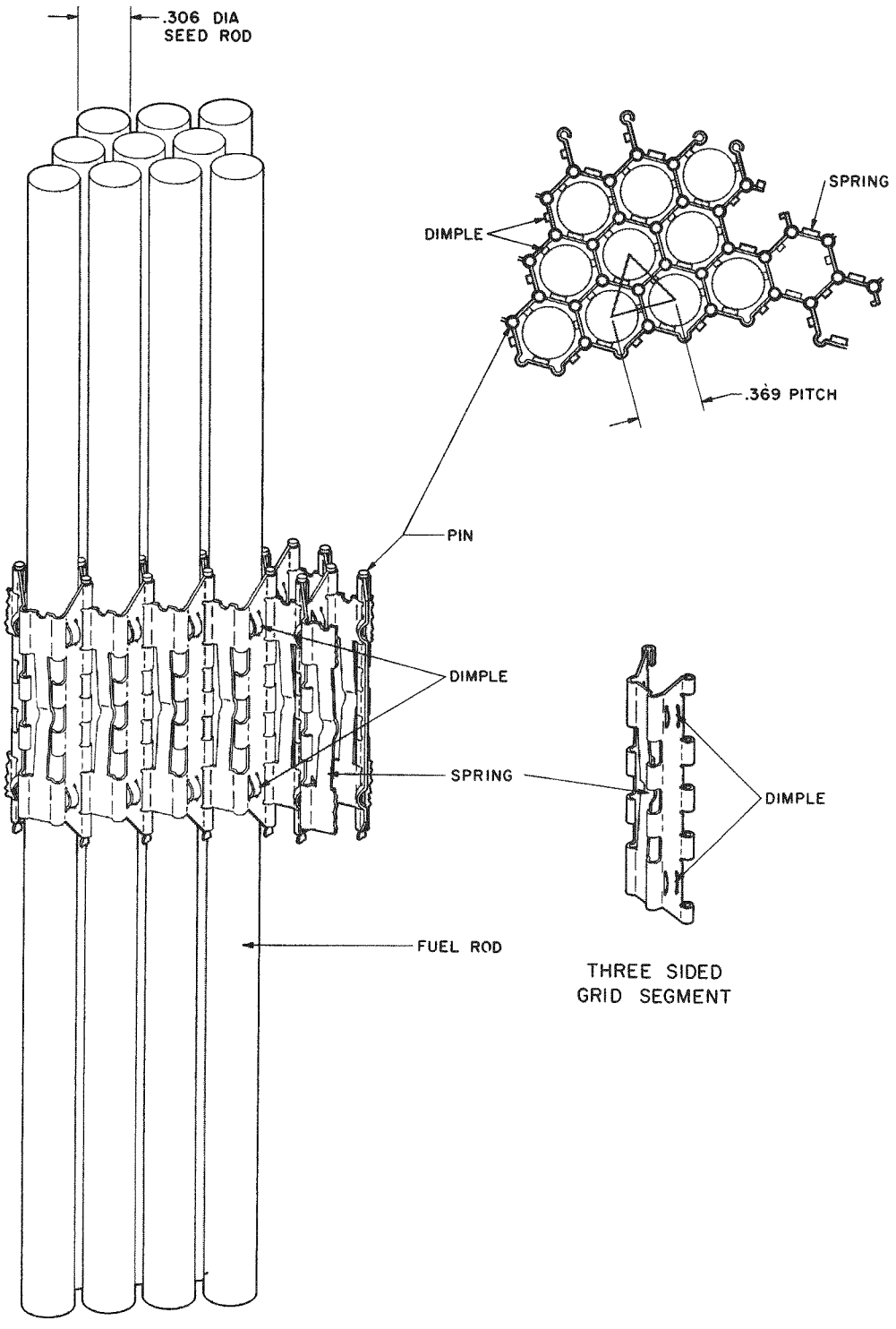

Figure 11. Typical LWBR Seed Rod Support Grid

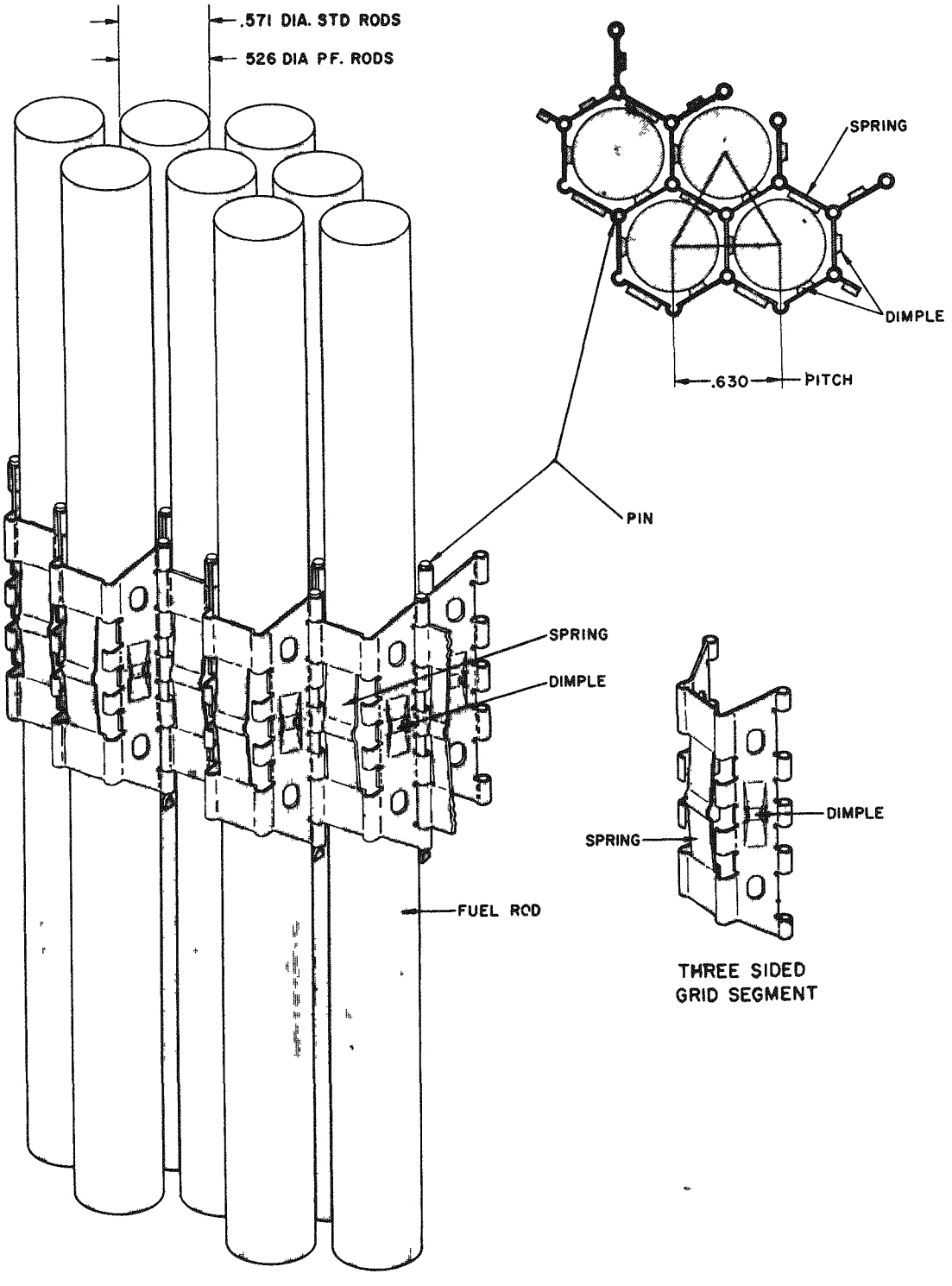

Figure 12. Typical LWBR Blanket Rod Support Grid

The numbers of rods of each size in the LWBR fuel modules are listed in Table 1.

Table 1 - Number of Fuel Rods in the LWBR Core

		Seed Rods	Standard Blanket Rods	Power Flattening Blanket Rods	Reflector Rods
I.	Number of Rods Per Module				
	Seed	619			
	Blanket Type I		444		
	Blanket Type II		261	303	
	Blanket Type III		187	446	
	Reflector Type IV				228
	Reflector Type V				166
II.	Number of Rods in Core	7428	3234	3581	3047
III.	Total of All Rods in Core*		17,290		

*Eight neutron flux measurement tubes occupied positions which otherwise would have been filled with fuel rods.

2.3 - FUEL CLADDING DESIGN

The fuel rod cladding material used in LWBR was Zircaloy-4, which is used in the majority of operating light water reactors. In addition to exhibiting high strength and good corrosion resistance, Zircaloy-4 has a low thermal neutron absorption cross section, a necessary characteristic for a water breeder reactor. The Zircaloy-4 tubing used as rod cladding in LWBR had lower limits established for allowable hafnium content (45 ppm) than standard (100 ppm) Zircaloy-4 to further minimize neutron absorption in this (hafnium) neutron poison material. Chemistry requirements and fabrication steps from the Zircaloy ingot to the finished tubes are given in Reference (5).

Cladding designs of seed, blanket, and reflector rods were tailored to enable the different core regions to carry out their individual functions: the seed to provide neutrons as efficiently as possible in burning of fissile uranium-233 fuel, and the blanket and reflector to use neutrons efficiently in producing new fissile fuel by neutron absorption in the fertile thorium fuel. Desired characteristics of each fuel region were met by setting the metal-to-water ratio and by using "freestanding" or "nonfreestanding" cladding.

The metal-to-water ratio is a measure of the rod volume relative to the volume of water surrounding the fuel rod. A higher metal-to-water ratio means that less water surrounds the rods and results in more neutrons being captured in the rod itself. It was important to have a high metal-to-water ratio for those rod regions containing greater amounts of fertile thorium, namely, the standard blanket region and the reflector regions. The standard blanket rods had a relatively high metal-to-water ratio of 2.98. The metal-to-water ratio for the reflector rods, 3.51, was the highest of the LWBR rods. Lower metal-to-water ratios for the seed (1.73) and power flattening blanket (1.75) rods were necessary to provide more water to meet minimum rod spacing requirements with smaller diameter rods and to produce adequate cooling in the high power density seed.

The gap between the fuel pellet and the cladding was specified to optimize performance and to meet limits imposed by fuel and cladding mechanical interaction and fuel pellet temperatures. The need to maximize neutron capture in the fertile thorium demanded a small radial gap between the fuel pellet and cladding. Small radial gaps, however, close during power operation. Gap closure causes pellet-cladding interaction and higher cladding strains. Conversely, large radial gaps lead to increased fuel and cladding temperatures by effectively reducing heat transfer capability. Fuel temperatures were limited by operating conditions to avoid undesirable fuel structural changes and the risk of cladding failure.

The gap in the blanket rod and reflector rod regions was specified to be small (0.004 to 0.007 inch diametral in the binary region of the blanket rods

and 0.005 to 0.008 inch diametral in the thoria regions of the blanket and reflector rods) to maximize neutron capture and to control fuel temperatures. This resulted in cladding that was "nonfreestanding," that is, the small gap between the cladding and pellet closed because of cladding creepdown onto the pellets as a result of hydrostatic presssure during core operation.

Larger gaps could be tolerated in the smaller diameter seed rods and, in fact, were desirable to minimize the potential for pellet-cladding interaction. The gap between the fuel pellet and cladding in the binary fuel region of the seed rods was specified to be 0.0085 to 0.0115 inch. This gap, in combination with a relatively small diameter-to-thickness ratio for the cladding, resulted in the seed fuel rod cladding being "freestanding," that is, it did not collapse onto the fuel. Because of the large fabricated gap and the freestanding nature of the cladding, the cladding remained separated from the fuel pellets during core life. Mechanical properties of the freestanding seed cladding and the nonfreestanding blanket and reflector cladding were optimized by varying the final tubing heat treatment and by controlling the cladding diameter-to-thickness ratio. Final heat treatment for the blanket and reflector cladding was typical of commercial LWR fuel rods. The cladding was highly cold worked (60 to 80 percent final reduction) followed by a stress relief anneal (SRA) heat treatment (1 to 5.5 hours at 900 to 950°F). The stress relief anneal for the blanket and reflector tubing provided the higher strength needed at beginning of life to prevent collapse of the cladding onto the fuel early in core life.

Enhanced creep resistance during irradiation was provided for seed cladding by a final tube reduction of 50 to 70 percent, followed by a recrystallization anneal (RXA) heat treatment (2 to 5 hours at 1200 to 1250°F). The reduced strength of the recrystallization annealed seed tubing early in core life was acceptable because the relatively large fuel pellet to cladding gap delayed pellet-cladding interaction until the cladding had experienced considerable irradiation hardening. Resulting Zircaloy-4 tubing tensile strengths are given in Table 2 (Reference (5)).

Table 2 - Average As-Built LWBR Zircaloy-4 Tubing Tensile Strength

Tube	Final Anneal	Room Temperature YS	U/Y	ELONG	Elevated Temperature (700°F) YS	U/Y	ELONG
Seed	RXA	54,660	1.472	29.20	17,100	1.951	35.76
PFB	SRA	80,710	1.359	19.63	53,130	1.254	18.17
STB	SRA	79,770	1.363	21.87	51,140	1.259	20.61
Reflector	SRA	77,790	1.367	23.57	49,490	1.288	21.87

YS 0.2 percent offset yield strength, psi
U/Y Ratio of ultimate strength to 0.2 percent offset yield strength
ELONG Elongation in 2-inch gage length measured after rupture, percent
PFB Power flattening blanket
STB Standard blanket
RXA Recrystallization Anneal
SRA Stress Relief Anneal

The fuel rod cladding diameter-to-thickness ratio for the seed rods (13.9) was set lower than that for the blanket and reflector rods (20.6, 20.1, and 19.8 for the standard blanket, power flattening blanket, and reflector, respectively). This lower ratio was intended to help the seed cladding to remain freestanding. The higher ratios for the blanket and reflector cladding were designed to minimize the volume of Zircaloy and thus enhance breeding. Nonfreestanding cladding in the blanket and reflector rods was acceptable because the cladding stresses were lower due to less fuel swelling. Fuel swelling was lower because the fuel burnup requirements in the blanket rods were only about half the burnup requirements in the seed rods and only about 10 percent of the seed requirements in the reflector rods.

2.4 - FUEL PELLET DESIGN

Relevant fuel pellet dimensional parameters are given in Reference (4) and are repeated in Table 3 for convenience. The pellets were right circular cylinders. Lengths were varied in part to facilitate confirmation during nondestructive inspection of the assembled rod that the pellets were correctly

Table 3 - Fuel Element Dimension Specifications*

Zircaloy-4 Cladding	Seed	Standard Blanket	Power Flattening Blanket	Reflector
Outside Diameter	0.306 ± .0015 avg +.003 −.002 local	0.5715 ± .0015 avg ± .0025 local	0.5275 ± .0015 avg ± .0025 local	0.832 ± .003 avg ± .003 local
Inside Diameter	0.262 ± .002 local ± .001 avg	0.516 ± .002 local ± .001 avg	0.475 ± .002 local ± .001 avg	0.748 ± .001 avg ± .0025 local
Nominal Wall Thickness	0.022	0.02775	0.02625	0.042
Outside Diameter to Thickness Ratio	13.9	20.6	20.1	19.8
Cladding Heat Treatment**	RXA	SRA	SRA	SRA
UO_2-ThO_2 Fuel Pellets				
Diameter	0.252 ± .0005	0.5105 ± .0005	0.4695 ± .0005	-
Length	0.445 ± .020	0.530 ± .020	0.870 ± .020	-
	0.615 ± .020	0.870 ± .020	0.785 ± .020	-
		0.785 ± .020	0.700 ± .020	-
End Shoulder Width	0.046 ± .008	0.055 ± .015	0.055 ± .015	-
Endface Dish Depth	0.009 ± .003	0.014 ± .004	0.014 ± .004	-
Chamfer or Taper-				
Depth	0.015 ± .005	0.001 - 0.004	0.001 - 0.004	-
Length	0.015 ± .015	0.100 - 0.200	0.100 - 0.200	-
Range of Individual Pellet Densities, % of Theoretical	94.55 - 99.27	96.55 - 99.38	95.26 - 98.60	-
Fuel-Cladding Diametral Gap	0.0085 - 0.0115	0.004-0.007	0.004-0.007	-
ThO_2 Fuel Pellets				
Diameter	0.2555 ± .0005	0.5105 ± .0005	0.4695 ± .0005	0.7415 ± .0005
Length	0.530 ± .020	0.615 ± .020	0.445 ± .020	0.740 ± .060
End Shoulder Width	0.055 ± .010	0.055 ± .010	0.055 ± .010	0.074 ± .010
Endface Dish Depth	0.009 ± .003	0.014 ± .004	0.014 ± .004	0.014 ± .004
Edge Configuration	0.015 ± .005 Chamfer	0.006 ± .004 Chamfer	0.006 ± .004 Edge	Square
Range of Individual Pellet Densities, % of Theoretical	95.14 - 99.75	93.10 - 99.36	95.37 - 99.95	93.08 - 99.08
Fuel-Cladding Diametral Gap	0.005 - 0.008	0.004 - 0.007	0.004 - 0.007	0.005 - 0.008

* All dimensions are in inches, except as noted.
** RXA = Recrystallization Annealed
SRA = Stress Relief Annealed

positioned in the stack. This was important because of the requirement for different fuel compositions and stack lengths in the various rod types, as discussed below. The different fuel compositions of pellets of the same diameter were also identified by indentation marks in the pellet ends; one, two, or three circles or squares were indented in each pellet end.

The LWBR pellets were fabricated with a concave dish in each end. This dish condition prevented the pellet ends from developing a convex contour during power operation because of the temperature distribution, as observed during irradiation tests for pellets with flat ends. The increased stack length of rods with nondished, convex-shaped pellet ends tended to increase pellet-cladding interaction (PCI), which in turn caused increased cladding axial strain and fuel rod length. By dishing the pellet ends, room for fuel thermal expansion was provided, thereby minimizing axial expansion and PCI. The dish depth was nominally 0.009 inch for the seed pellets and 0.014 inch for the blanket and reflector pellets. A dish diameter of approximately 75 percent of the full pellet diameter was used in the design. The remaining land on the pellet ends was cooler and was adequate to carry pellet-to-pellet bearing forces.

The one exception to dished pellets was the top fuel pellet in each rod. To provide an acceptable bearing surface for the plenum spring, this top (thoria) pellet had its top end ground flat.

All seed and blanket fuel pellets were either chamfered or tapered at their ends. The seed binary and thoria pellets and the blanket thoria pellets had a small chamfer of 45 degrees by 0.006 inch (blanket thoria) or 0.015 inch (seed binary and thoria) at both ends of the pellets. Pellet chamfers served two basic purposes. First, during loading of pellets into cladding, the chamfers eased the loading and minimized formation of chips which could cause increased local cladding strains during core operation. It was important to minimize such strains to prevent cladding failure. Second, the chamfers, in combination with pellet end perpendicularity control, were specified to minimize the forces necessary for the fuel stack to slide within the cladding. Expansion and contraction of the fuel stack occurs during power excursions.

By reducing both the frictional force needed to slide through the cladding and the tendency for pellets to become cocked, PCI and local cladding radial strains were minimized. Because of the combination of low power demands in the reflector region of the core and the vertical loading process used only for reflector fuel rods, fuel pellets in the reflector rods were not chamfered.

The binary fuel pellets in the blanket region contained shallow tapers at the pellet ends rather than chamfers. Tapers were required because the nonfreestanding cladding in the blanket binary region resulted in pellet-cladding contact early in core life. Irradiation tests showed that nonfreestanding cladding creeps down onto a pellet without tapers. A ridge generally develops in the cladding at pellet-to-pellet interfaces. Ridges are regions of larger cladding diameter resulting from the nontapered pellets assuming an hourglass shape at power.

Use of tapers at the pellet ends in the blanket binary fuel elements reduced circumferential cladding strains associated with cladding ridging. The tapers extended radially inward at each pellet end from 0.001 to 0.004 inch, and axially 0.100 to 0.200 inch from each end. It was anticipated that these tapers would be sufficient to avoid cladding ridging, with the possibility that the maximum radial depth taper would result in a slight grooving of the cladding at pellet interfaces. The latter condition would also result in a change in cladding strain distribution, but one that was minor in comparison to ridging.

Pellet end tapers were not required in the seed region because of the relatively thicker, freestanding cladding, nor in the blanket thoria and reflector (thoria) regions of the core because of the lower power operating conditions.

LWBR contained approximately 1.6 million binary (thoria-urania) fuel pellets and 1.3 million thoria fuel pellets.

2.5 - OTHER FUEL ELEMENT COMPONENT DESIGN FEATURES

In addition to the cladding and fuel pellets, the fuel rods contained other components (Figures 8 through 10). A plenum region was provided at the

top of all fuel rods to accommodate fission gas released from the fuel during core operation. The plenum extended from the top inside surface of the end stem to the top of the fuel stack. The as-built plenum length was 10.0 inches long in the seed rods, 9.9 inches long in the blanket rods, and 3.955 inches long in the largest diameter, lowest power reflector rods.

Coiled springs of Inconel X-750 exerted a downward force on the fuel pellet stack to prevent the formation of axial gaps between pellets in the stack during rod handling, normal reactor operation, and shock loading such as from check valve slams and earthquakes. The beginning-of-life plenum spring dimensions and forces are listed in Table 4.

Table 4 - LWBR Fuel Rod Plenum Spring Force at Beginning of Life

Spring Data	Seed Rod	Standard Blanket Rod	Power Flattening Blanket Rod	Reflector Rod
Total Coils	190	125	135	33
Active Coils	188	123	133	31
Coil Spacing (in.)	0.024	0.036	0.032	0.048
Wire Diameter (in.)	0.043	0.072	0.066	0.109
Mean Spring Diameter (in.)	0.207	0.361	0.332	0.527
Spring Load Rate (lb/in.)	3.060	6.960	5.850	46.800
Nominal Free Length (in.)	12.620	13.410	13.400	5.100
Installed Length (in.)*	10.000	9.900	9.900	3.955
Installed Load (lb)*	8.030	24.400	20.500	53.600

* At room temperature

A support sleeve of Type 348 stainless steel was positioned between the cladding inner diameter and the plenum spring in the blanket and reflector fuel rods. Because the cladding was nonfreestanding in these regions and,

therefore, was expected to collapse onto internal rod components, the sleeve was added to provide support for the cladding in the plenum region. This avoided the increased local cladding strains which would develop if the cladding came into contact with the coils of the plenum spring. The sleeve was pinned at the top to the top end stem to maintain correct axial position. To accommodate axial expansion of the fuel stack during core life, the sleeve length was sized to provide an axial gap at beginning of life between the bottom end of the sleeve and the top of the pellet stack. This gap was 0.53, 0.50, and 0.23 inch, respectively, for the standard blanket, power flattening blanket, and reflector rods. A support sleeve was not necessary in the seed fuel rods because of the freestanding cladding.

Top-mounted fuel rods had their unattached "free" end located at the bottom end of the core near the coolant inlet. Their free end was hemispherical to minimize rod vibration from the upward coolant flow. The free (top) end of the bottom-mounted rods was square, with chamfers, for ease of machining and to accommodate an internal threaded hole used during assembly to pull the rod through the support grids.

Zircaloy-4 fuel rod fasteners (nuts) attached the Zircaloy-4 fuel rods to the Inconel-600 baseplates (Figure 13). Torquing of the fastener against the high-nickel bearing baseplate was of concern because of the potential for nickel smearing on the Zircaloy-4 fastener. Nickel contamination on the surface of Zircaloy has been shown to serve as a window for hydrogen ingress and consequent heavy hydride formation (References (6) and (7)). If the hydride formation becomes massive, cracking of the Zircaloy metal and degradation of mechanical properties results. To prevent the development of excessive Zircaloy hydrides in the blanket region, thin (0.032-inch thick), flat, chromium-plated 17-4 PH washers were placed between the fastener and the baseplate. Such washers were not used in the reflector region because of its low neutron flux and power levels. The lower torque requirements for the smaller fasteners in the seed region also presented less concern for massive hydriding and, consequently, washers were not used.

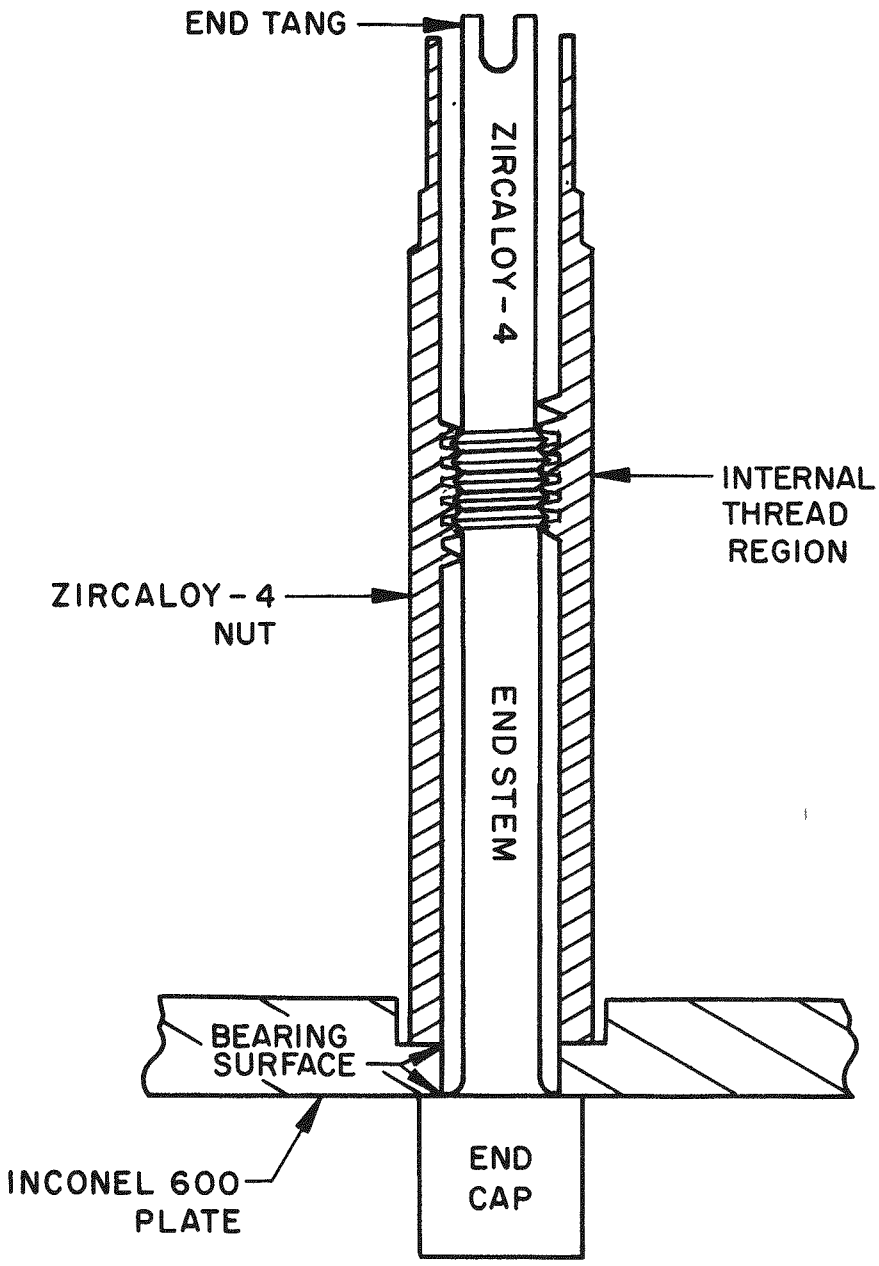

Figure 13. Attachment of Fuel Rod to Baseplate with Fastener

Sealing of the Zircaloy-4 tubing to the solid Zircaloy-4 end stems was accomplished by full penetration fusion welding. The bottom end was welded prior to loading, the top end after loading.

A unique seven-digit serial number was machine engraved into the end stems of all rods. The first digit designated the basic type of rod: 0 for seed, 1 for standard blanket, 2 for power flattening blanket, and 3 for reflector. The second digit designated a specific fuel composition and loading within each basic rod type. It also identified the rod mounting: even numbers indicated the rod was top-mounted, and odd numbers indicated the rod was bottom-mounted. For example, a rod serial number beginning with 02 was a top-mounted seed rod; a rod serial number beginning with 15 was a bottom-mounted standard blanket fuel rod. Rod types are listed in Table 5.

2.6 - FUEL STRUCTURE AND COMPOSITION

The fuel used in LWBR was composed of thoria (ThO_2) or a binary solid solution of thoria with a low weight-percent (1.211 to 5.195) of urania (ThO_2-$^{233}UO_2$). Thoria and thoria-urania are ceramic fuel materials similar to uranium dioxide but have higher melting temperatures, lower thermal expansions, more creep resistance at high temperature, better corrosion resistance if exposed to reactor coolant, and less fission gas release (Reference (8)).

LWBR fuel pellets were fabricated from the two oxides in powder form. The binary pellets were obtained from well-mixed powders of thoria and urania to achieve a nearly homogeneous structure. Homogeneity was important to prevent local areas of increased fission rate with consequent increased depletion, temperature, and fission gas release.

Because neutron capture in impurities reduces the number of neutrons available for capture in the fertile thorium, the amount of impurities permitted in the fuel powder was controlled to be very low to enhance breeding. Similarly, the level of residual contaminants permitted in the as-fabricated pellets was controlled. Such residuals as carbon monoxide and hydrogen gases

Table 5 - LWBR Core Rod Fuel Loadings at Beginning of Life

Rod Type	Mounting	Binary Fuel Stack Length Within the Middle 84 Inches (In.)		Binary Pellet U-Fissile Content (w/o)
Seed				
01	Bottom	LZ	42	4.327
02	Top	LZ	42	4.327
03	Bottom	LZ	56	4.327
04	Top	LZ	70	4.327
05	Bottom	HZ	84	5.195
06	Top	HZ	84	5.195
07	Bottom	LZ	42	4.327
08	Top	LZ	42	4.327
Standard Blanket				
11	Bottom	LZ	42	1.211
12	Top	LZ	42	1.211
13	Bottom	HZ	70	2.000
14	Top	MZ	56	1.662
15	Bottom	MZ	84	1.662
16	Top	HZ	84	2.000
Power Flattening Blanket				
21	Bottom	LZ	42	1.649
22	Top	LZ	42	1.649
23	Bottom	HZ	70	2.733
24	Top	MZ	56	2.005
25	Bottom	HZ	84	2.733
26	Top	HZ	84	2.733
27	Bottom	MZ	84	2.005
Reflector				
31	Bottom	--	0	0
32	Top	--	0	0

HZ = High Zone Fuel
MZ = Medium Zone Fuel
LZ = Low Zone Fuel

and hydrocarbons could become trapped within the fuel during the sintering operation. At power, these gases could then be released into the rod atmosphere, degrading the thermal conductivity of the gas atmosphere, increasing gas pressure within the rod, and possibly causing internal cladding hydriding in the case of hydrogenous gases. Residual gases were reduced to acceptable levels with a special degassing operation on the pellets. Pellet surfaces were inspected by comparison against visual standards for the presence of dark spots, indicating surface inclusions from impurities picked up during manufacturing, and for color changes, indicating the presence of trace impurities.

After the powder was blended and compacted into pellets of the desired geometry, the "green" pellets were exposed to a thermal treatment to remove the blending binder (Carbowax) and the compacting lubricant (Sterotex). This thermal pretreatment was followed by a sintering operation at high temperatures for a long period of time to develop high density (typically 97 to 98 percent of theoretical) pellets. This operation also developed a homogeneous solid solution of the mixed and blended thoria and urania powders as described in Reference (9).

The main technical objective of the high-density fuel was to maximize the breeding potential by having the maximum amount of fuel per unit volume. There were additional advantages to having high-density fuel: the higher thermal conductivity permitted higher power production at the maximum permissible fuel centerline temperature; and the enhanced in-pile dimensional stability (resulting from the fact that fewer pores were available for closure) was important to minimize axial shrinkage of the fuel stack, thereby minimizing the potential for collapse of unsupported cladding.

Limits on internal and external structural attributes were established for core fuel pellets. Internal structural attributes which were controlled included grain size, granular segregation, pore size and distribution, internal cracks, and foreign inclusions. External structural attributes included chip-void and end land defects, incipient chips, surface cracks, and surface pores and blowholes.

Grain size limits were established to coincide with successful irradiation test results and, in the case of the fine-grain size limit, to prevent excessive creep and fission gas release associated with very fine grain size fuel. Grain size limits ranged from a coarse-grain limit of ASTM 3 (127 microns) for thoria fuel or ASTM 4 (90 microns) for binary fuel to a fine grain size varying from ASTM 10.5 (9.4 microns) to ASTM 13 (4.0 microns), depending on the type of fuel and location within the pellet.

Metallographic specimens were evaluated to determine the extent that the spherical granules of powder and binder were delineated by intergranular porosity following the cold pressing and sintering steps in fabrication. Normally, the original granules could not be detected. On occasion, however, a portion of the outline of these granules could be observed. The principal concerns with fuel having such granules were inadequate thermal conductivity, pellet strength, and resistance to fission gas release. Fabrication limits were established on the basis of irradiated fuel test results.

Internal pore size, shape, and distribution affect thermal conductivity and structural integrity of the fuel pellets. Because some amount of internal porosity exists even in high density pellets such as those in LWBR, limits were established on the maximum allowable pore size and distribution on the basis of irradiation test experience.

Metallographic samples of the fuel pellets were examined for the presence of internal cracks. Limits of acceptability were established to limit the size (area) and orientation of the cracks. There were two technical concerns with internal cracks: chips from the crack area could become wedged between the pellet and cladding, locally increasing cladding strains; and complete fracture of the pellet could result in pellet jamming and cladding deformation from pellet-cladding interaction.

Foreign inclusions consisting of metallic particles or second phase impurities were limited to prevent such deleterious effects as high neutron absorption cross section, a low-melting eutectic, differences in thermal

expansion or mechanical properties, and reaction with cladding at the outer surface.

With respect to external fuel structural attributes, pellets having incipient chips (chips loosely attached to the pellet), edge cracks, surface blowholes (surface porosity interconnected to internal porosity), and excessive surface pores were rejected for core use. The magnitude of a cavity on the surface of the pellet resulting from inadvertent chipping, called a chip-void, was restricted by performance and fuel loss considerations. Chip-voids on the pellet cylindrical surface were limited in size to avoid local cladding deformation into the void region and to avoid excessive fuel temperatures. In the end land region, chip-voids were limited to ensure that the end land load carrying capability and the pellet cocking stability were not adversely affected.

The LWBR core contained both radial and axial variation of fuel composition. An example of the fuel compositions is shown in Figure 14. The fuel stack length was 104 inches and included axial thoria regions of 10-inch length at the top and bottom of each rod to capture neutrons which might otherwise escape from the core in this direction. Of the 15 rows of rods in a seed module located from the module center to the outer row, rods in the 11 innermost rows contained high-zone $^{233}UO_2$-ThO_2 binary pellets in the middle 84 inches of length. High-, medium-, and low-zone refers to the weight percent of fissile uranium in the fuel pellets. Rods in the outer four rows contained low-zone binary pellets in stack lengths of 70, 56, and 42 inches, the remainder of the middle 84-inch stack being thoria fuel pellets. Blanket modules contained high-, medium-, and low-zone binary pellets and thoria pellets. The zoned rods reduced power peaking near metal and water channels and increased the reactivity worth of the movable seed modules as the latter changed elevation relative to the fixed elevation blanket modules.

Rod loadings and binary stack lengths for each of the 23 types of fuel rods used in the LWBR core are listed in Table 5.

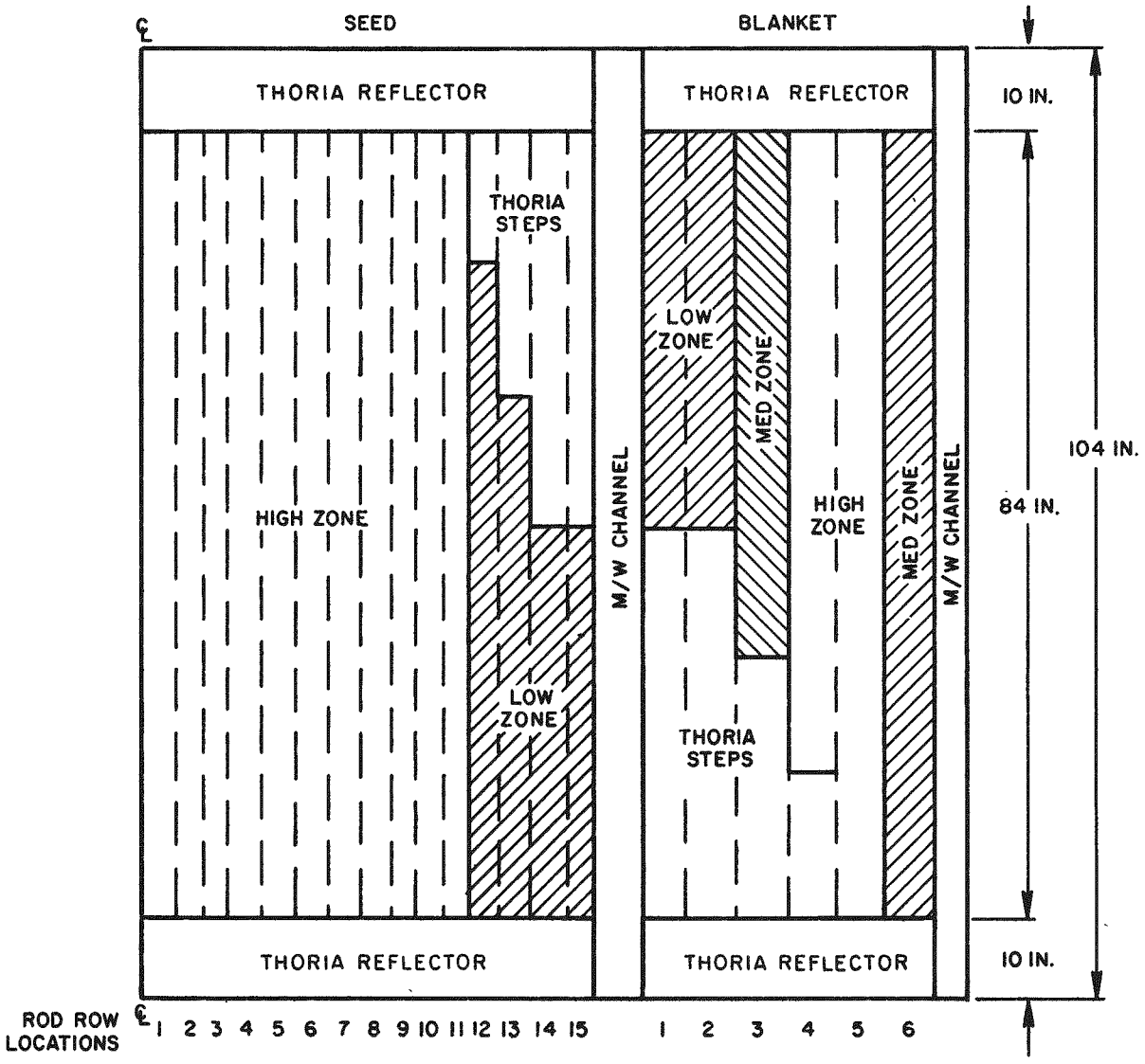

Figure 14. Variations in Fuel Composition in the Seed and Blanket Regions

2.7 - LWBR CORE OPERATION

The LWBR core was designed to operate for 18,000 effective full power hours (EFPH) and for approximately three years. One EFPH is the equivalent of operating the core for one hour at rated power, namely, 236.6 Mw (thermal).

The core was actually operated 60 percent beyond the design life, achieving 29,047 EFPH and approximately five years operation. During most of the core life, LWBR operated as a base load station. In the first two years, the core was subjected to 204 swing load cycles to demonstrate the core transient capability and generating system load follow to simulate operation of a large commercial nuclear reactor. A swing load cycle was defined as a power reduction from about 90 percent to between 35 and 60 percent for periods of four to eight hours, followed by a return to 90 percent or higher power. In spite of shutdowns for special testing and for maintenance and the deliberate swing load operation, the reactor achieved a high capacity factor of 65 percent and a high availability factor of 86 percent.

For the initial 18,000 EFPH, maximum allowable reactor power was established as 72 Mw gross (electric) and the average coolant temperature was 531°F. System pressure was initially 2000 psia, with reductions to 1940 psia at 4325 EFPH, to 1870 psia at 7132 EFPH, and to 1815 psia at 10,932 EFPH to reduce the probability of fuel rod cladding collapse. At approximately 18,500 EFPH, maximum allowable reactor power was reduced to 58 Mw gross (electric), system pressure was reduced to 1615 psia, and average coolant temperature was reduced to 521°F.

Maximum allowable power was further reduced to 54 Mw gross (electric) at 27,419 EFPH and to 43 Mw gross (electric) in 12 steps until the end of core life because of reductions in core excess reactivity late in life. Again, the pressure reductions were made to ensure against cladding collapse. Decreases in coolant temperature and reactor power were made to meet core performance limits for critical heat flux and fuel element stress at the reduced pressures.

During core operation, the LWBR fuel rods were subjected to 60 reactor startups (a change in power from below 1 percent to above 20 percent), 58 reactor scrams (in which the movable seed modules were unlatched and dropped

through the inner blanket guide tube from any power level), 204 swingload cycles, and 68 other power cycles in excess of 20 percent change. Additional details regarding LWBR operation are presented in Reference (10).

2.8 - SELECTION OF THE TWELVE DESTRUCTIVE EXAMINATION FUEL RODS

The 12 rods chosen for destructive examination (DE) were selected to cover a broad range of as-built and core operating characteristics. Principal operating characteristics of the twelve rods are listed in Table 6. As much as possible, the DE rods covered a range of power density, fuel burnup, and rod neutron fluence.

Because only 12 of the 39 core fuel modules were prepared for fuel rod removal, the number of module locations represented in the DE rods was limited. Four of the DE rods were from the seed region, four were from the standard blanket region, three were from the power flattening blanket region, and one was from the reflector region. All four seed rods were selected from a Type I seed module (I-1) which were most representative of those likely to be used in a large-scale breeder reactor. Only one reflector rod was examined since LWBR reflector modules would not be typical of large-scale breeder reactors. The blanket fuel rods were selected from Type I blanket modules at the center of the core and from Type II blanket modules between the inner blanket modules and the outer reflector modules to observe any radial fuel element performance differences.

Table 6 - Operating Characteristics of the 12 LWBR DE Fuel Rods at End of Life

Module Type	Rod S/N	Peak Power (Kw/ft)	Peak Depletion (10^{20} f/cc)	Peak Burnup MWD/MTM*	Peak Fast Fluence (>1 Mev) (10^{20} n/cm^2)
Seed I-1	0400736	6.7	9.52	44,500	85.0
Seed I-1	0606773	4.4	8.81	41,200	96.5
Seed I-1	0205071	5.5	11.43	53,400	75.5
Seed I-1	0507672	4.2	10.12	47,300	87.9
Blanket I-3	1606710	8.7	5.07	22,300	73.0
Blanket I-3	1105717	8.6	5.18	22,800	71.4
Blanket I-3	1504272	7.4	4.37	19,200	64.2
Blanket II-2	1208823	6.9	4.25	18,700	55.4
Blanket II-2	2610746	8.7	5.70	25,200	57.7
Blanket II-2	2514164	8.3	5.05	22,300	38.6
Blanket II-2	2607600	8.4	5.53	24,400	58.6
Reflector IV-3	3102657	3.4	0.96	4,100	25.9

* MWD/MTM = Megawatt days per metric ton of metal (uranium plus thorium)

(Intentionally Blank)

SECTION 3 - DESCRIPTION OF DESTRUCTIVE EXAMINATIONS

Destructive examinations of the fuel rods were performed both at Argonne National Laboratory-West (ANL-West) in Idaho Falls, Idaho, and at Argonne National Laboratory-East (ANL-East) in Argonne, Illinois. After the rods were nondestructively examined in the Rod Examination Station (REX) at the Expended Core Facility (ECF), the rods were shipped to ANL-West, where they were neutron radiographed and punctured to obtain fission gases. The neutron radiography procedure and examination findings are given in Reference (3).

The approximately 10-foot long rods were cut in half to facilitate handling and were shipped to ANL-East. Samples were cut from each rod half; some of the samples were shipped back to ANL-West for examination while other samples were examined at ANL-East. The procedures used to prepare and examine the DE rods are described in this section. Results of the examinations are presented and discussed in Section 4.

3.1 - FUEL ROD PUNCTURE AND GAS ANALYSIS

Puncturing of each fuel rod to permit collection of the internal gases was performed in a hot cell with a laser beam as a drill. The rod, in a vertical position, was clamped and sealed against a collection chamber in front of the laser instrument. An elastic washer served as a gas seal between the rod and the chamber. The laser beam was fired through the transparent wall of the collection chamber onto a predetermined spot on the rod surface in the plenum region. The spot was chosen from review of the neutron radiographs of the rod to lie between the coils of the plenum spring, which would act as a heat sink and reduce the drilling action of the laser. Typically, the Zircaloy-4 cladding was penetrated in approximately 60 seconds.

Upon puncturing of the cladding wall, the internal gases, consisting of fission products and the initial helium atmosphere, were released by way of the collection chamber into a low pressure (30 to 40 millitorr) argon gas region of the collection system. After allowing three to five minutes for the gas pressure to reach equilibrium between the collection chamber and the fuel rod, the gases were directed into a sample collection tube. By backfilling

the system with an inert atmosphere to a known pressure and bleeding off the gases, the gas volume and pressure of the fuel element were calculated. The gas sample was analyzed by mass spectrometry to determine composition and quantity of the constituent gases, particularly of the fission gases, xenon and krypton, present in the sample.

3.2 - FUEL ROD SECTIONING

Each rod was cut approximately in half using a modified tube cutter. The rod was positioned in a V-trough by two clamps on either side of a 15-inch access opening in the trough. With the tube cutter assembly clamped onto the rod, an integral cutter blade on the end of a micrometer-type screw was directed against the cladding. As the cutter was rotated around the stationary fuel rod, metal chips were removed from the cladding. The cutter blade was advanced a small amount (1 to 2 mils) and the cutter was rotated again. The micrometer continued to be advanced by this amount until the cladding was sectioned. The intent was to cut the rod at pellet-pellet interfaces to contain the pellets within the cladding after cutting.

During the initial cut of the first two (seed) rods, the plenum spring pushed out several pellets from the cut end of the top rod section. For subsequent fuel rods, an initial cut of the rod was made at the interface between the top fuel pellet and the bottom of the plenum spring. This relieved the plenum spring without having fuel pellets become displaced from the cladding. The rods were then cut in half and capped with either shrink-fit tubing or epoxy.

Examination samples were removed from the rod by making transverse cuts at designated locations with an abrasive cutoff wheel. An in-cell manipulator (slave) was used to pivot a counterweighted arm holding the cutoff wheel onto the fuel rod. A chuck (Jacob's) gripped the rod near the cut location and rotated the rod during the cutting operation. Again, the rod was sectioned at pellet-pellet interfaces to minimize separation forces and to eliminate having a portion of a pellet protruding from one end of the cladding. Control of the cut location along the rod axis was provided by sliding a steel block (attached to the rod end away from the cut) in the V-trough until the desired location was obtained, then clamping the block to the V-trough.

3.3 - METALLOGRAPHIC EXAMINATION

Sections of the fuel rod, one pellet in length, were removed and prepared for metallographic examination of the fuel and cladding. Locations of the samples were specified to provide a range of end-of-life fuel conditions, such as burnup, neutron fluence, and power levels. In some cases, the samples were mounted to provide a transverse view in which grinding of the metallographic mount revealed a plane perpendicular to the axis of the rod. In other cases, the samples were mounted to provide a longitudinal view to reveal a plane parallel to and essentially through the rod axis. The orientation of each cladding-fuel metallographic mount was determined from the results of neutron radiography performed prior to rod sectioning.

Microstructural features were observed at magnifications of 50X, 250X, and 500X. Composites of the complete pellet section were made at 35-50X, with the final photograph of the mosaic at approximately 10-20X.

In the as-polished condition, the fuel was evaluated for the size and spatial distribution of porosity, as well as for the presence of cracks in the ceramic fuel. Grain size was determined by direct counting of the number of grains in a 3 inch x 3 inch area on 250X micrographs. This data was converted to equivalent grains per square inch at 100X, n, from which the equivalent ASTM grain size number, Q, was calculated by means of the following formula:

$$Q = (\log n/\log 2) + 1.00$$

Accuracy was reported to be ±5μm for the average grain diameter and ±0.2 for the ASTM grain size.

Metallographic examination of the cladding in the as-polished condition was performed to assess corrosion (oxide) of both the external (water side) and the internal (fuel side) cladding surfaces. These mounts were also used to look for evidence of fuel and cladding mechanical and chemical interaction, cracking, or other defects. To observe the concentration and orientation of the hydrides, both longitudinal and transverse metallographic samples were examined in the etched condition. The etchant consisted of 60 cc H_2O_2, 40 cc HNO_3, and 10 drops HF. Hydrogen concentration in the cladding was estimated

by comparison of 250X photographs of the examined cladding to the 250X photographic standards in Reference (11).

Longitudinal metallographic samples of selected cladding-to-end stem welds were examined in the as-polished condition to evaluate weld integrity (the presence of cracks, holes, corrosion, or other unusual features), and in the etched condition for the presence of hydrides. Similarly, longitudinal metallographic samples through selected end stems were examined in the etched condition for the presence and distribution of hydrides and for cracks. Because the top "shoulder" of the end stem in the seed and reflector regions was in direct contact with the high nickel baseplate of Inconel-600, the possibility existed for significant hydride formation at the shoulder. The end stem metallographic sample was evaluated to determine the presence and extent of any hydride concentration gradient in this area.

The Inconel X-750 plenum spring samples and the Type 348 stainless steel support sleeve samples were visually examined at low magnification (approximately 5X) for the presence of cracks. The spring length in the cold (room temperature) free (unloaded) condition was measured to evaluate stress relaxation. Transverse metallographic samples through the springs were examined at 250X for the presence of cracks or corrosion effects.

The principal concern for the Zircaloy-4 fasteners (Figure 13) used in the seed and reflector fuel regions to secure the fuel rods to the Inconel-600 baseplates was the potential for rapid hydriding of the fastener at the bearing surface. Rapid hydriding could occur if the protective prefilm was removed during the installation torquing operation. Smearing and bonding of Inconel onto local regions of the Zircaloy fastener at the regions of the removed oxide layer could provide a "window" for rapid hydriding.

To evaluate whether this mechanism was operative during core life, transverse and longitudinal metallographic samples of the Zircaloy-4 fuel rod fasteners were examined. In the unpolished condition, the fasteners were examined at 500X for oxide appearance and thickness. In the etched condition, the fasteners were examined at 250X for hydride content and orientation. The same etchant used for the Zircaloy-4 cladding was used to etch these fuel rod fasteners.

Most of the fasteners were mounted to observe a transverse view through the cross section. A 0.7-inch long section of the fastener containing the bearing surface was mounted in Micarta with epoxy potting material. The first transverse plane examined was located within 1 mil of the bearing surface. Serial grinding and polishing through several layers to depths between approximately 15 and 50 mils were performed to determine the extent, if any, of the hydride gradient from the bearing surface.

3.4 - HYDROGEN ANALYSIS OF THE CLADDING

The hydrogen content of Zircaloy-4 cladding sections was determined by the inert-gas fusion technique. Cladding sections, each consisting of a full-diameter ring approximately 0.125 inch in length, were cut from designated fuel rods. Prior to analysis, the cladding rings were prepared by rinsing in distilled water, ultrasonically cleaning with acetone to remove any loose fuel particles, degreasing in carbon tetrachloride, rinsing again in acetone, and air drying. The cladding ring was sectioned into four pieces, individually weighed, and wrapped in a preweighed piece of 1-mil thick platinum foil of a known hydrogen content. Hydrogen in the cladding was measured in two runs in the inert-gas fusion apparatus, each run involving two adjacent pieces of cladding. This provided an indication of both uniformity of hydrogen distribution and average hydrogen concentration.

The amount of hydrogen in the cladding sample was determined by measuring the H_2 gas, which is evolved when the sample is fused in an inductively heated graphite crucible containing a platinum bath at about 1950°C. Purified helium carries the released gases through an initial trap to remove any water vapor, then through hot copper oxide (fine copper wire filaments) to oxidize the H_2 to H_2O, then through a capillary cold trap to solidify the H_2O. The carrier gas is extracted, the ice crystals are heated, and the water vapor subsequently passes through capacitive manometers into a calibrated volume chamber for quantitative determination of hydrogen.

The inert-gas fusion system was calibrated against National Bureau of Standards Standard Reference Materials (SRM). The hydrogen determination has an estimated standard deviation (including measurement uncertainties and

variations in the platinum-foil blanks) of approximately 5 percent at a level of 100 ppm hydrogen. Calibration checks were performed against the standard reference material values before and after the cladding samples. The reported values included a correction for an apparent bias of 6.8 ppm (6.4 percent), relative to the National Bureau of Standards SRM.

3.5 - DETERMINATION OF FUEL DEPLETION

Fuel depletion is defined in terms of fissions per cubic centimeter of fuel. Depletion, also known as burnup, is often given in terms of megawatt days per metric ton of metal (uranium plus thorium). Fuel pellets to be analyzed for depletion (burnup) were removed from the cladding and dissolved in an acid solution (HNO_3-HF) without comminution. Total thorium and uranium, isotopic uranium, and stable fission products ^{139}La and ^{148}Nd were measured by isotopic dilution mass spectroscopy after decontamination of the analytes from interferences and radioactive fission products. The mass spectrometer was calibrated with isotopically pure ThO_2 and an NBS uranium standard. In addition to these isotopes, ^{137}Cs and ^{144}Ce were measured by gamma-ray spectroscopy on fractions of the dissolver solution. A lithium-drifted germanium detector calibrated with NBS traceable standards for ^{137}Cs and ^{144}Ce was used to detect and measure the fission products for these analyses. Fuel burnup was determined from the measured quantities of these isotopes.

Two of the 12 DE fuel rods were destructively examined to determine fuel burnup. Seed rod 0205071 and standard blanket rod 1606710 were analyzed and compared with calculated burnup values to qualify the calculational model. For each of the two fuel rods examined for burnup, one of the samples was taken from the top thoria region and the second sample was taken from the adjacent top binary pellet. Results of the fuel burnup analyses are given in Section 4.3.

3.6 - IODINE AND CESIUM ANALYSIS OF THE FUEL AND CLADDING

Stress corrosion cracking of metallic components, such as the Zircaloy-4 cladding, has historically been a problem concerning reactor safety and fuel performance. Iodine and cesium have been identified as possible corrosive

agents causing stress corrosion cracking. Under reactor conditions, fission product iodine can react with Zircaloy. Measurement of fission product iodine and cesium inventories in the fuel rod samples was performed to determine the fraction of these nuclides that migrate to the gap region and into the cladding. (The gap region was defined as the fuel-cladding gap, fuel cracks, and the interconnected, open porosity in the fuel.) The quantity of fission products ^{129}I and ^{137}Cs in the fuel-cladding gap and, separately, dissolved in the fuel and cladding were determined for two seed fuel rods and two standard blanket fuel rods.

Fission products ^{129}I and ^{137}Cs deposited in the gap were determined by immersing the fuel and cladding, separately, in 2N HCL for 30 minutes. Ultrasonic vibration was applied to aid in dissolving any iodine and cesium deposits from the cladding surface only. Fuel particles remaining in the cladding and fuel wash solution were removed by filtration. After diluting the solution to a know volume, an aliquot was taken for ^{137}Cs measurement by gamma-ray spectroscopy. The remaining solution was analyzed for ^{129}I by adding carrier iodine and separating the iodine by solvent extraction. The separated iodine was precipitated as palladium iodide (PdI_2) and counted for ^{129}I with a calibrated lithium-drifted germanium detector.

The ^{129}I and ^{137}Cs inventory in samples of ThO_2 and ThO_2-UO_2 fuel was determined after comminution and dissolution of the powdered fuel samples in HBr-HF solution containing carrier iodine. Cesium-137 and ^{129}I were determined from the dissolver solution in the same manner as for the gap wash solutions.

In order to determine the fission product ^{129}I and ^{137}Cs inventory in the cladding, the cladding was first washed, dried, weighed, and measured to calculate the inside surface area. A one-gram sample of cladding was dissolved in a HCL-HF mixture containing carrier iodine. The dissolver solution was diluted to a know volume and an aliquot was taken for ^{137}Cs analysis. The cesium and iodine inventories were then obtained in the same manner as for the gap wash solutions. Results of the analyses are given in Section 4.4.

3.7 TENSILE TESTING OF THE CLADDING

Tensile tests were performed on RXA cladding from the seed region and on SRA cladding from the standard blanket and reflector regions. Seven to eight inch long sections were cut from the fuel rod to be tested and the fuel was removed, leaving the cylindrical cladding intact. Cladding sample locations along the length of the rod were selected between support grid levels to ensure that the gage length surface was free from wear marks. Four fuel rods (two seed, one standard blanket, and one reflector) were tested at room temperature. Three fuel rods (two seed and one reflector) were tested at 500°F to determine elevated temperature mechanical properties. Heat lamps were used to achieve the elevated test temperature. Elevated temperature tests at end of life were conducted at 500°F rather than the 700°F temperature used for beginning of life because annealing of radiation damage in Zircaloy occurs at temperatures above about 500°F. Difficulty in separating fuel from blanket cladding precluded testing of additional blanket rods.

Tensile tests were conducted in-cell on an Instron machine at a strain rate of 0.058 inch/inch of gage per minute in accordance with References (12) and (13) for room temperature and elevated temperature testing, respectively. Mechanical properties measured and reported were 0.2 percent offset yield strength, the ratio of ultimate strength to yield strength, percent elongation in a 2-inch gage length upon rupture, and percent reduction in area. Results of the cladding tensile tests are given in Section 4.5.

SECTION 4 - RESULTS OF DESTRUCTIVE EXAMINATIONS

4.1 - FISSION GAS RELEASE

Plenum gases were tapped from 11 of the 12 destructively examined (DE) fuel rods. The gas sample from the twelfth DE rod was lost during the plenum tap. In a previously conducted proof-of-breeding program, plenum gases from 17 additional Light Water Breeder Reactor (LWBR) core fuel rods were collected and analyzed at Argonne National Laboratory-East (ANL-E), providing a total of 28 rods that were analyzed for fission gas released volume and composition. The total moles of collected gas for each fuel rod were determined from calibrated volumes. Gas compositions were analyzed by mass spectrometry of samples from the calibrated volumes.

Helium was the major component of the tapped gas and comprised more than 94 percent of the analyzed sample in each case. High amounts of helium were expected because it was the initial fill gas and additional helium was generated in the fissioning process. The remainder of the gas sample was xenon and krypton generated in the fissioning process and hydrogen and carbon dioxide residual from pellet fabrication. All five gases were expected and were considered in fuel rod design.

The ratio of total fission gas (xenon plus krypton) generated in the fuel to the amount released is an important indication of fuel temperatures achieved during reactor operation. As described in Reference (14), the transition temperature (boundary temperature) between low temperature and high temperature fuel during power operations is that temperature at which gas bubbles coalescing at dislocations in the fuel begin to be released. For operations below the boundary temperature, gas release occurs only from recoil and knockout at free surfaces. Low-temperature release is normally less than 0.5 percent for rod-average depletions to 10×10^{20} f/cc. The boundary temperature for LWBR (thoria-based fuel and 29,047 EFPH operation) was 2580°F.

Measured fission gas releases from the 28 LWBR fuel rods are listed in Table 7, expressed as a percentage of calculated fission gas generated in fissioning. The gas release percentages, normalized to 100 percent fuel density, are plotted against rod-average depletion in Figure 15. All rods are shown to

Table 7 - LWBR Fuel Rod Fission Gas Release at End of Life

Rod S/N	Cell	Module	Rod-average Depletion (10^{20} f/cc)	Fission Gas: Generated in Fuel* (mol)	Fission Gas: Measured in Plenum Tap (10^{-5} mol)	Fission Gas: Recovered Fraction**	Fission Gas: Released (%)***
0606773	6B4	SI-1	5.4	0.02683	1.22	0.803	0.06
0507672	5L31	SI-1	6.4	0.03198	2.51	0.725	0.11
0504042	5L29	SI-1	6.0	0.03007	2.37	0.734	0.11
0507057	5C10	SI-1	5.1	0.02575	1.30	0.744	0.07
0400736	4M33	SI-1	5.3	0.02631	1.51	0.912	0.06
0401744	4M49	SI-1	4.8	0.02398	3.76	0.849	0.18
0307602	3N63	SI-1	4.2	0.02120	1.36	0.767	0.08
0205071	2Q41	SI-1	4.5	0.02266	1.02	0.782	0.06
0201562	2P39	SI-1	3.8	0.01890	1.06	0.816	0.07
1606710	16E57	BI-3	2.9	0.05723	3.10	0.662	0.08
1605519	16E56	BI-3	2.9	0.05693	2.76	0.659	0.07
1504272	15F11	BI-3	2.5	0.04831	1.90	0.726	0.05
1400544	14C3	BI-3	1.9	0.03791	1.77	0.959	0.05
1302864	13D24	BI-3	2.4	0.04582	1.49	0.675	0.05
1200830	12A49	BI-3	2.1	0.04051	1.37	0.695	0.05
1208823	12A12	BII-2	1.8	0.03436	0.89	0.788	0.03
1105717	11A46	BI-3	2.2	0.04304	2.27	0.722	0.07
2610746	26E68	BII-2	3.3	0.05531	3.22	0.646	0.09
2606481	26E31	BIII-6	3.1	0.05424	3.43	0.743	0.09
2514164	25K13	BII-2	2.9	0.04741	1.63	0.629	0.06
2513854	25F73	BIII-6	2.6	0.04345	1.46	0.655	0.05
2502102	25H1	BIII-6	1.3	0.02209	0.22	0.770	0.01
2400408	24C13	BIII-6	1.4	0.02319	0.38	0.725	0.02
2300711	23D29	BIII-6	2.8	0.04622	2.54	0.633	0.09
2102187	21B62	BIII-6	1.5	0.02380	0.44	0.729	0.03
3102657	1A1	RIV-3	0.5	0.01856	0.17	0.983	0.01
3211456	2B1	RIV-3	0.4	0.01659	0.12	0.788	0.01
3110505	1E3	RIV-3	0.2	0.00687	0.04	0.999	0.01

* Calculated from rod-average depletion

** Ratio of helium recovered to calculated amount present from initial fill and $\{n,\gamma\}$ reaction

*** Gas release = (Amount measured in plenum tap)/(Amount generated)/(Recovered fraction)

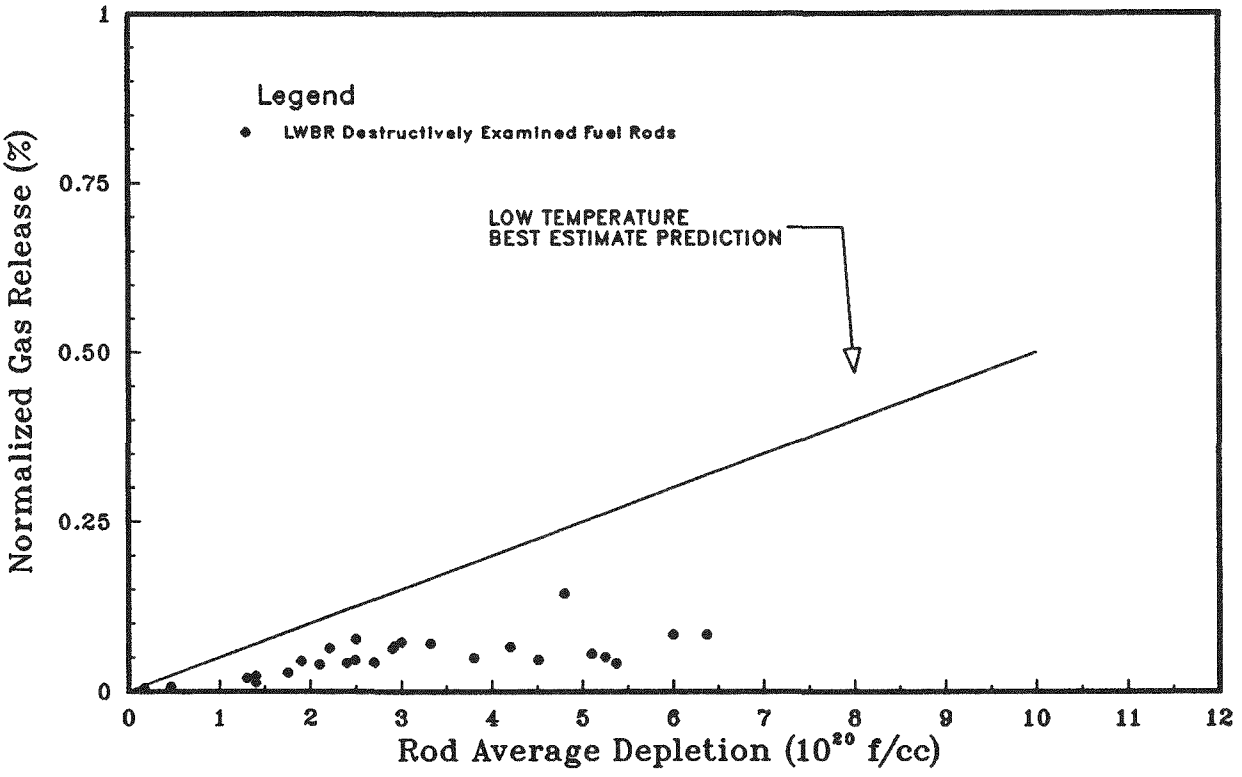

Figure 15. Fission Gas Release Versus Depletion

have gas release levels below the low-temperature prediction line. Because fuel rods from peak temperature and peak depletion locations were included among those rods examined, all fuel was considered to have operated at temperatures below 2580°F.

Low temperature operation and the resulting low fission gas release were favorable to fuel rod performance and indicate that rod internal pressure and Loss of Coolant Accident (LOCA) adequacy were as expected (Reference (15)).

4.2 - METALLOGRAPHIC FEATURES

4.2.1 - Fuel Behavior

4.2.1.1 - Thoria Fuel

A view of whole thoria (ThO_2) pellets at end of life is shown in Figure 16 following removal from seed rod 0205071. The pellets were intact and could be handled remotely in the hot cell without fracturing. Metallographic examination revealed that at very low burnup (280 MWD/MT) and fast neutron fluence (4 x 10^{20} n/cm^2), thoria fuel (having no initial loading of UO_2) experienced little change from as-fabricated conditions. No pellet cracks were evident as shown in the transverse micrograph in Figure 17, and the smaller as-fabricated pores were still present (Figure 18). In general, the pore size was small compared to binary (ThO_2-UO_2) fuel which experienced high burnup.

At significantly higher burnup and fast neutron fluence (13,750 MWD/MT and 71 x 10^{20} n/cm^2), the thoria fuel pellets experienced internal cracking, many of which were circumferential in orientation as shown in Figure 19. Little change in grain size was noted between the low and high fast fluence thoria fuel as reported in Table 8. Figure 20 shows that the pore size remained small and the pores were located principally at the grain boundaries. Grain pullout was observed in a band along the pellet surface and internal cracks; however, the central portion of the high fast fluence thoria pellet showed very little grain pullout (Figures 19 and 20).

A gap between the cladding I.D. and the pellet surface of one to two mils was observed for the low fast fluence and low burnup thoria rod in the reflector region (Figure 18, top micrograph). This differed from the finding for

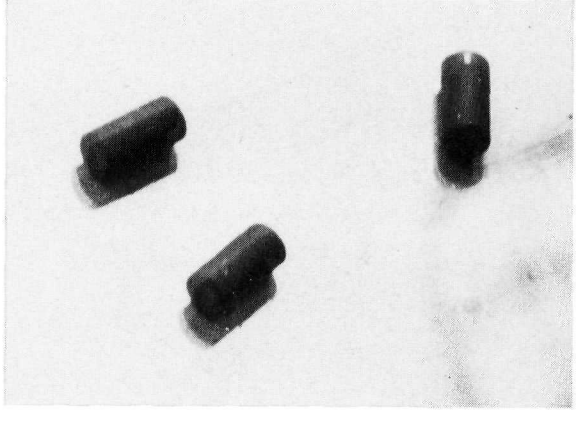

Figure 16. LWBR Thoria Pellets at End of Life

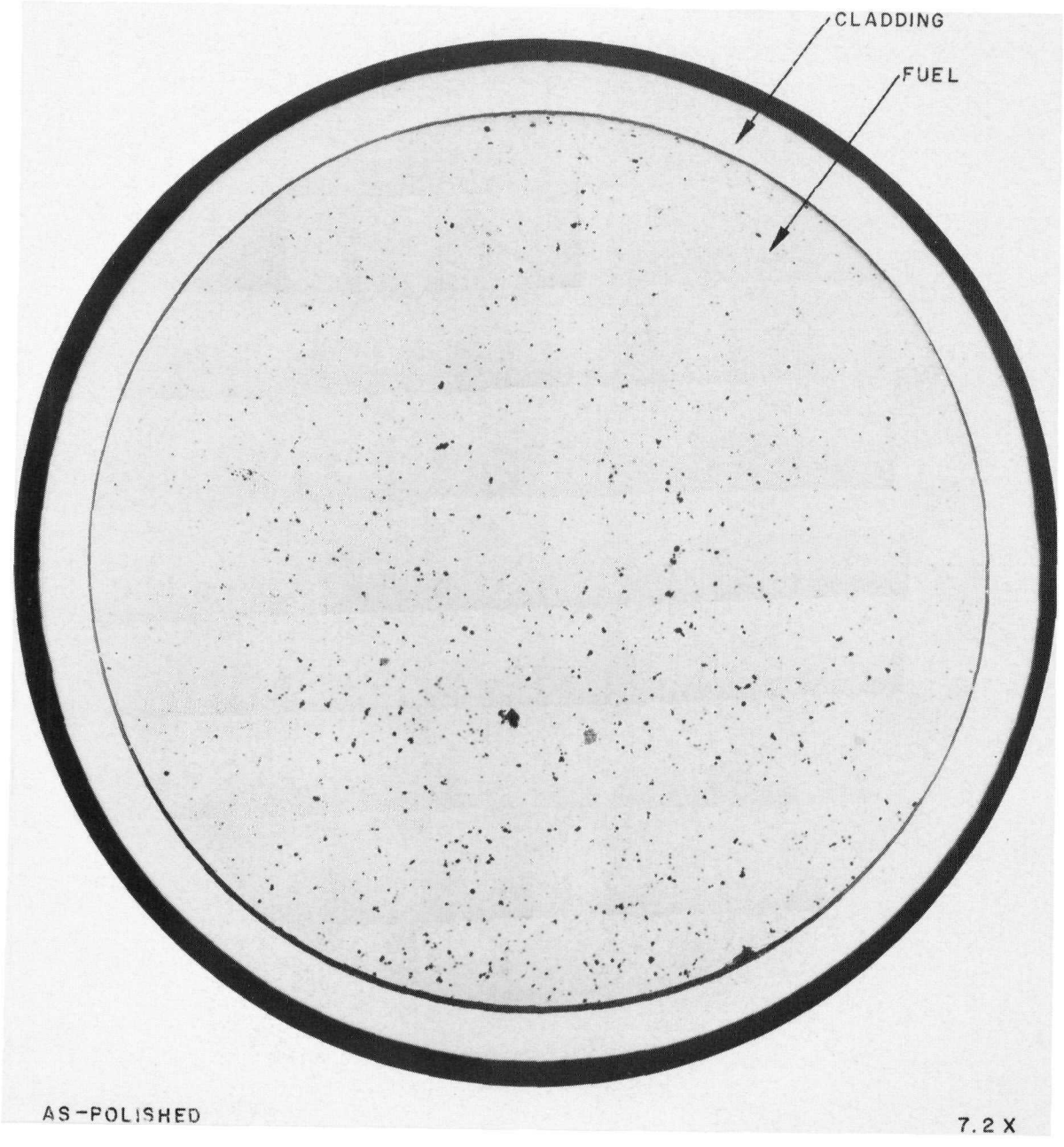

Figure 17. Transverse Section Through Thoria Fuel Pellet from Reflector Rod 3102657 (4×10^{20} n/cm^2 Fast Fluence, 280 MWD/MT Burnup)

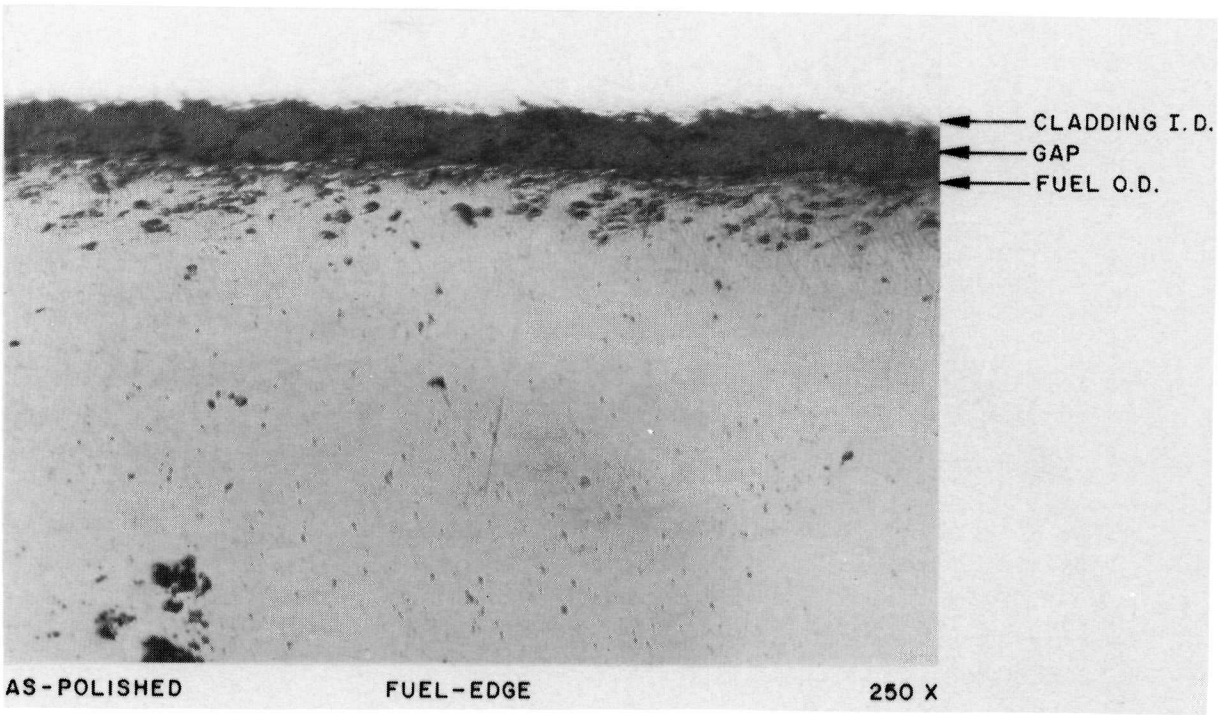

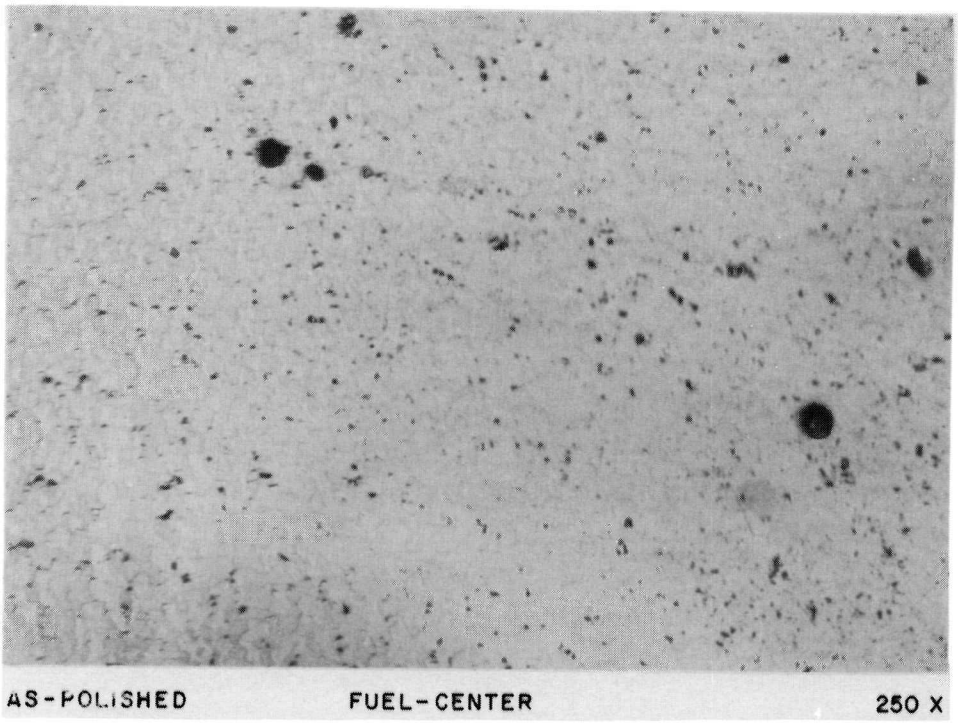

Figure 18. Thoria Fuel at End of Life from Reflector Rod 3102657 (4×10^{20} n/cm^2 Fast Fluence, 280 MWD/MT Burnup)

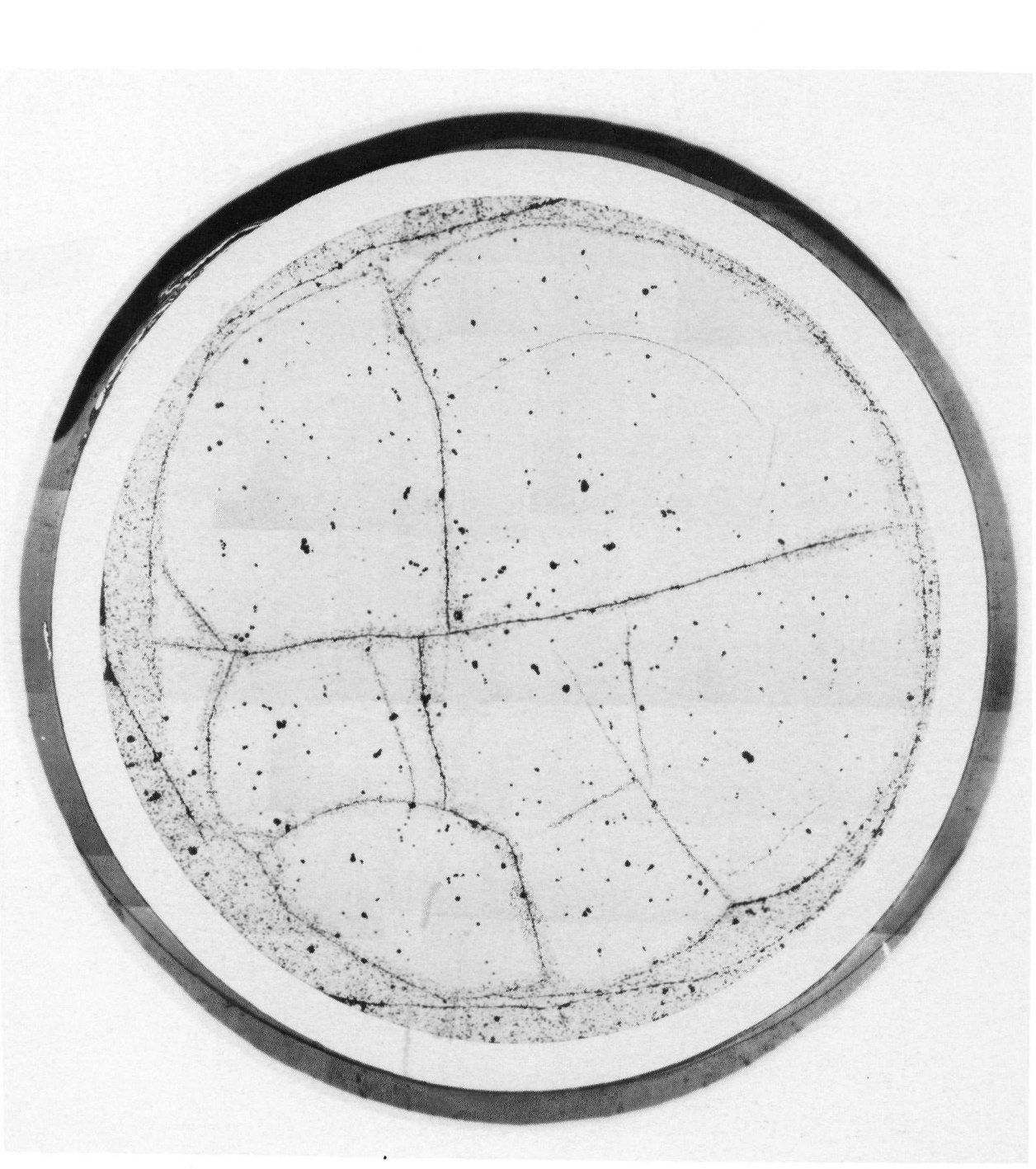

As-Polished 10.5X

Figure 19. Transverse Section Through High Fast Fluence Thoria Fuel Pellet from Standard Blanket Rod 1105717 (71×10^{20} n/cm^2 Fast Fluence, 13,750 MWD/MT Burnup)

Table 8 - Grain Size of LWBR Fuel at End of Life

Rod Type	Rod S/N	Fast Neutron Fluence 10^{20} n/cm^2	Burnup (MWD/MTM)	Grain Diameter, μm		ASTM Grain Size		Type Pellet
				Edge	Center	Edge	Center	
Seed	0400736	49	24,850	60	70	5.3	4.6	Binary
		54	36,990	40	40	6.3	6.4	Binary
	0606773	96	40,870	70	80	4.8	4.3	Binary
		33	17,300	65	80	5.0	4.5	Binary
	0205071	75	51,580	N/M	N/M	N/M	N/M	Binary
	0507672	86	46,900	95	125	3.8	3.0	Binary
Standard Blanket	1606710	73	22,350	150	80	2.6	4.3	Binary
		58	18,910	125	70	3.0	4.6	Binary
	1504272	64	19,130	115	105	3.3	3.6	Binary
	1105717	71	23,090	150	105	2.6	3.6	Binary
		71	13,750	65	50	5.0	5.6	Thoria
	1208823	51	10,180	75	N/M	4.6	N/M	Thoria
Power Flattening Blanket	2514164	39	22,320	70	45	4.6	6.0	Binary
	2607600	42	17,520	80	45	4.5	5.9	Binary
		59	24,290	150	85	2.6	4.2	Binary
	2610746	57	24,790	75	55	4.6	5.3	Binary
Reflector	3102657	4	280	45	N/M	6.0	N/M	Thoria

N/M = Not Measured
MWD/MTM = Megawatt days per metric ton of metal (uranium plus thorium)

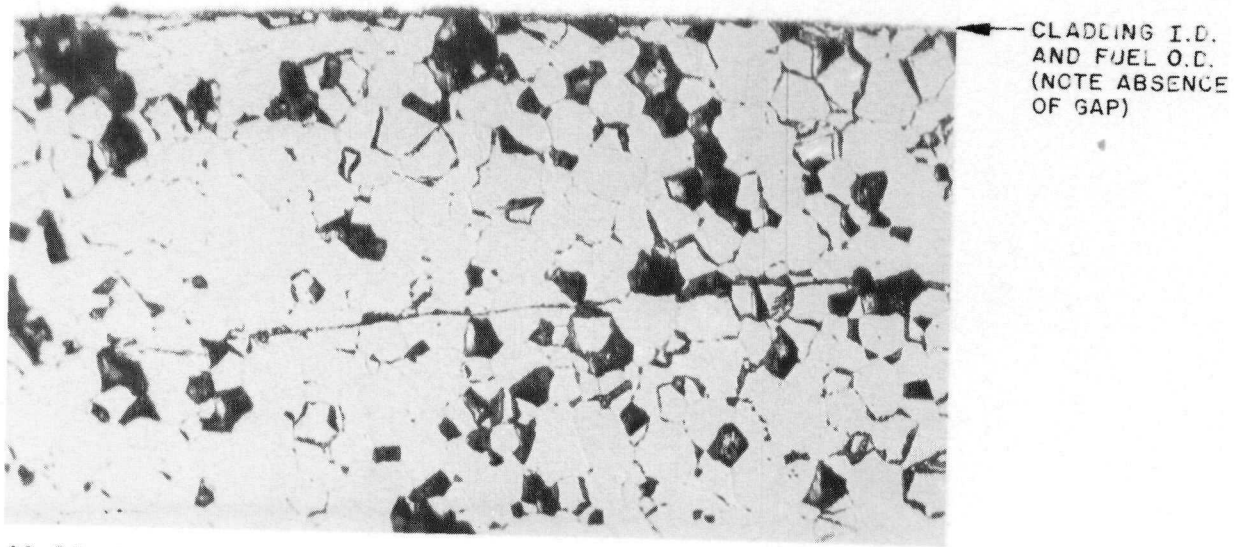

AS-POLISHED FUEL-EDGE 250 X

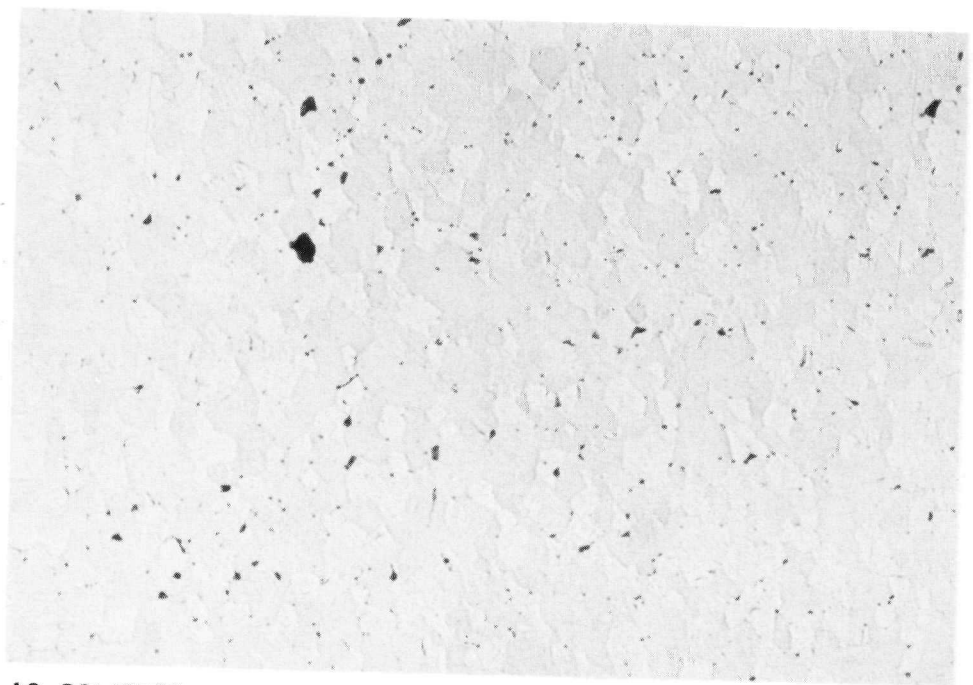

AS-POLISHED FUEL-CENTER 250 X

Figure 20. High Fast Fluence Thoria Fuel from Standard Blanket Rod 1105717 (71×10^{20} n/cm^2 Fast Fluence, 13,750 MWD/MT Burnup)

binary fuel in the blanket region in which no gap between the cladding I.D. and pellet surface was observed.

4.2.1.2 - Binary Seed Fuel

Fuel pellets from the seed region remained cylindrical and well-formed in shape after a core lifetime of 29,047 EFPH. In contrast to thoria fuel pellets, binary (ThO_2-UO_2) fuel pellets were often cracked, such that the pellets fractured if handled in-cell, but their basic cylindrical shape was maintained (Figures 21 and 22). During sectioning of the seed rods, it was observed that the fuel pellets were free to slide within the cladding. This indicated that pellet-cladding interaction did not occur and that these rods remained freestanding as designed.

Fuel coring was not observed (Figures 21 and 22). This was consistent with irradiation test results for similar high-density (approximately 98 percent theoretical) ThO_2-UO_2 pellets.

Fuel porosity was very fine in binary pellets at lower depletion and fluence levels (Figure 23) for the transverse sample from seed rod 0400736. Burnup and fast neutron (greater than 1 Mev) fluence estimates for the specific fuel samples examined metallographically are listed in Table 9. The fuel burnup for the pellet from seed rod 0400736 in Figure 23 was estimated at 24,850 MWD/MTM and the fast neutron fluence at 49×10^{20} n/cm^2. For pellets at higher burnup and fast fluence levels, such as that shown in Figure 24 from seed rod 0606773 at an estimated burnup of 40,870 MWD/MTM and a fast fluence of 96×10^{20} n/cm^2, a greater quantity of fission gas porosity is evident. Porosity in the more highly depleted fuel was observed to be concentrated principally at the grain boundaries, such that the grains were nearly ringed by the porosity. The magnitude and distribution of the porosity was not sufficient to develop the classical "necklace" porosity, but it appeared to be sufficient to cause more grain pullout during metallographic preparation than for the less depleted fuel.

The appearance of binary fuel from the most highly depleted region examined was unusual. A transverse section through the cladding and fuel pellet from seed rod 0205071 after experiencing a burnup of 51,580 MWD/MT

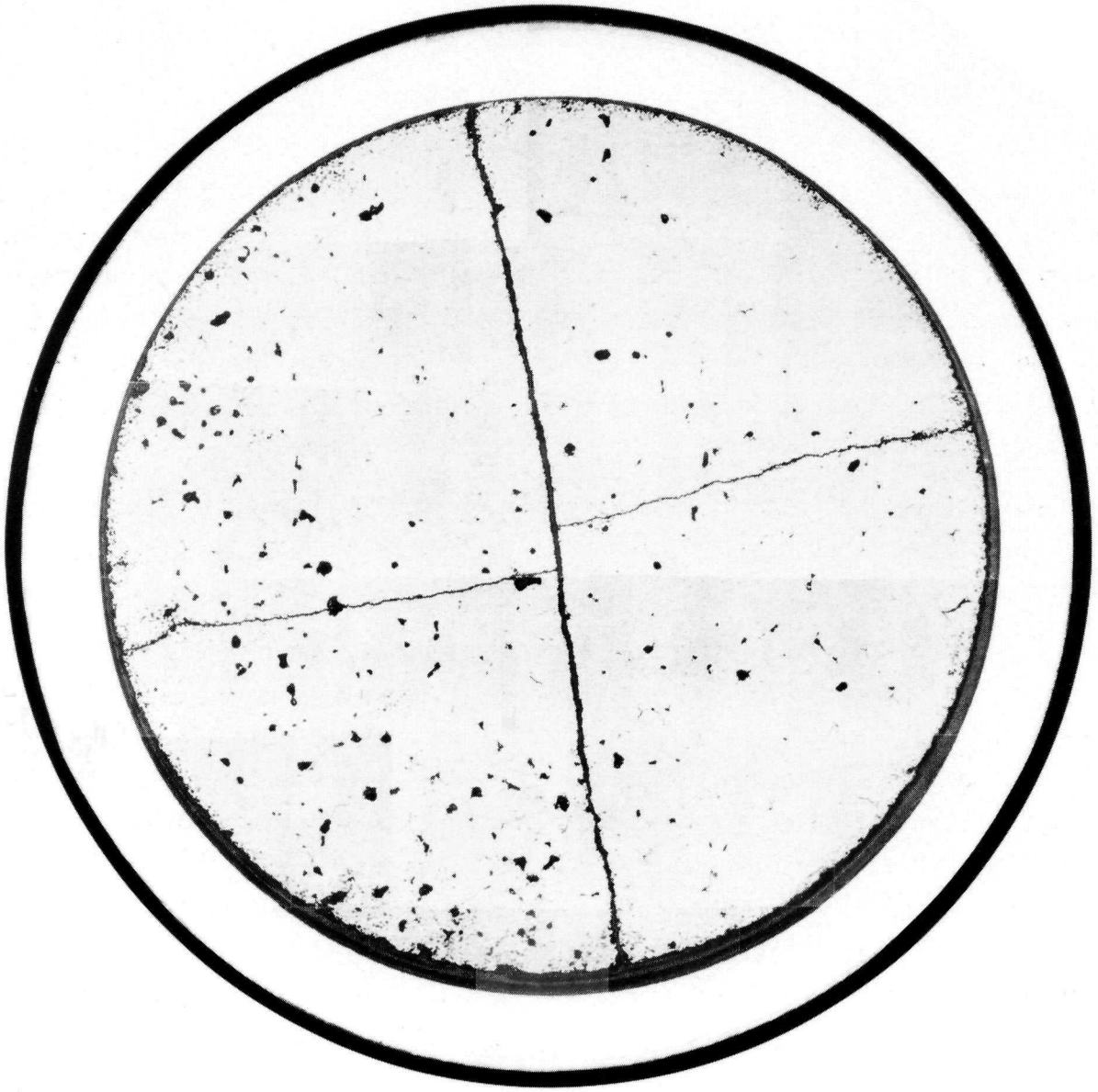

As-Polished 19.8X

Figure 21. Transverse Section Through Binary Fuel at End of Life from Seed Rod 0400736 (49 x10^{20} n/cm^2 Fast Fluence, 24,850 MWD/MT Burnup)

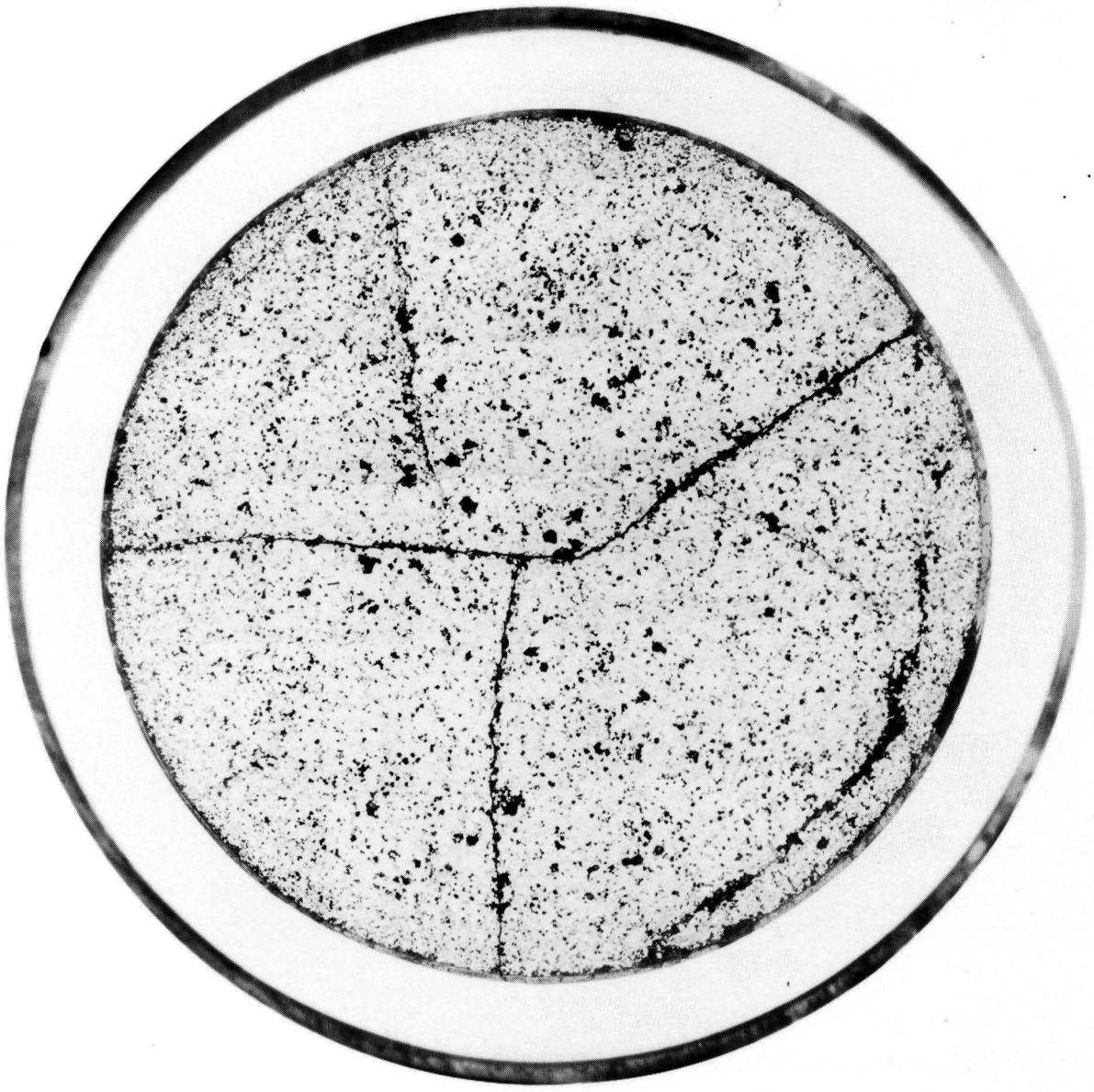

As-Polished 19.7X

Figure 22. Transverse Section Through Binary Fuel at End of Life from Seed Rod 0606773 (96 x 10^{20} n/cm^2 Fast Fluence, 40,870 MWD/MT Burnup)

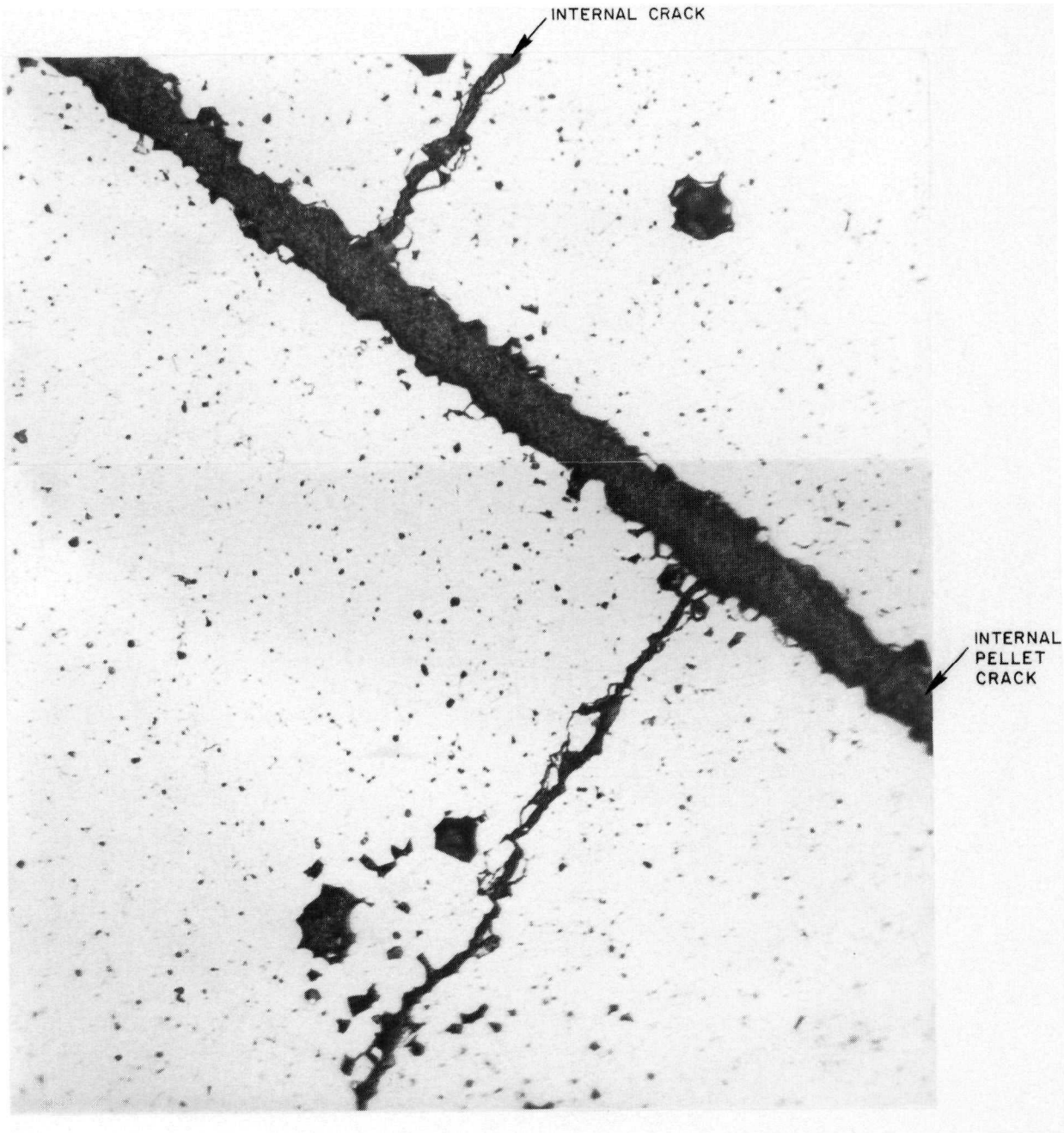

As-Polished Fuel-Center 250X

Figure 23. Fine Porosity in Binary Fuel from Seed Rod 0400736 (49×10^{20} n/cm^2 Fast Fluence, 24,850 MWD/MT Burnup

Table 9 - End-of-Life Conditions of the Cladding-Fuel Metallographic Sections from the 12 DE Fuel Rods

Fuel Region	Rod S/N	Type Pellet	Orientation	Fuel Depletion (10^{20} f/cc)	Fuel Burnup (MWD/MTM)	Fast Neutron Fluence (10^{20} n/cm^2)
Seed	0400736	Binary	L	7.9	36,990	54
		Binary	T	5.3	24,850	49
	0606773	Binary	L	3.7	17,300	33
		Binary	T	8.7	40,870	96
	0205071	Binary	T	11.0	51,580	75
	0507672	Binary	L	10.0	46,900	86
Standard Blanket	1606710	Binary	T	5.1	22,350	73
		Binary	L	4.3	18,910	58
	1208823	Thoria	T	2.3	10,180	51
	1105717	Thoria	T	3.1	13,750	71
		Binary	T	5.2	23,090	71
	1504272	Binary	T	4.3	19,130	64
Power Flattening Blanket	2610746	Binary	T	5.6	24,790	57
	2514164	Binary	T	5.1	22,320	39
	2607600	Binary	T	4.0	17,520	42
		Binary	L	5.5	24,290	59
Reflector	3102657	Thoria	T	0.1	280	4

L = Longitudinal to pellet axis
T = Transverse to pellet axis
MWD/MTM = Megawatt days per metric ton metal (uranium plus thorium)

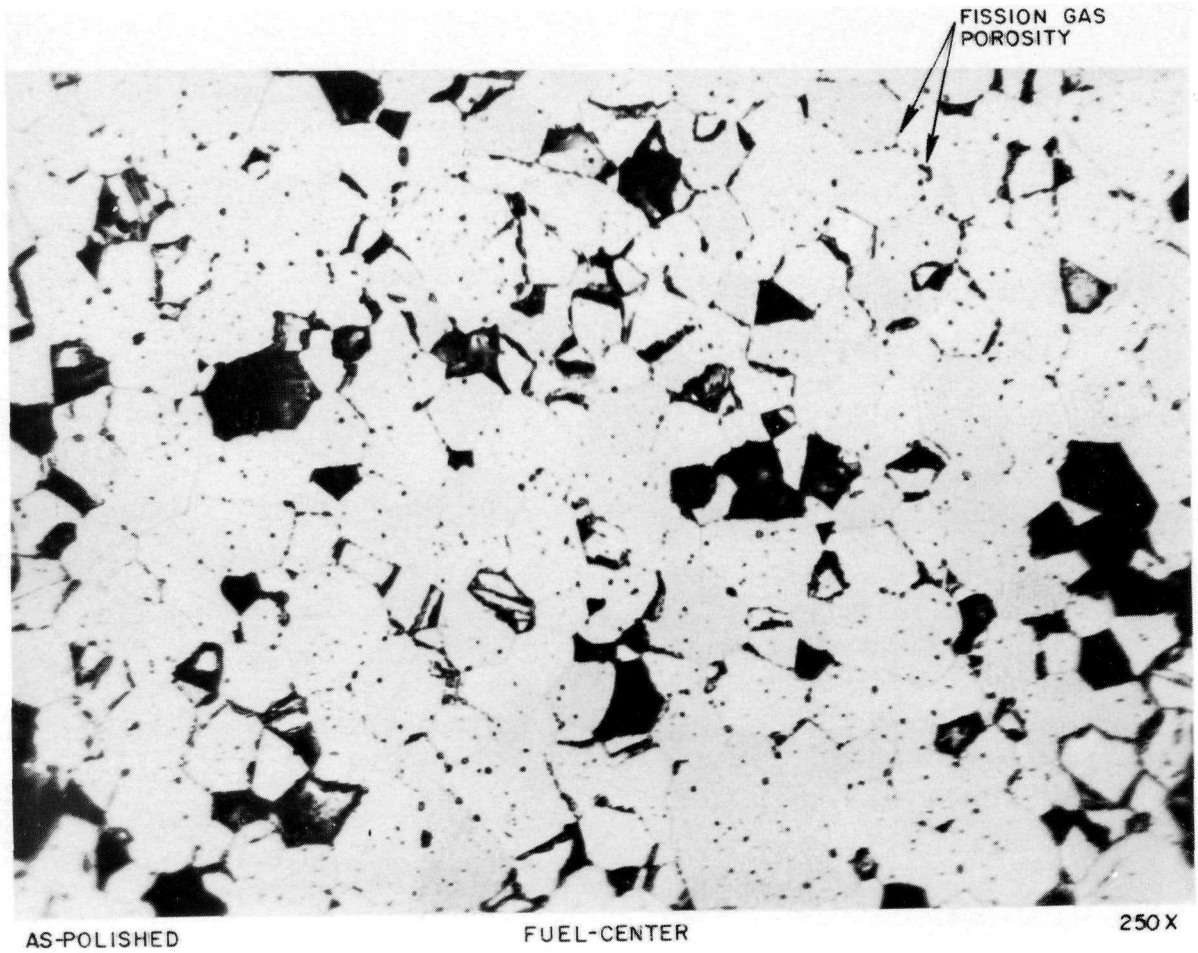

Figure 24. Increased Fuel Porosity (Fission Gas Bubbles) in Binary Fuel from Seed Rod 0606773 (96×10^{20} n/cm^2 Fast Fluence, 40,870 MWD/MT Burnup)

(11 x 10^{20} f/cc depletion) is shown in Figure 25. The micrograph reveals features typical of seed rods, such as a fuel-cladding gap and pellet cracks. From the 500X micrographs in Figure 26, however, it appears that fuel grain fragments, rather than whole grains, have been pulled out. The result was an unusual combination of porosity and partial grain pullout. This highly depleted fuel was also unusual in that white metallic inclusions were observed, primarily in the fuel cracks, as shown in Figure 27. The reason for these observations is not understood; further work, not planned as part of the present examination, would be required to explain these observations.

The amount of grain pullout was also greater at the pellet surface. In Figure 22 a 0.015-inch band at the pellet circumference showed increased grain pullout. A similar 0.030-inch band of increased grain pullout at the surface of the longitudinal section of a pellet from seed 0606773 resulted in a "picture frame" appearance (Figure 28). Grain size may have had an effect on this "picture frame" phenomenon since the grain size at the surface was smaller than throughout the remainder of the pellet cross sections. In this sense, the "picture frame" effect was the reverse of that occasionally noted during pellet fabrication development, in which the "picture frame" portion exhibited a larger, rather than smaller, grain size than the remainder of the pellet cross section.

No evidence of fuel bonding to the Zircaloy cladding I.D. was observed in the seed region. The cladding I.D. appeared to be unoxidized and without evidence of corrosion. A gap between fuel and cladding was observed in all examined seed fuel pellets. Fuel in the nonfreestanding blanket rods, however, was in contact with the cladding. This was expected in these nonfreestanding cladding rods, although cool-down of the rods to room temperature should have resulted in a small fuel-cladding gap because of the greater thermal contraction of the fuel.

4.2.1.3 - Blanket Binary Fuel

Binary fuel examined from the blanket region ranged from 17,520 MWD/MT to 24,790 MWD/MT burnup and 39 x 10^{20} n/cm^2 to 73 x 10^{20} n/cm^2 fast fluence.

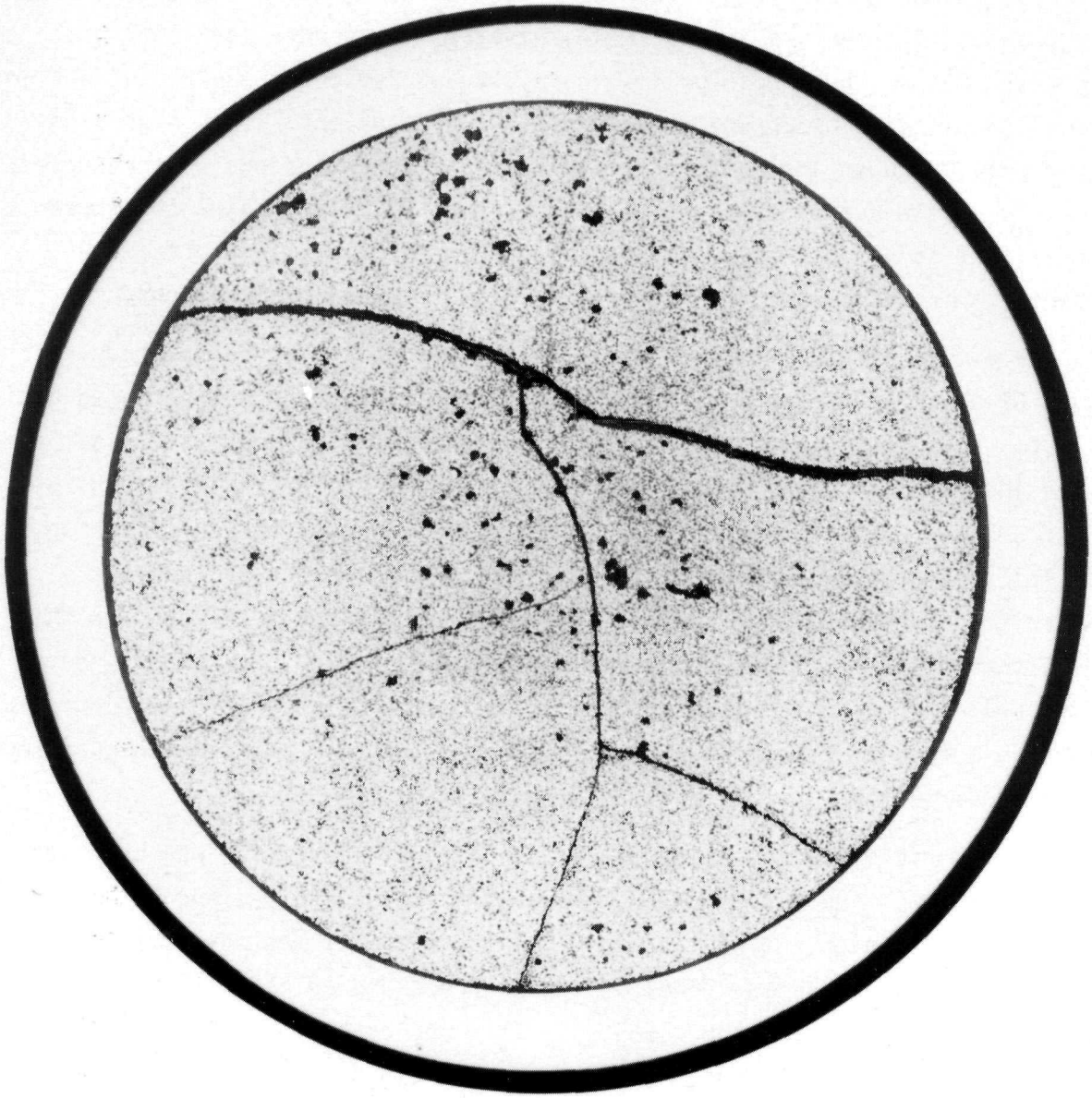

As-Polished 19.6X

Figure 25. Transverse Section Through the Highest Burnup Fuel Pellet Examined from Seed Rod 0205071 (75×10^{20} n/cm^2 Fast Fluence, 51,580 MWD/MT Burnup)

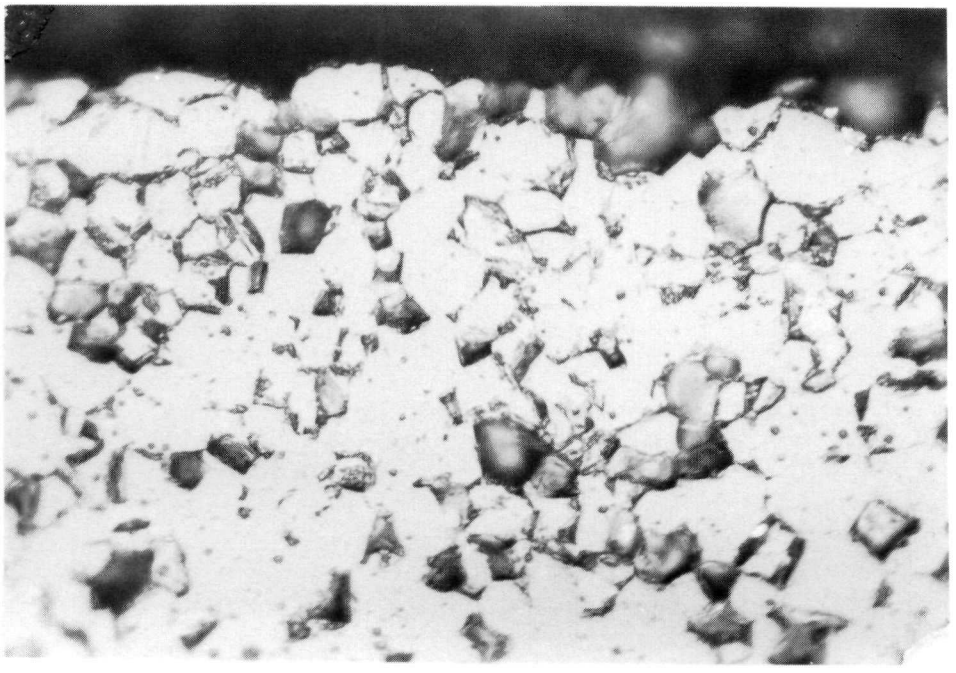

As-Polished Fuel-Edge 500X

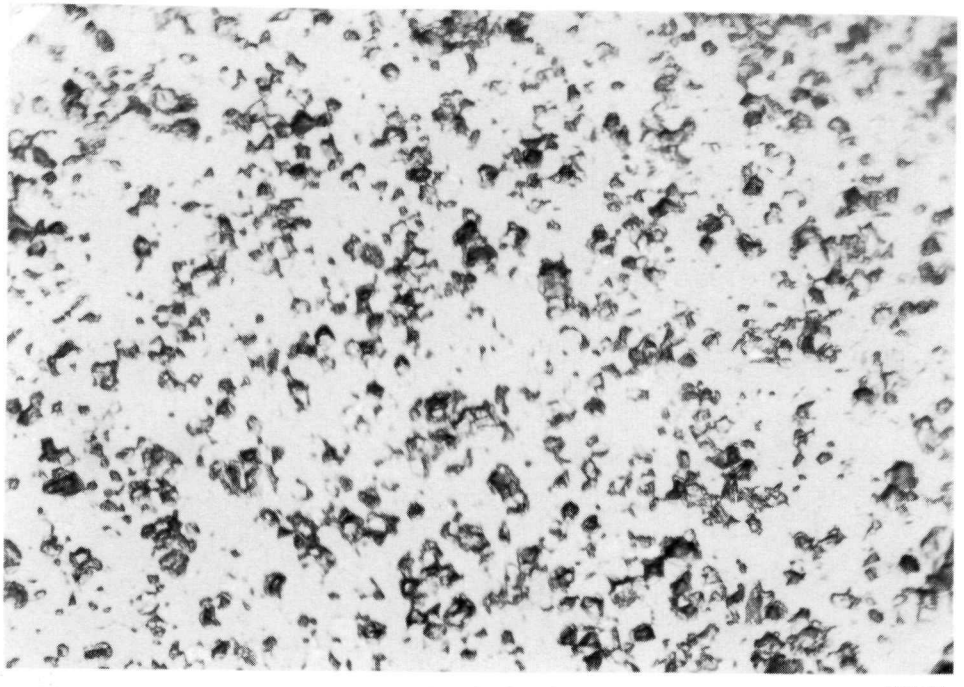

As-Polished Fuel-Center 500X

Figure 26. Unusual Appearance of Highly Depleted Binary Fuel from Seed Rod 0205071 (11×10^{20} f/cc Depletion, 51,580 MWD/MT Burnup)

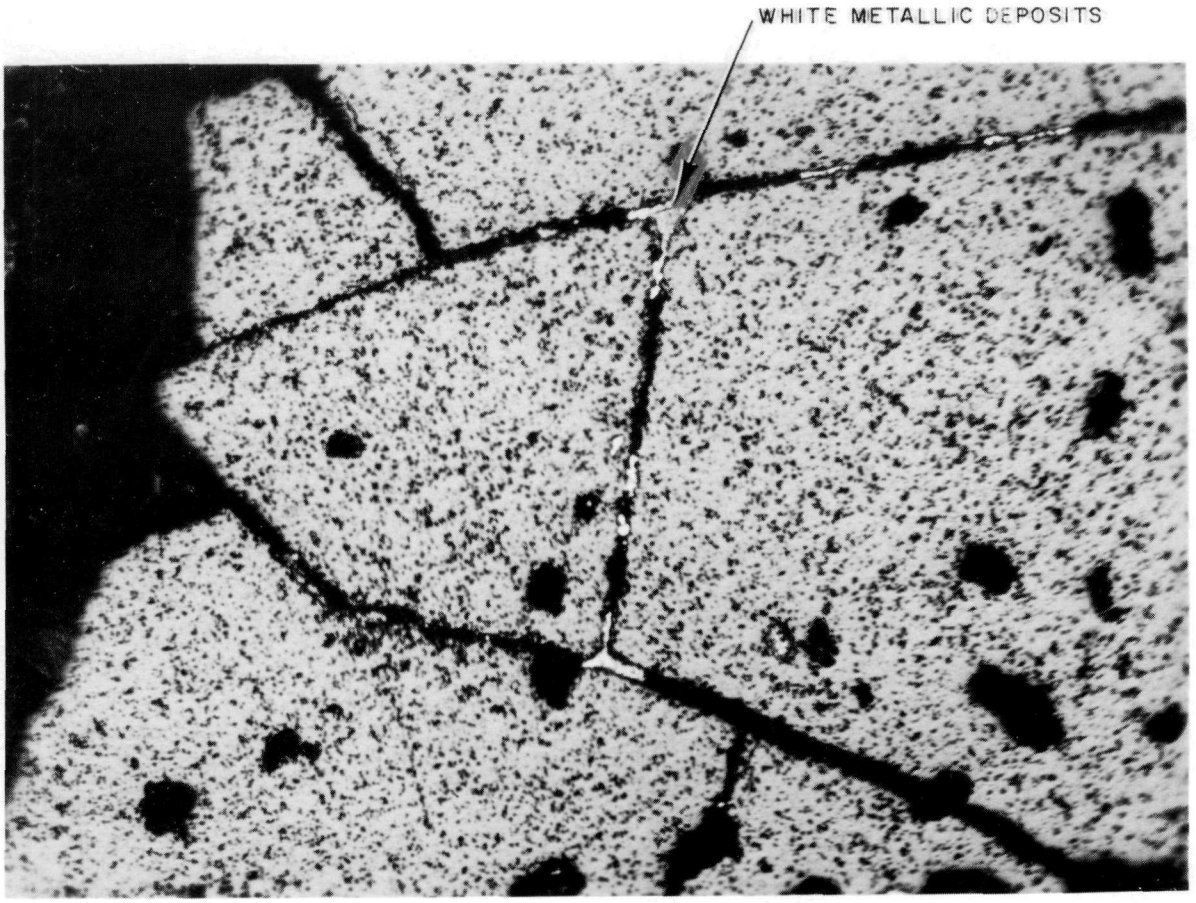

As-Polished 100X

Figure 27. Highly Depleted Binary Fuel from Seed Rod 0205071 Showing Metallic Inclusions (11×10^{20} f/cc Depletion, 51,580 MWD/MT Burnup)

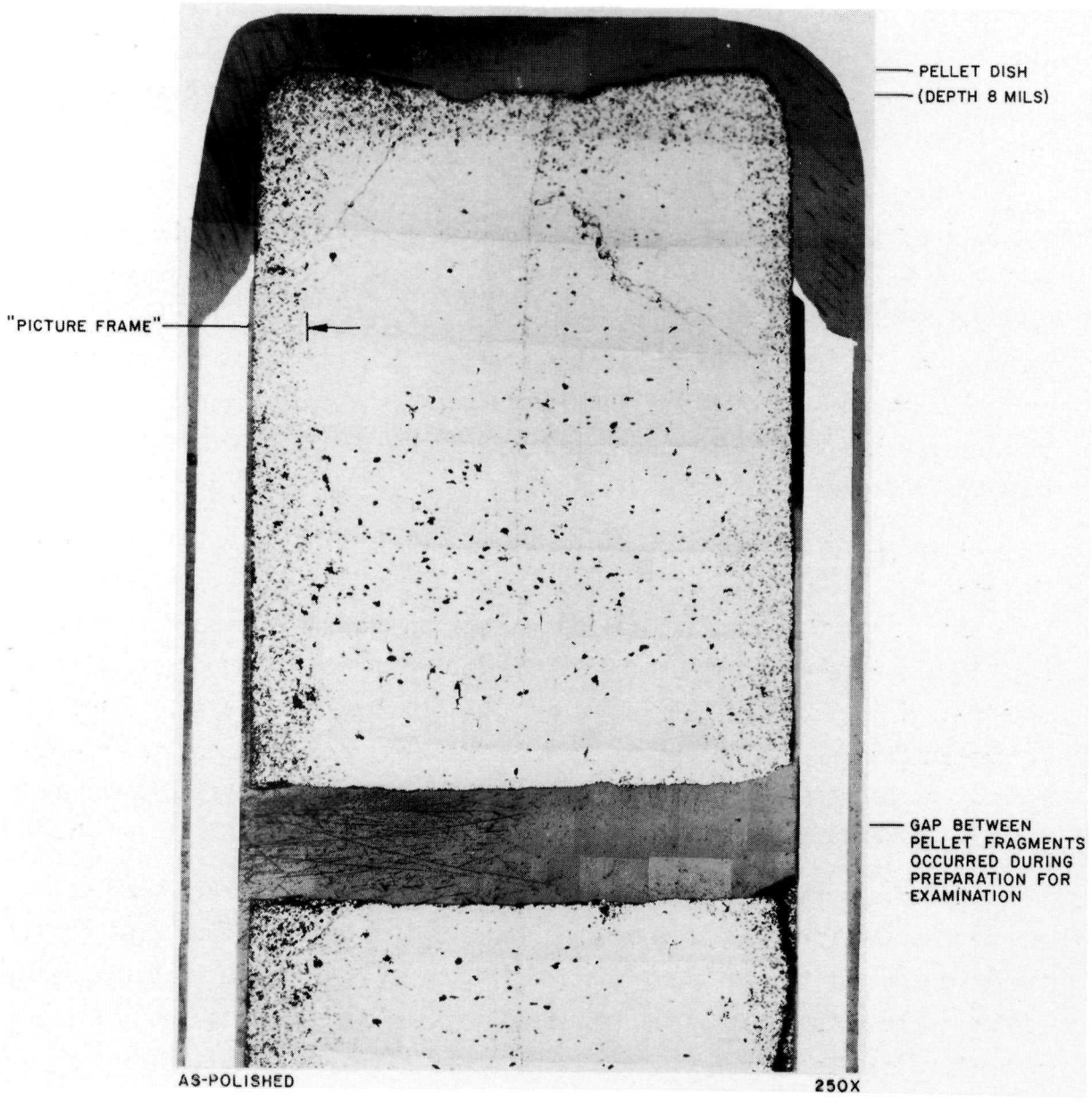

Figure 28. Longitudinal Section Through Binary Fuel Pellet from Seed Rod 0606773 (33×10^{20} n/cm^2 Fast Fluence, 17,300 MWD/MT Burnup)

At the lower end of the burnup and fast fluence ranges examined, both small size "micropores" and larger size "macropores" were visible, as shown in Figure 29 for rod 2607600. The pores appeared to be equally distributed intergranularly and intragranularly.

At higher burnup and the highest fast fluence examined in the blanket region (rod 1606710), the pore size appeared to be larger and to be concentrated at the grain boundaries (Figure 30). Some pores were large enough to make it difficult to distinguish between pores and grain pullout. At intermediate levels (19,130 MWD/MT burnup and 64 x 10^{20} n/cm^2 fast fluence), the porosity appeared to be principally located at the grain boundaries, but was smaller in size than at higher levels of fluence and burnup, as shown for rod 1504272 in Figure 31.

All binary fuel examined exhibited pellet cracks, as noted in Figures 32 through 34. The pellet cracks were primarily radial across the pellet diameter. From the longitudinal cross section through the pellets (Figure 32), it was observed that cracks existed both in transverse planes across the section and in longitudinal planes parallel to the pellet axis. (Some of the larger cracks are considered to be artifacts of metallographic mount preparation.) At higher magnification, some of the narrower cracks appeared to be intragranular in nature, as shown in Figure 35 for rods 1105717 and 2610746.

Photomicrographs of several rods showed regions of darker shading surrounding pellet cracks, as shown in Figure 36 for rod 2607600. Inspection of these regions at higher magnification (Figure 37) indicated that the darker regions were a combination of increased fission gas porosity and small grain pullout. The reason for the increases observed is not known.

The absence of a gap between cladding I.D. and fuel pellet O.D. in all blanket fuel, both binary and thoria, is clearly observed in the 250X photomicrographs of this region, shown in Figures 29 through 31. Contact between the cladding and the fuel in blanket and reflector rods was expected, since these rods were designed to be nonfreestanding.

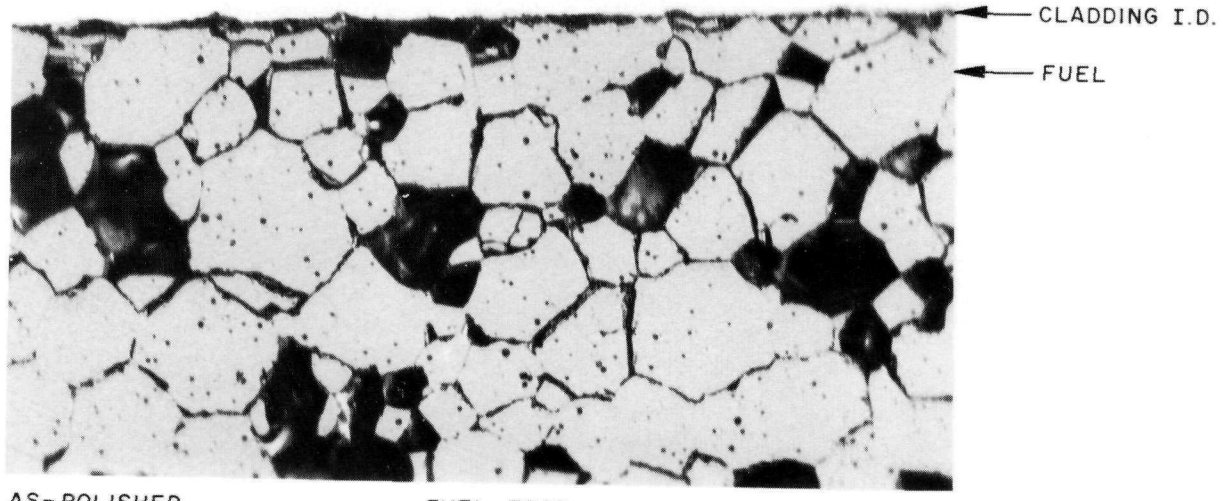

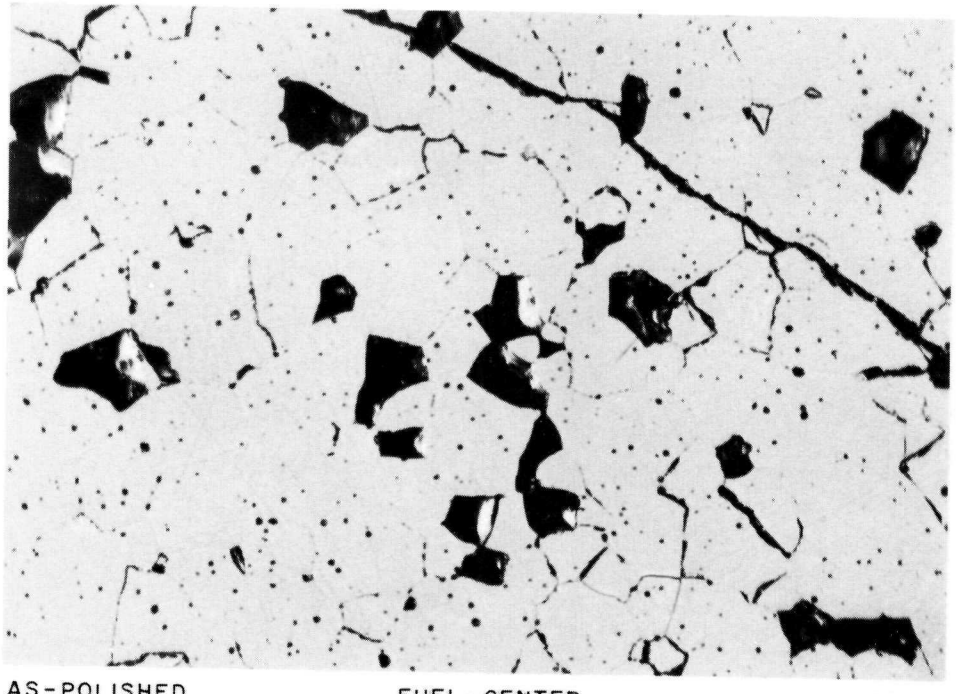

Figure 29. Binary Fuel at End of Life from Power Flattening Blanket Rod 2607600 (42×10^{20} n/cm^2 Fast Fluence, 17,520 MWD/MT Burnup)

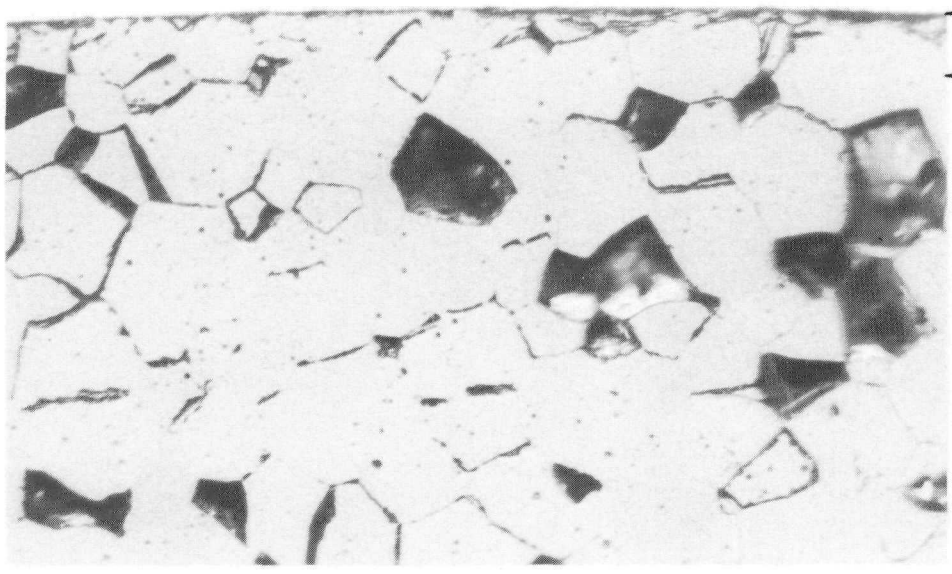

AS-POLISHED FUEL-EDGE 250 X

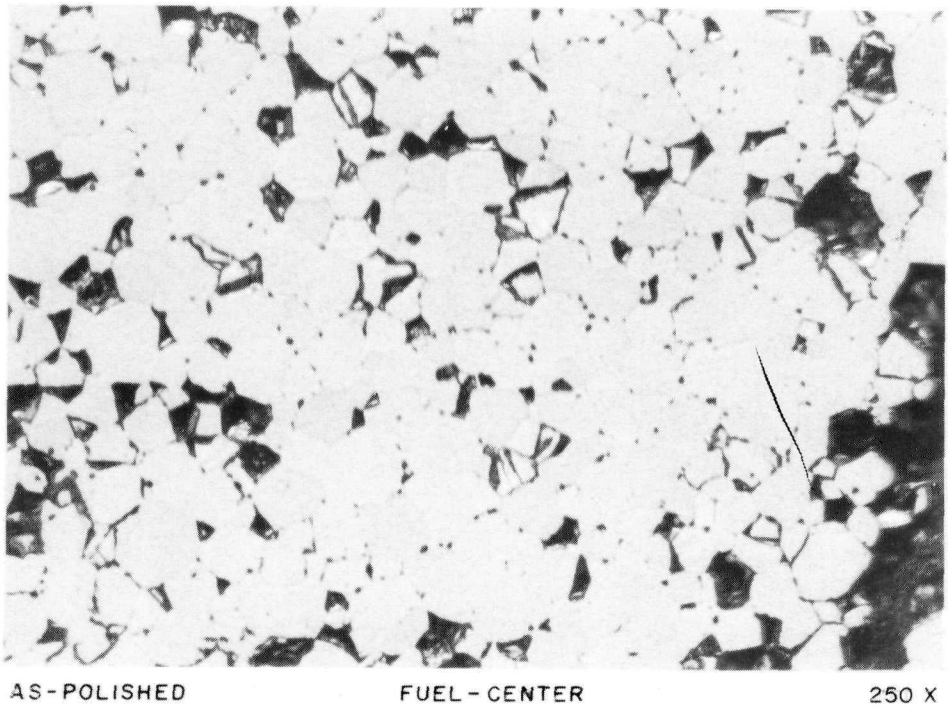

AS-POLISHED FUEL-CENTER 250 X

Figure 30. Binary Fuel at End of Life from Standard Blanket Rod 1606710 (73×10^{20} n/cm^2 Fast Fluence, 22,350 MWD/MT Burnup)

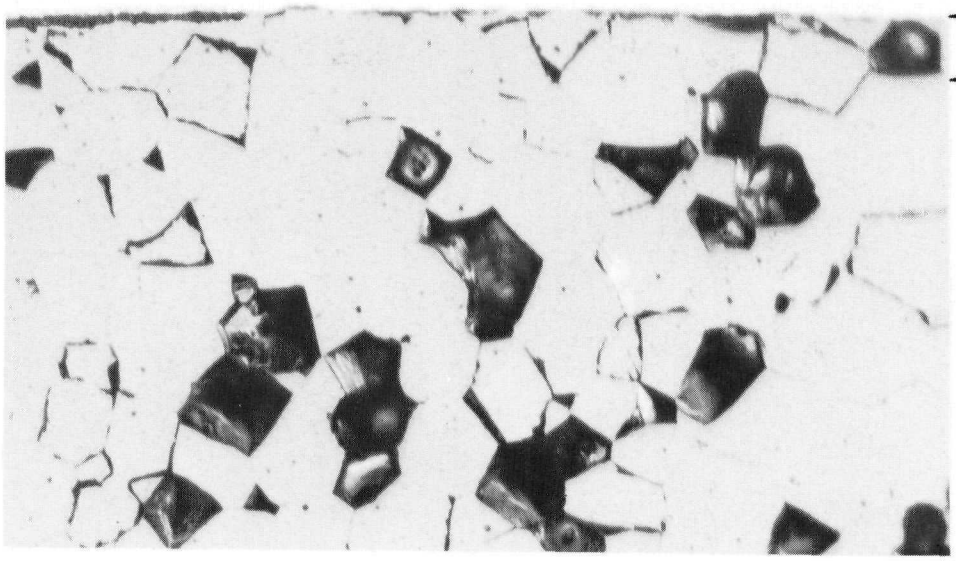

AS-POLISHED FUEL-EDGE 250 X

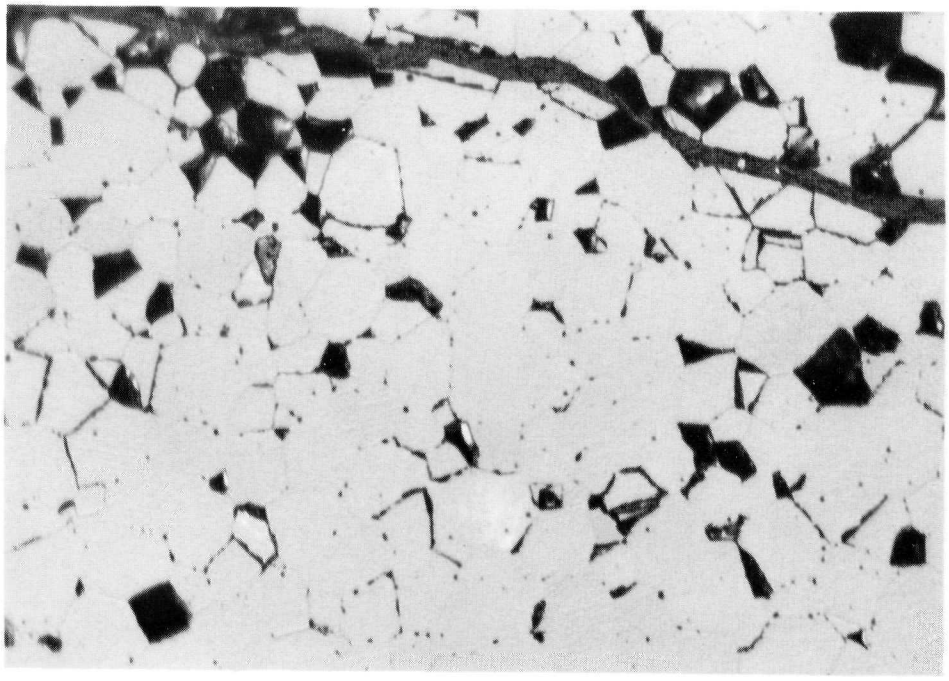

AS-POLISHED FUEL-CENTER 250 X

Figure 31. Binary Fuel at End of Life from Standard Blanket Rod 1504272 (64×10^{20} n/cm^2 Fast Fluence, 19,130 MWD/MT Burnup)

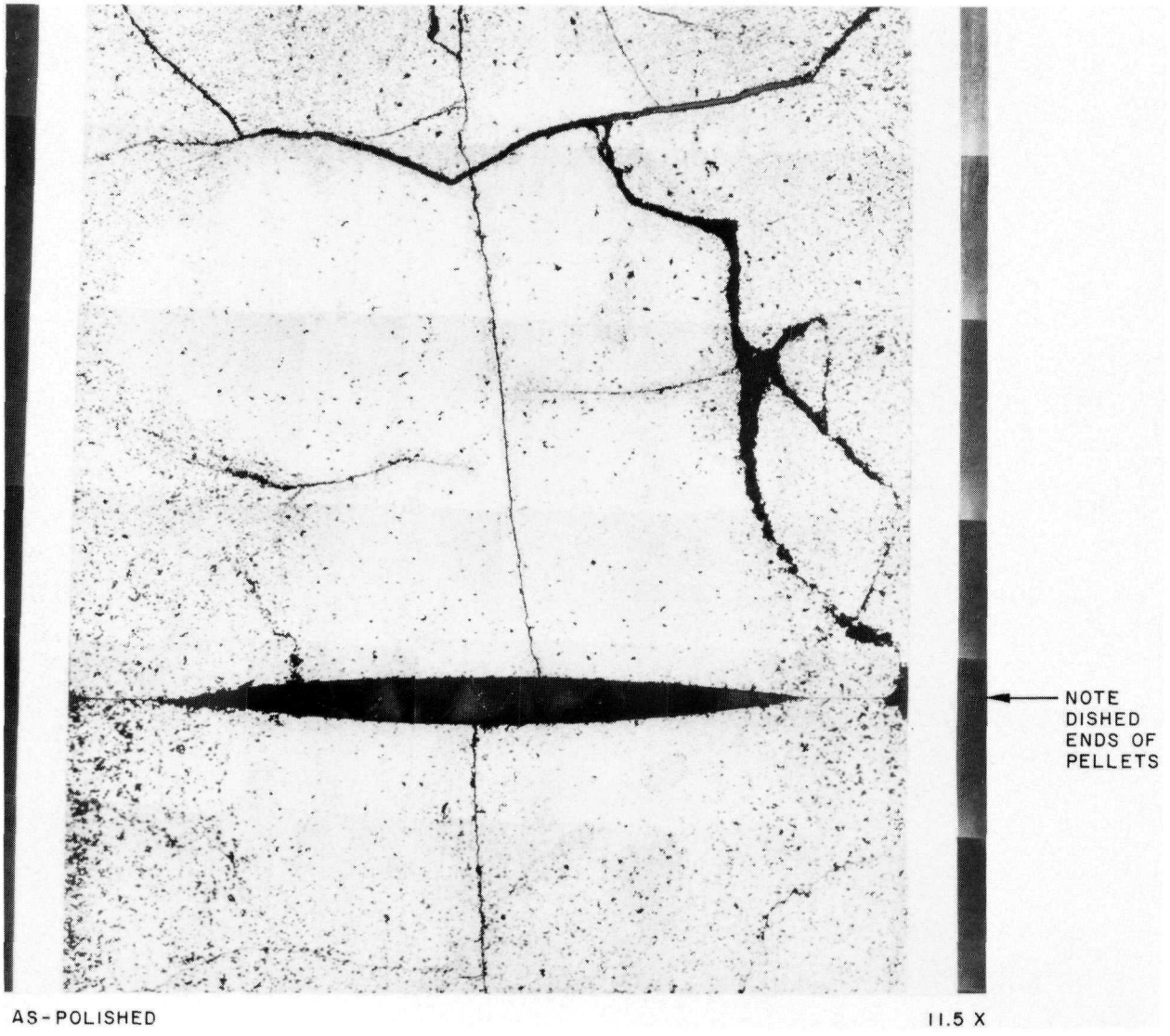

Figure 32. Longitudinal Section Through Pellet-Pellet Interface in Power Flattening Blanket Rod 2607600 (42×10^{20} n/cm^2 Fast Fluence, 17,520 MWD/MT Burnup)

As-Polished 10.5X

Figure 33. Transverse Section Through Standard Blanket Rod 1504272 (64×10^{20} n/cm^2 Fast Fluence, 19,130 MWD/MT Burnup)

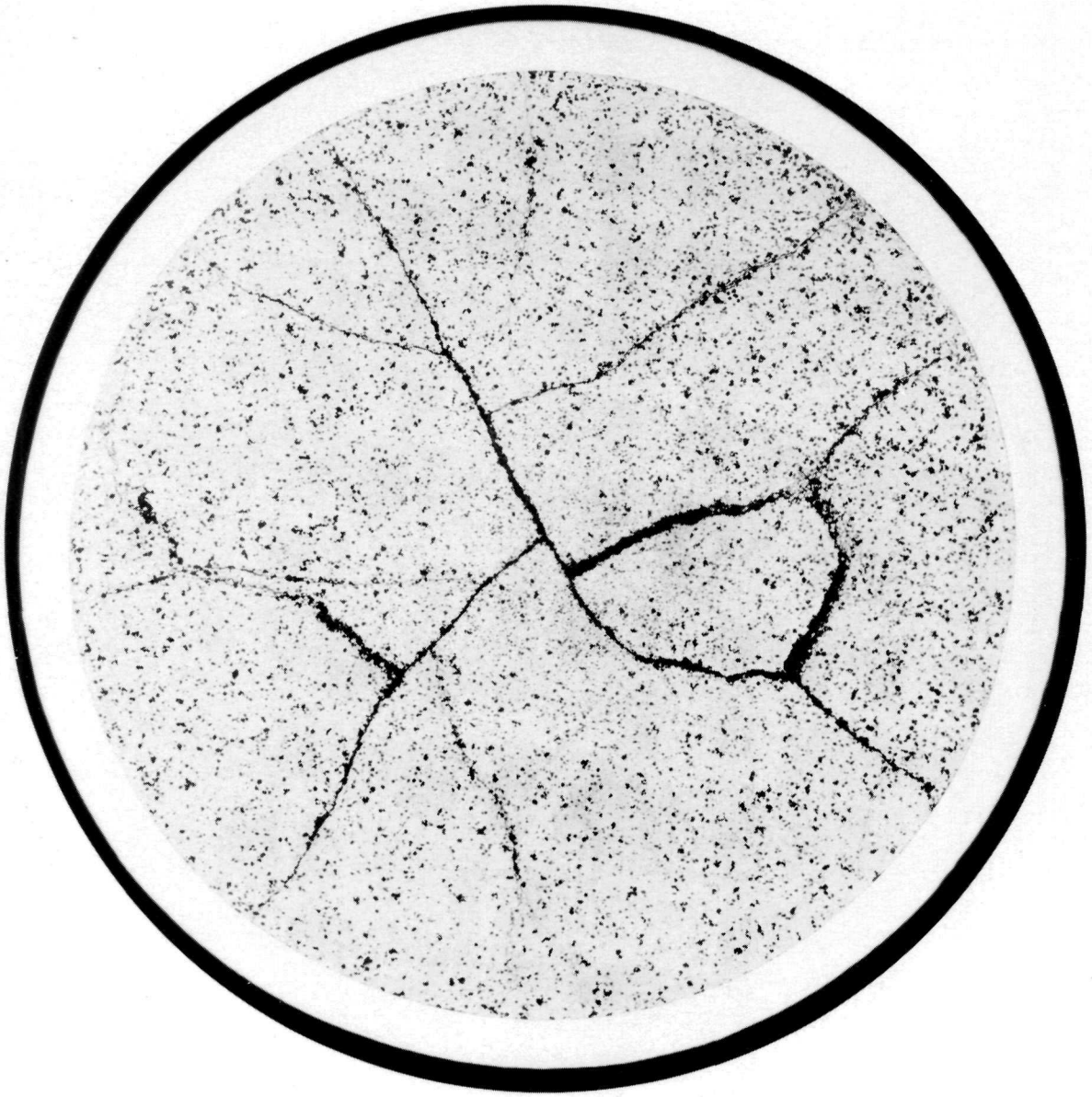

As-Polished 10.5X

Figure 34. Transverse Section Through Binary Fuel from Standard Blanket Rod 1606710 (73×10^{20} n/cm^2 Fast Fluence, 22,350 MWD/MT Burnup)

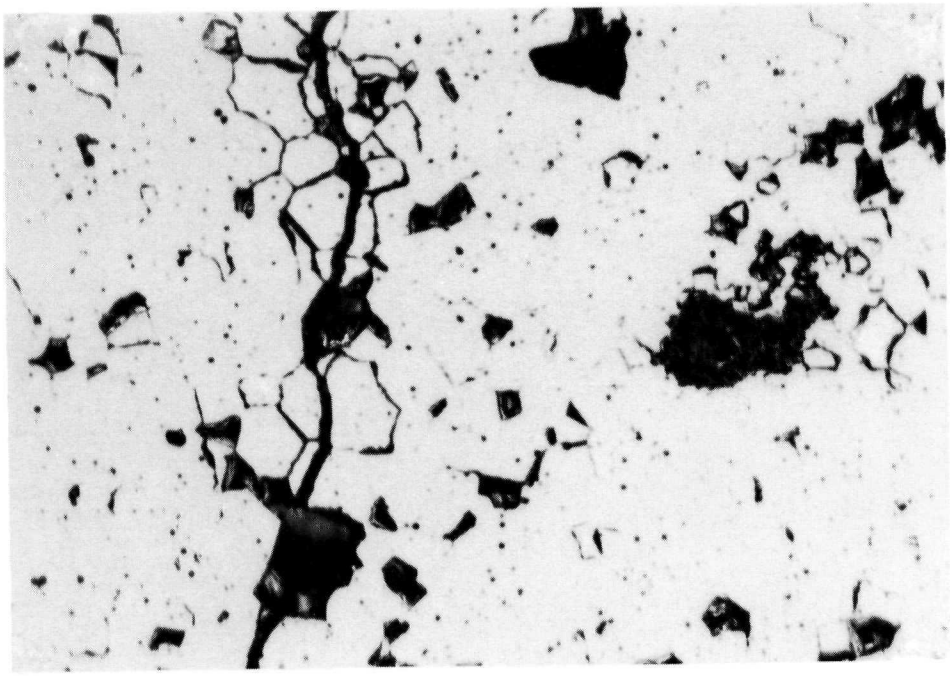

As-Polished Fuel-Center 250X
Rod 2610746 (57 x 10^{20} n/cm^2 Fast Fluence)
(24,790 MWD/MT Burnup)

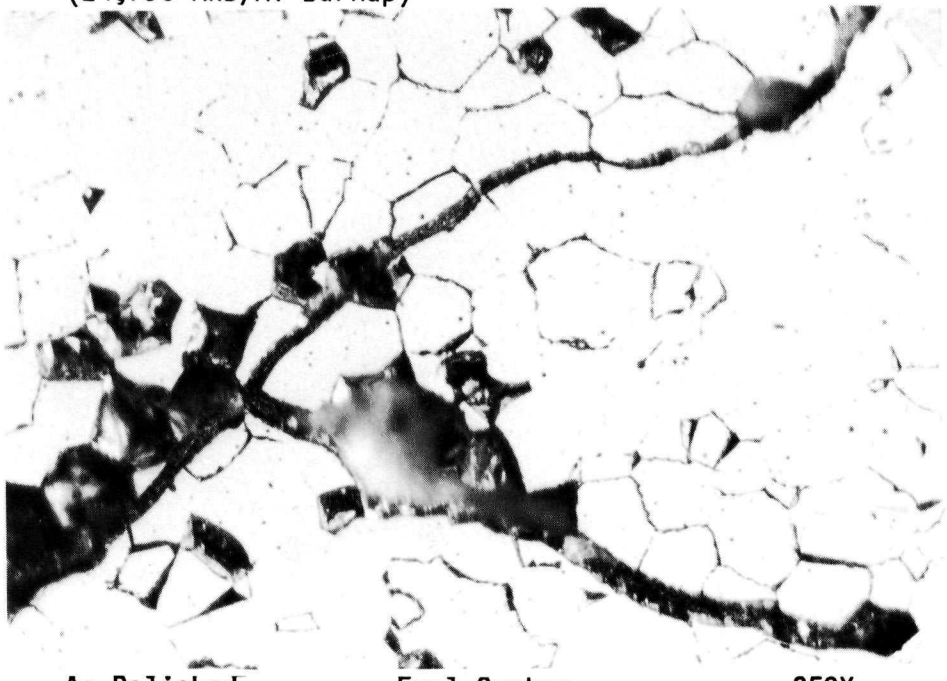

As-Polished Fuel-Center 250X
Rod 1105717 (71 x 10^{20} n/cm^2 Fast Fluence)
(23,090 MWD/MT Burnup)

Figure 35. Intragranular Cracks Through Binary Blanket Fuel Rods at End of Life

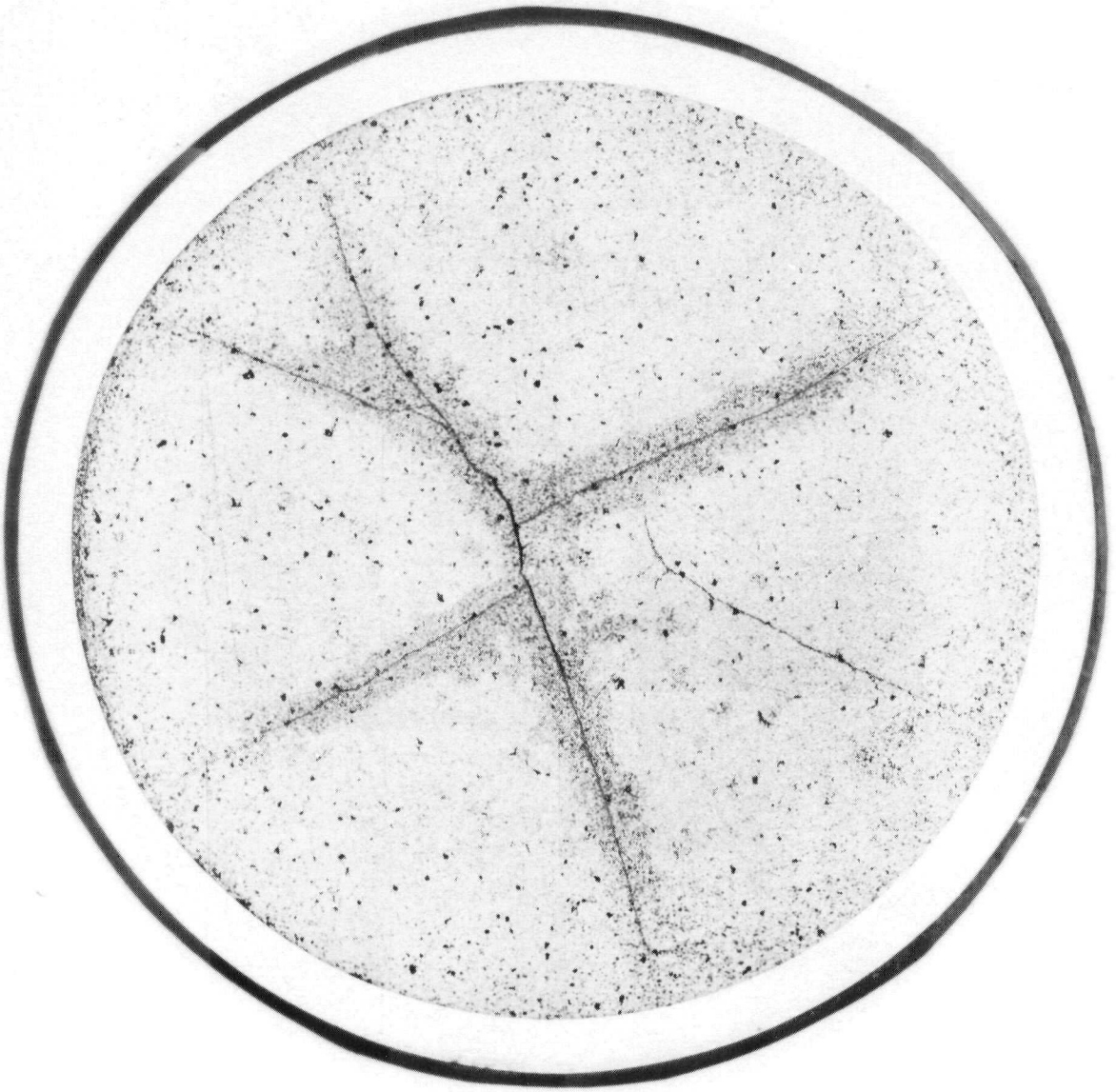

As-Polished 10.5X

Figure 36. Transverse Section Through Binary Fuel from Power Flattening Blanket Rod 2607600 (59×10^{20} n/cm^2 Fast Fluence, 24,290 MWD/MT Burnup)

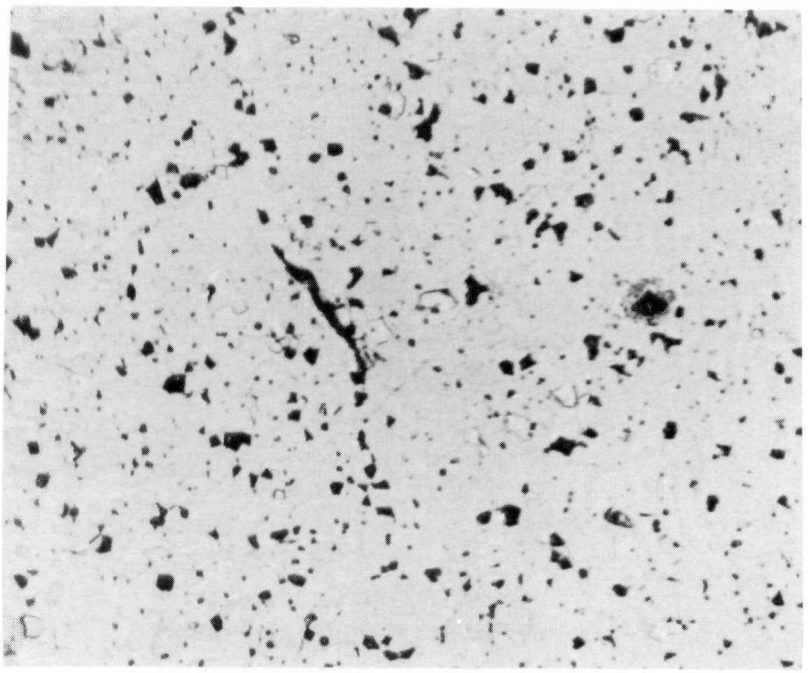

As-Polished 250X
Fuel Away from Pellet Cracks

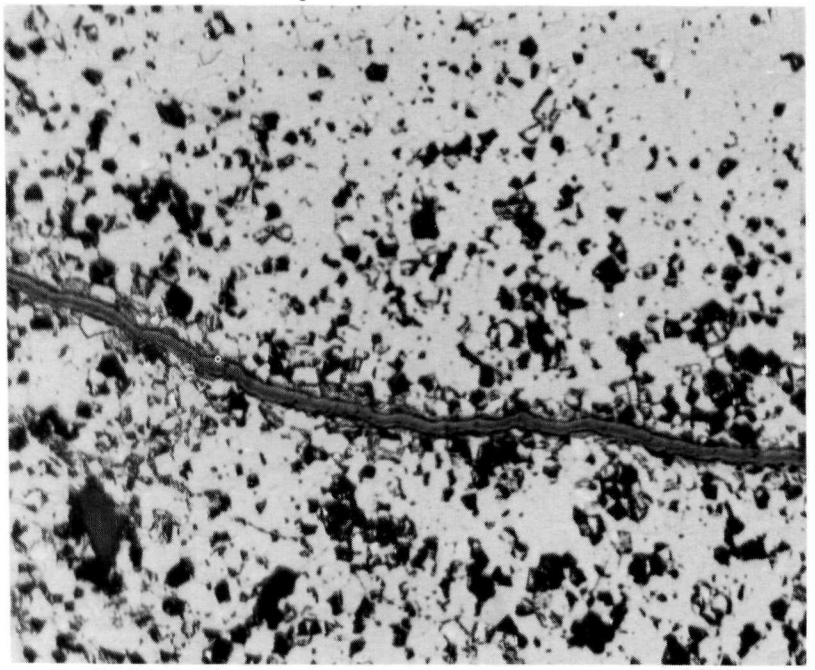

As-Polished 250X
Fuel at Pellet Cracks

Figure 37. Binary Fuel from Power Flattening Blanket Rod 2607600 Showing Increased Porosity and Grain Pullout in Areas Surrounding Pellet Cracks (59×10^{20} n/cm^2 Fast Fluence, 24,290 MWD/MT Burnup)

A general correlation between fuel grain size and fluence or burnup levels was noted for binary fuel in the blanket region. (The correlation with fluence appeared to be better than with burnup.) As shown in Table 8 and in Figure 38, fuel grain size at lower fluence tended to be smaller than fuel at higher fluence. The correlation in binary fuel in the seed region was less distinct, as shown in Figure 39.

Also, from Figure 38, the grain size at the edge of binary fuel in the blanket fuel rods was larger by approximately 50 percent than the fuel at the pellet center. This observation was the reverse of that for seed fuel in which the smaller grain size fuel was located at the pellet edge (Figure 39).

Grain growth in the fuel is governed by temperature, time, and a characteristic activation energy (Reference (16)). High fuel temperatures are needed for grain growth. The peak power density of 8.9 Kw/ft in the LWBR core rods (8.7 Kw/ft for the 12 DE rods) was not high enough to cause high fuel temperatures. In addition, the very low levels (less than 0.2 percent) of released fission gas provides further evidence that LWBR fuel operated at relatively low temperatures (below the 2580°F threshold level where increased fission gas is released). Grain growth at these low fuel temperatures would not be expected in LWBR fuel elements. Lack of significant grain growth was confirmed in the micrographs shown in Figures 24, 29 through 31 and in Table 8. Grain size measured at end of life was within one ASTM number of the as-fabricated limits of ASTM 4 (90 microns) for binary fuel and ASTM 3 (127 microns) for thoria fuel.

4.2.1.4 - Mechanical Stability

Mechanical stability of the fuel was exceptional. Neutron radiographs of all 12 DE rods revealed no closure of the dishes at pellet ends. The 0.008-inch depth of the end dish in seed pellet 0606773 (Figure 28) is within the as-built specification of 0.009 ±0.003 inch.

Note also from Figure 32 that pellet dishes at the pellet-pellet interface are clearly visible. The gap between pellet ends measured approximately 0.028 inch, indicating an endface dish depth of 0.014 inch for each pellet. Since the fabrication limit on pellet endface dish depth, given in Table 3,

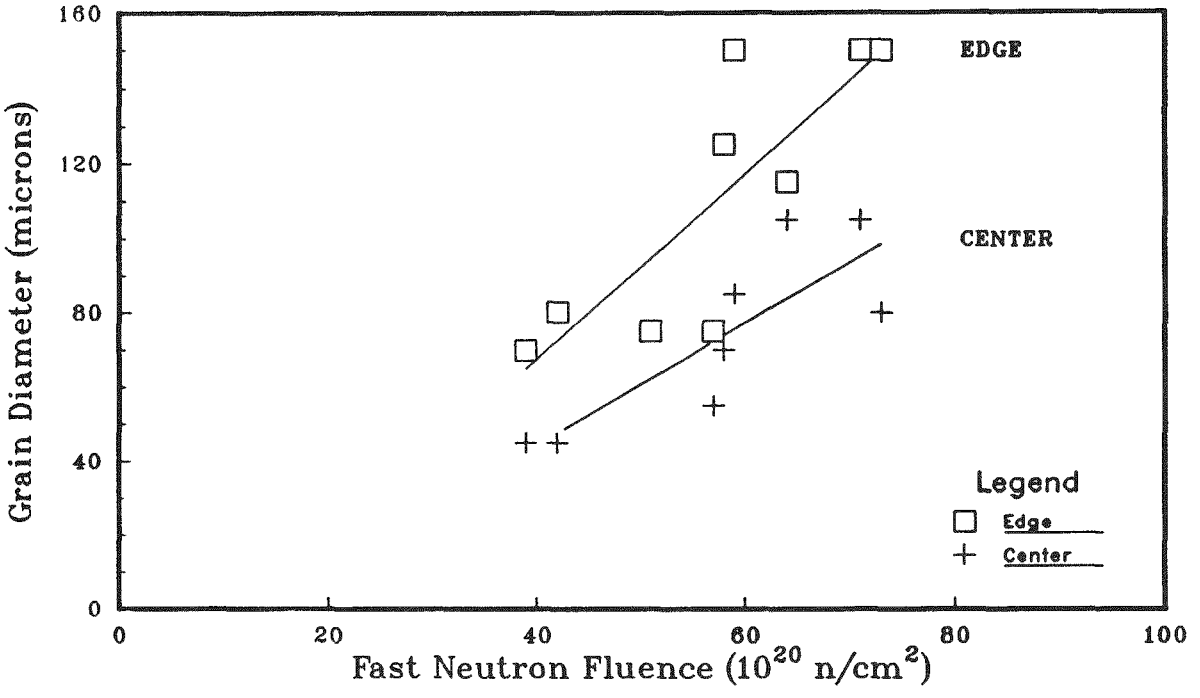

Figure 38. Blanket Fuel Grain Size at End of Life

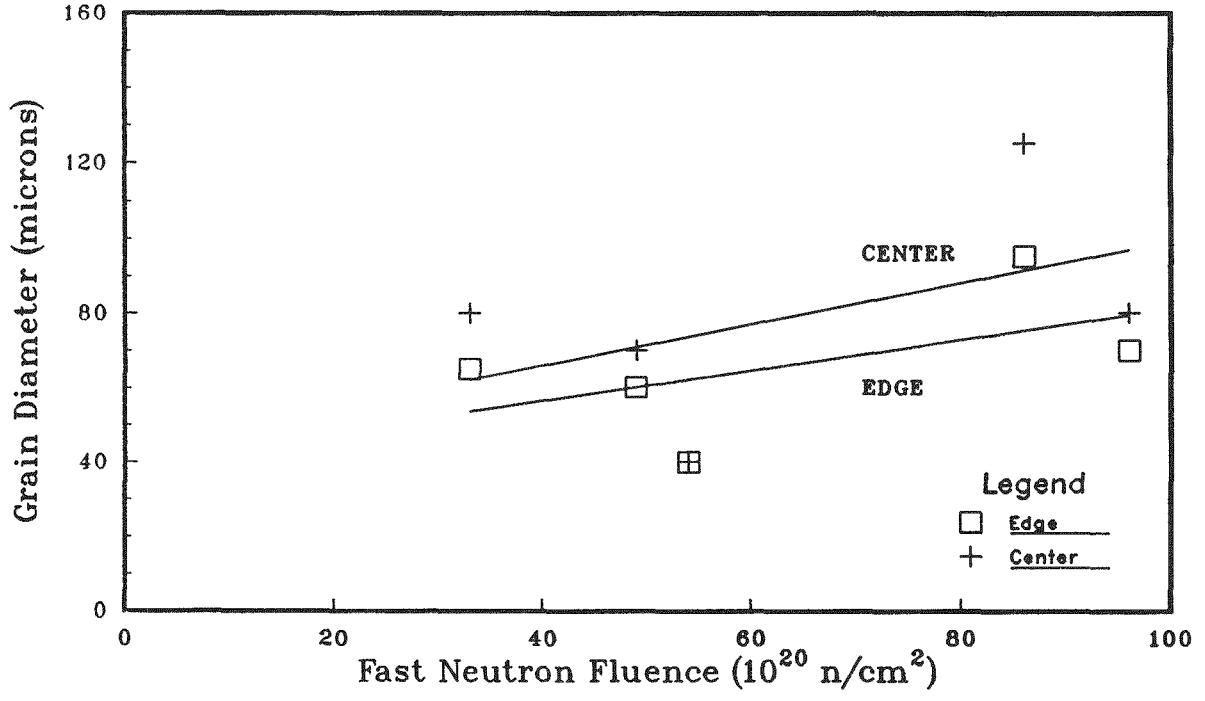

Figure 39. Seed Fuel Grain Size at End of Life

was 0.014 ±0.004 inch for blanket binary fuel, no change occurred from as-fabricated conditions. Significant axial fuel swelling into the pellet end-face dishes, therefore, did not occur.

The extensive chipping and cracking observed in some pellets from irradiation test rods were not present in the examined core rods. Some fuel cracks, both transverse and circumferential were present (Figures 21 and 22); however, the cracks did not lead to breakup of the fuel pellets and no chips were observed.

4.2.2 - Cladding Behavior

Performance of both the recrystallization annealed seed cladding and the stress relief annealed blanket and reflector cladding throughout core life was excellent. No condition indicative of a cladding defect was observed for the 12 DE rods. If present, through-cladding defects would be detected during water chemistry checks by the presence of fission products, during detailed visual examination of the rod surface by the presence of unusual water patterns around the defect, such as streamers downstream of the defect, or during metallographic examination by the presence of cracks or through-holes in the cladding. No such condition was found.

Although the balance of the 17,290 fuel rods in the LWBR core was not examined individually, a defected rod condition would be detected by the presence of fission products in the water coolant chemistry checks during core operations or water pit storage. Fission product chemistry checks were consistently within limits, indicating there were no cladding defects.

In addition, during preparation of the fuel modules for long-term storage, each module was individually placed into a storage liner. Water was removed from the liner, the liner was purged with an inert gas during the drying period, and the purged gas was analyzed for the presence of fission products. Of the 48 liners containing irradiated fuel from the LWBR core, only two gave indication of possible defected fuel rods (seed III-5 and seed III-6). Information concerning these two modules was inconclusive as to whether actual fuel rod cladding defects existed. The possibility of defected fuel rods is discussed in Reference (17).

4.2.2.1 - Cladding Oxide

Typically, the cladding had an essentially unbroken oxide layer on the O.D. surface (Figure 40) but no oxide on the I.D. surface (Figures 29 through 31). Oxide thickness around the cladding circumference, however, could vary by several tenths of a mil. The maximum oxide thickness observed metallographically for each cladding sample is listed in Table 10. Thickness of the oxide ranged from approximately 0.05 mil for cladding with the thinnest oxide layer (over a thoria fuel pellet (Figure 41, top) to 1.75 mils for cladding with the thickest oxide layer (over a blanket binary fuel pellet, Figure 41, bottom). On occasion, the oxide layer had small locally decreased thickness spots, or the oxide thickness was irregular and wavy (Figure 42). Erosion of the cladding surfaces, both outer and inner, was not observed.

A correlation between fast neutron fluence and cladding oxide thickness was observed. The correlation differed for RXA (seed) cladding and SRA (blanket and reflector) cladding. For the highest fast fluence RXA cladding section evaluated metallographically (seed rod 0606773 having a fast fluence calculated at 96×10^{20} n/cm^2), the O.D. oxide thickness measured 1.0 mil. At fluence levels approximately half this amount, the cladding O.D. oxide thickness was 0.35 to 0.5 mil. The fast fluence and cladding oxide thickness correlation for RXA cladding is shown in the lower curve in Figure 43.

For SRA cladding over binary fuel in the blanket region, the correlation between neutron fluence and cladding O.D. oxide thickness is presented in the upper curve in Figure 43. The maximum SRA cladding oxide thickness of 1.75 mils was observed at the peak fluence location for the examined blanket samples. At low fast fluence levels, below about 40×10^{20} n/cm^2, oxide thicknesses for both RXA and SRA cladding were comparable. At higher fluence levels, the observation that the oxide thickness for SRA cladding for these LWBR fuel rods is greater than the oxide thickness for RXA cladding is in agreement with earlier studies, Reference (18).

The maximum measured oxide thicknesses for these rods using the EDCOT (Eddy Current Oxide Thickness) nondestructive technique at ECF are shown in

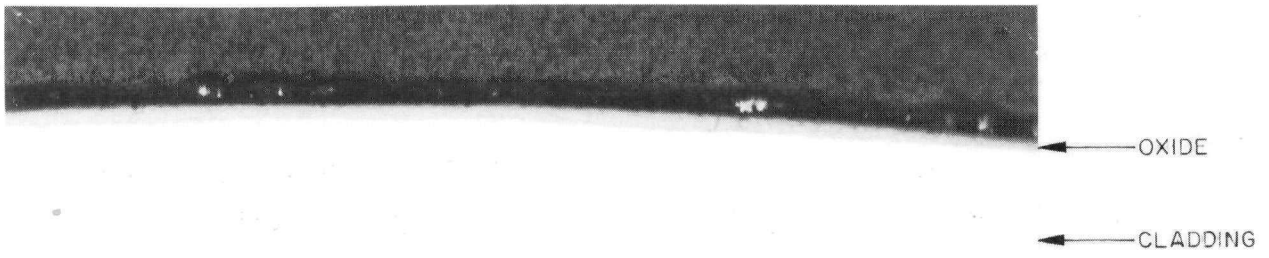

AS-POLISHED SEED ROD 0205071 250 X

(75 X 10^{20} n/cm^2 FAST FLUENCE, 0.4 mil OXIDE THICKNESS)

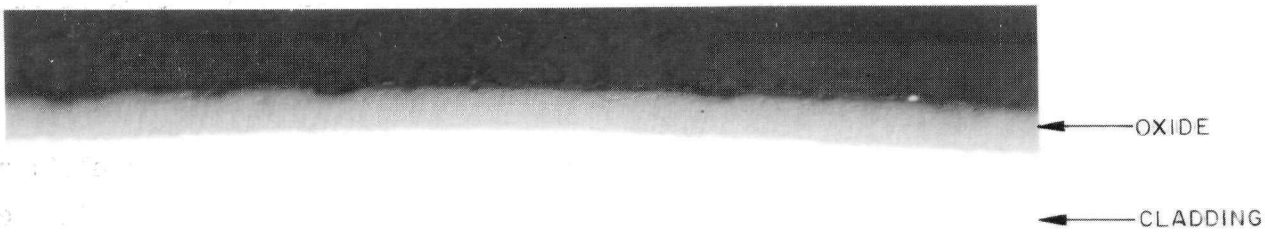

AS-POLISHED SEED ROD 0606773 250 X

(96 X 10^{20} n/cm^2 FAST FLUENCE, 1 mil OXIDE THICKNESS)

Figure 40. Typical Uniform Oxide Layer on RXA Cladding Waterside Surface

Table 10 - LWBR Zircaloy-4 Cladding Oxide Thickness at End of Life

Type Fuel	Orientation	Rod S/N	Fast Neutron Fluence 10^{20} n/cm^2	Maximum Observed Oxide Thickness (mils)		Minimum Observed Oxide Thickness (mils)	
				MET	EDCOT*	MET	EDCOT*
RXA Cladding							
Binary	L	0606773	33	0.40	1.56	0.30	1.37
Binary	T	0400736	49	0.35	1.46	N/M	1.17
Binary	L	0400736	54	0.50	1.46	0.25	1.17
Binary	T	0205071	75	0.50	0.84	0.30	0.67
Binary	T	0507672	86	0.80	1.36	0.70	1.12
Binary	T	0606773	96	1.00	1.56	0.95	1.37
SRA Cladding							
Binary	T	1504272	11	0.30	1.30	0.10	0.84
Binary	T	2514164	39	0.40	0.60	0.10	0.40
Binary	L	2607600	42	0.50	0.95	0.10	0.85
Binary	T	2610746	57	1.10	1.20	0.85	1.10
Binary	L	1606710	58	0.60	1.95	0.30	1.05
Binary	T	2607600	59	0.95	0.95	0.80	0.85
Binary	T	1105717	71	0.45	1.50	0.15	0.70
Binary	T	1606710	73	1.75	1.95	1.00	1.05
Thoria	T	3102657	4	0.25	0.75	0.05	0.50
Thoria	T	1208823	51	0.05	0.75	0.05	0.50
Thoria	T	1105717	71	0.45	1.50	0.15	0.70

*Reference (3)
L = Longitudinal section through cladding
T = Transverse section through cladding
N/M = Not Measured

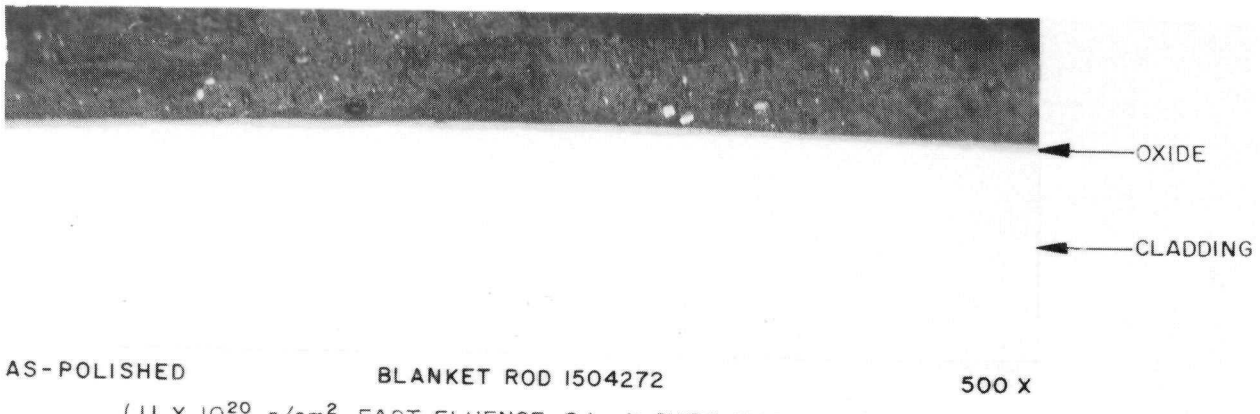

AS-POLISHED BLANKET ROD 1504272 500 X

(11 X 10^{20} n/cm^2 FAST FLUENCE, 0.1 mil OXIDE THICKNESS)

AS-POLISHED BLANKET ROD 2607600 500 X

(59 X 10^{20} n/cm^2 FAST FLUENCE, 0.95 mil THICKNESS)

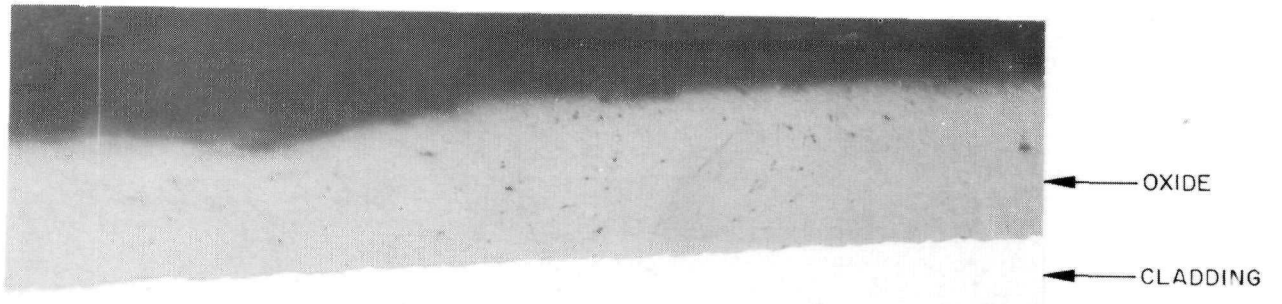

AS-POLISHED BLANKET ROD 1606710 500 X

(73 X 10^{20} n/cm^2 FAST FLUENCE, 1.75 mil THICKNESS)

Figure 41. Typical O.D. Oxide Layer on SRA Cladding

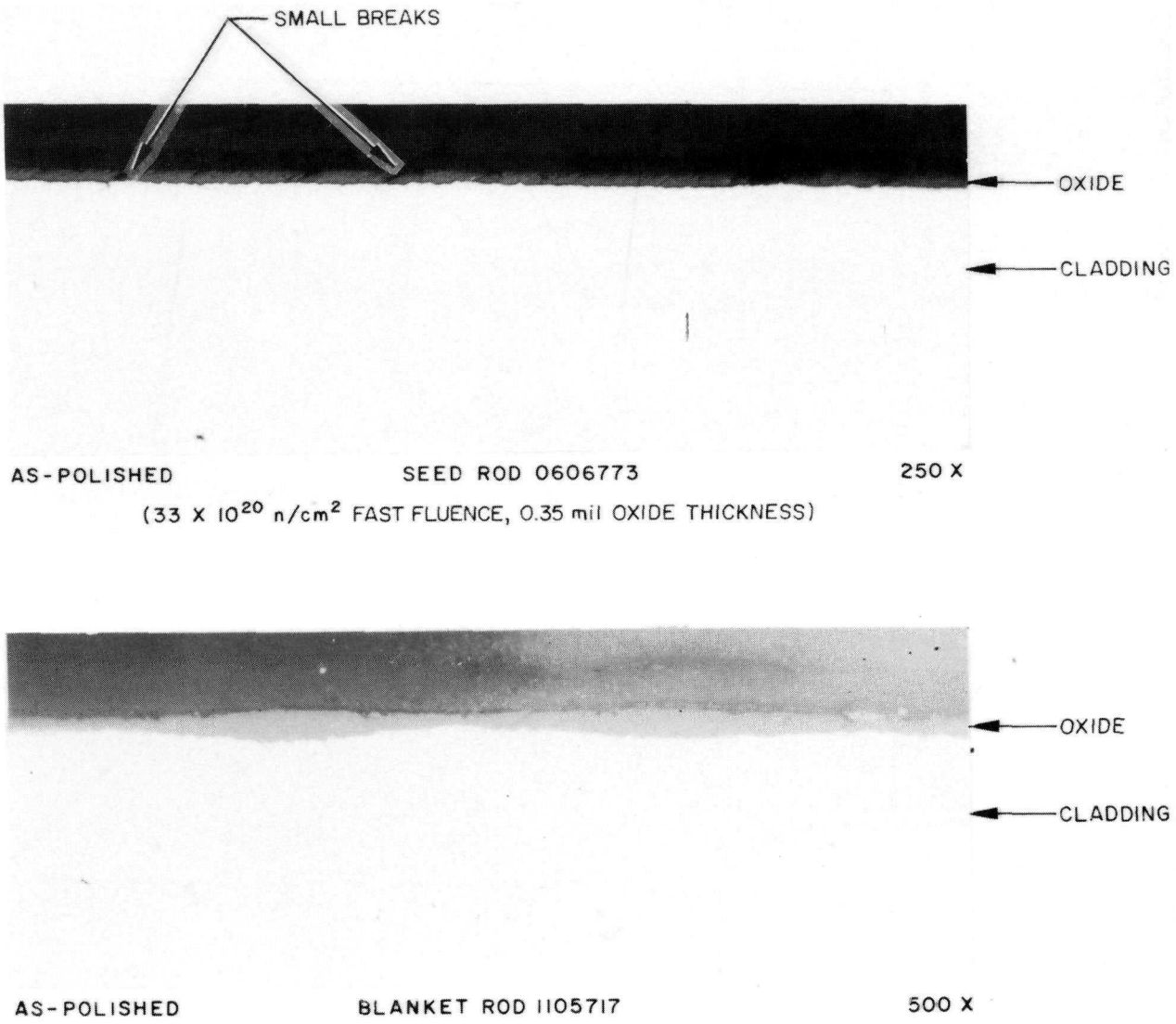

Figure 42. Cladding Oxide Layer (Waterside with Small Breaks (top) and Irregular (Wavy) Thickness (bottom)

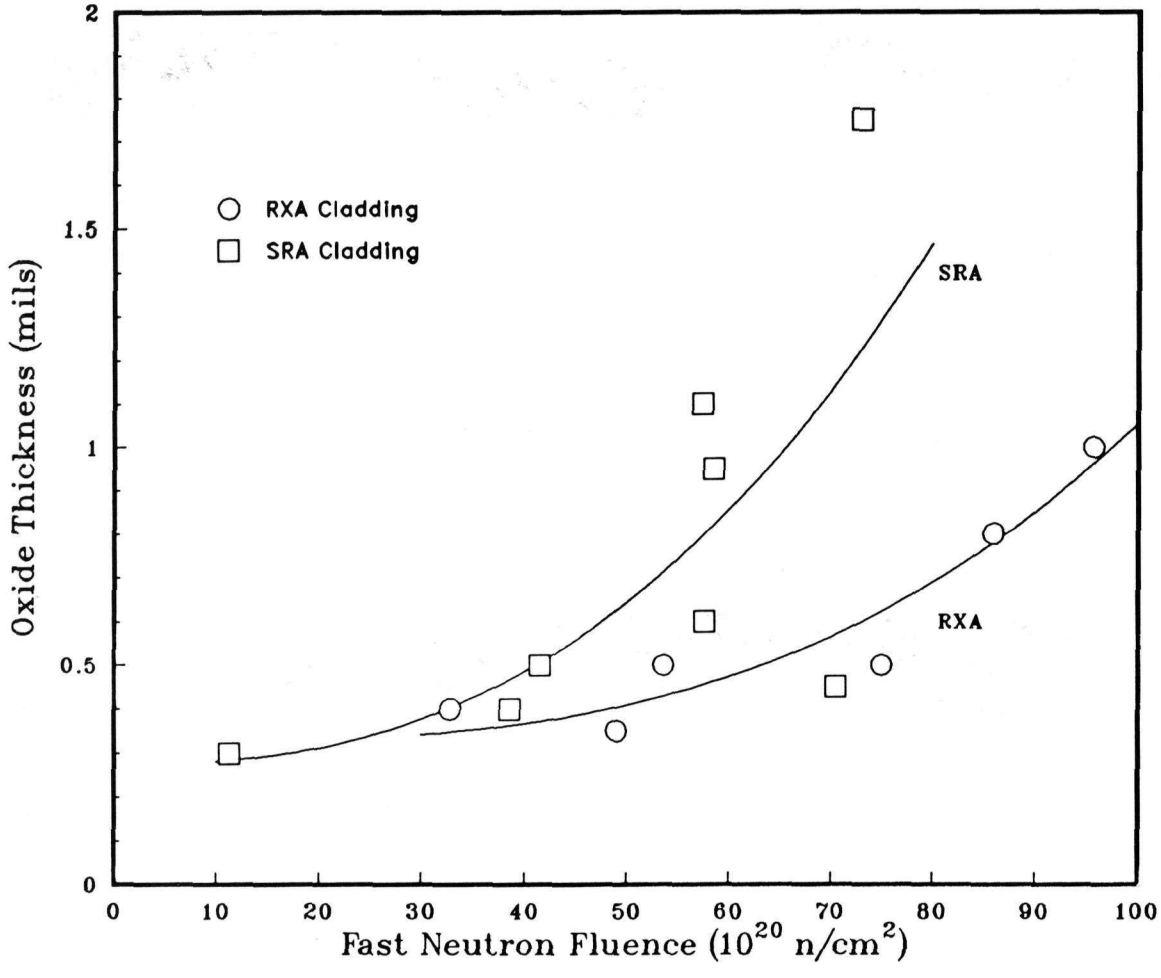

Figure 43. Comparison of Zircaloy Oxide Thickness on LWBR Rods at End of Life

Table 10. The EDCOT values were consistently higher and did not show a direct correlation with fluence.

The measured maximum waterside corrosion oxide film thicknesses at end of life (29,047 EFPH), as determined by metallography, are compared in Table 11 with values calculated in Reference (15) by a corrosion model designated CHORT (Corrosion and Hydriding of Reactor Tubing). The major variables in the CHORT model are Zircaloy cladding surface temperature, fast neutron flux (>1 Mev), and exposure time (References (18), (19), and (20)). The measured thicknesses listed in Table 11 are in reasonable agreement with CHORT predictions.

In the seed region and at least some regions of the reflector rods, the fuel-cladding gap was maintained throughout core life. Metallographic cross sections through the fuel pellet-cladding samples confirmed the presence of a gap completely around the pellets. No chemical interaction between the fuel and the cladding at the cladding inner surface was observed on any of the examined samples from the seed region and the one reflector region rod.

In the blanket region, however, the cross sections revealed that the cladding was in contact with the fuel over essentially all of the cladding I.D.

4.2.2.2 - Cladding Hydride

Etched sections of RXA Zircaloy-4 cladding from seed fuel rods typically revealed uniformly distributed hydrides throughout the cladding cross section, as shown in Figure 44. Hydride size and distribution in the SRA blanket rod cladding appeared to vary with the amount of cladding oxide thickness. For cladding with an oxide thickness of 1 mil or more, the hydrides were grouped in long (10 to 20 mils in length) stringers uniformly distributed throughout the cross section, as shown in Figure 45. Hydride stringers were usually located immediately beneath the oxide layer for these thicker oxide cladding samples. For cladding with an oxide thickness of less than 1 mil, the hydrides were shorter (2 to 5 mils in length), and only random hydrides were located at the oxide-cladding interface, as shown in Figure 46.

Table 11 - End-of-Life Oxide Corrosion Thickness of LWBR Cladding at Peak Power Position

Rod Type	Maximum Oxide Thickness (mils)	
	CHORT Best Estimate Prediction*	Metallographic Measurement
Seed	1.08	1.0
Standard Blanket	1.10	1.75
Power Flattening Blanket	1.03	1.1
Reflector	0.86	0.25

* Reference (15)

Hydride size and distribution in the reflector cladding was similar to that in the seed cladding, except that the hydride content was lower.

By comparing micrographs of the cladding cross sections, in both the transverse and longitudinal orientations, to the hydride visual standard in Reference (11), the total hydrogen content in the cladding was estimated to be on the order of 50 to 100 ppm in the seed region, 25 to 100 ppm in the blanket region, and 25 to 50 ppm in the reflector region. Analysis of cladding samples by the inert gas fusion technique confirmed these estimates. The results of this analysis are summarized in Table 12 along with values calculated by the CHORT model and from the oxide thickness correlation measured metallographically. For the seed, standard blanket and power flattening blanket rods, the hydrogen contents measured by metallography and inert gas fusion were significantly lower than the calculated values. For the one reflector rod, the measured hydrogen content was significantly lower than the CHORT estimate, but was equivalent to the calculated value based on the measured oxide thickness.

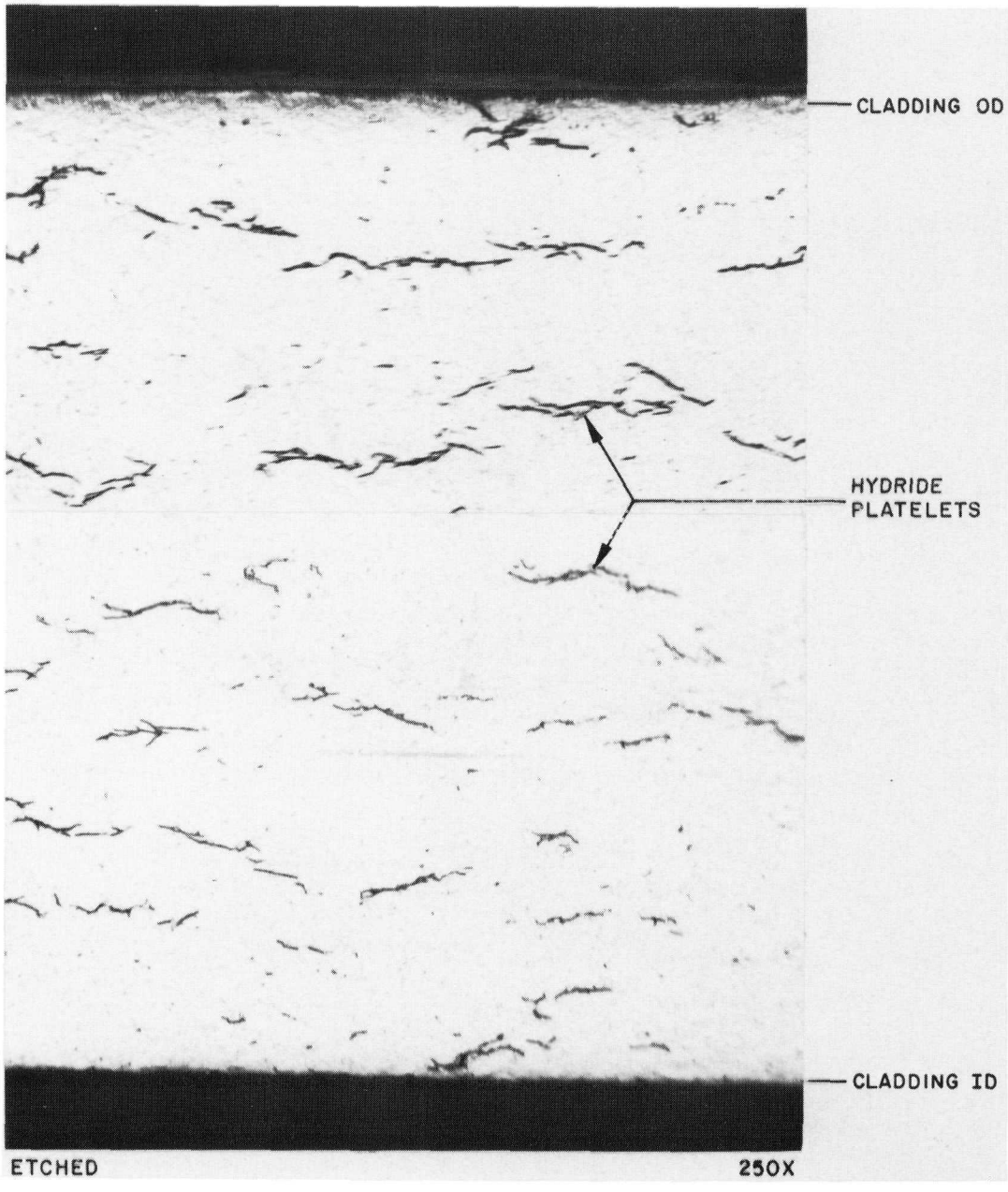

Figure 44. Typical Hydride Distribution in Cladding

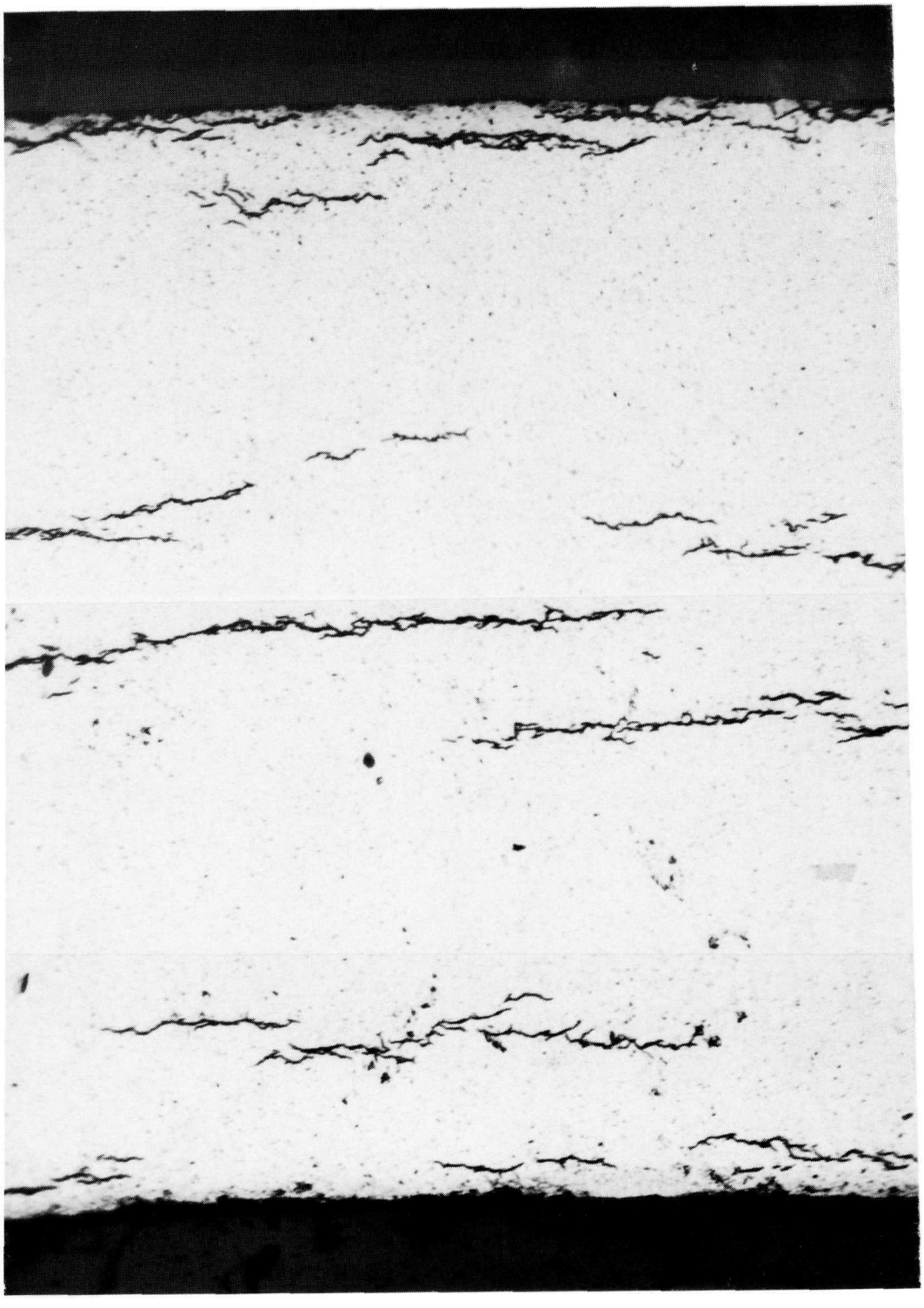

Cladding-Etched 250X

Figure 45. Hydride Distribution in Blanket Rod 2610746 Having Cladding Oxide Thickness Greater than 1 Mil

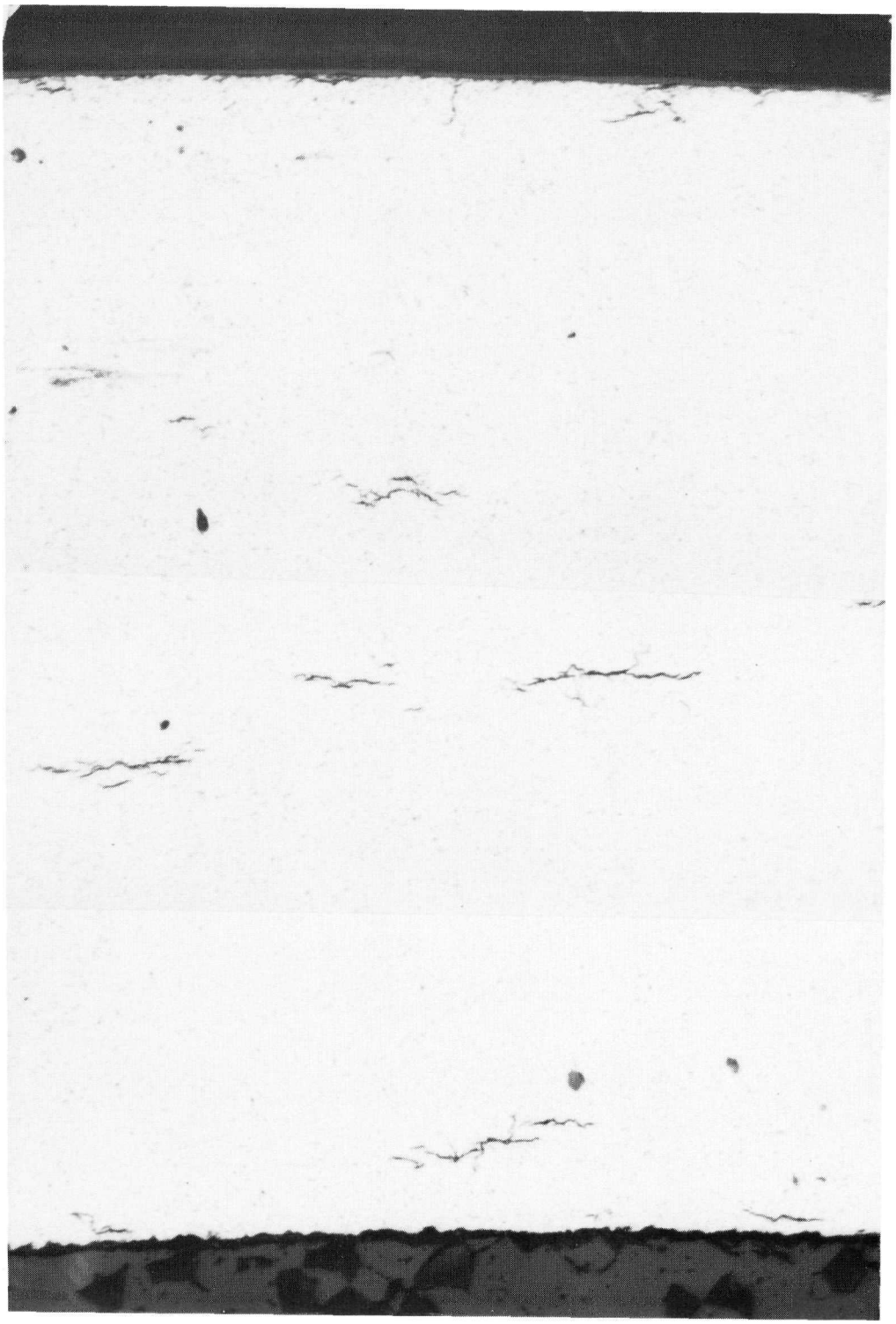

Cladding-Etched 250X

Figure 46. Hydride Distribution in Blanket Rod 2514164 With Cladding Oxide Thickness of 0.6 Mil

Table 12 - Hydrogen Content of LWBR Cladding at End of Life

Rod Type	Calculated Hydrogen Pickup (ppm)		Measured Hydrogen Pickup (ppm)			
	CHORT Best Estimate*	From Measured Oxide Thickness**	From Met.***	Inert Gas Fusion #1	#2	Average
Seed	345	92-320	50-100	79	92	86
Standard Blanket	277	73-446	25-100	94	110	102
Power Flattening Blanket	275	105-295	25-100	96	94	95
Reflector	144	40	25-50	33	35	34

* Reference (15)

** $\Delta H_{ppm} = \frac{(11.8987\ \Delta T - 0.1824)\ (0.6)}{t}$

where ΔT = oxide thickness in mils
t = cladding thickness in inches

*** Photomicrographs of metallographic sections were compared to the visual standards in Reference (11)

The two samples of each rod type analyzed by the inert gas fusion technique were taken from the same small cladding ring section but from different portions of the circumference. The results indicate that the circumferential distribution of hydrogen in the cladding was fairly uniform in the seed and blanket cladding and very uniform in the reflector cladding. This is in agreement with LWBR irradiation test data where uniform hydride concentrations in the fuel rod cladding were observed (Reference (21)). The lower hydrogen content in the reflector cladding is considered to be due to the thicker cladding (0.042 inch) and, hence, larger volume than for seed (0.022 inch) or blanket (0.02775 inch standard and 0.02625 inch power flattening) cladding.

No massive hydriding was observed. The hydride distribution at the inner and outer surfaces generally was the same as that through the cladding thickness (Figure 44). The cladding surrounding the high burnup binary pellet from seed rod 0205071, however, was unusual in that the hydride platelets were observed at both O.D. and I.D. surfaces and at the center of the cladding thickness but was generally absent in-between (Figure 47). The cause for this unusual hydride distribution was not apparent. No evidence of cladding cracking was observed in any of the samples examined metallographically.

The hydride platelets were circumferentially oriented (parallel to the cladding surface), as noted in both transverse and longitudinal metallographic cross sections (Figures 48 and 49). This orientation is preferred to avoid surface cracks. Since hydride platelets reduce ductility in the direction normal to the platelets, it is desirable to avoid radially oriented hydrides which would embrittle the cladding in the circumferential direction and make it susceptible to surface cracks. The preferred circumferential hydride orientation was clearly predominant in all rod types examined.

4.2.2.3 - Cladding I.D. Surface Features

Cladding samples from the four fuel rods examined to determine iodine and cesium content also were examined by Scanning Electron Microscopy (SEM) to determine typical and nontypical features on the cladding I.D. surface. Compositions of most features were determined with the energy dispersive X-ray (EDX) analyzer. A section of unirradiated Zircaloy-4 tubing of the same lot as one of the samples was also examined by SEM. Cladding surface images were obtained both by secondary electron modulation (S.E.) to identify topographic features, and by back-scattered electron (B.S.E.) modulation to produce an image in which the degree of "whiteness" in the image was directly proportional to the atomic number of the material.

The inner (fuel-side) surface of both the blanket and seed cladding was found to be covered with a thin film of approximately 15 weight percent thorium and 85 weight percent zirconium. Typical low magnification (8X - 13X) micrographs of the inner surfaces are shown in Figures 50 and 51. A coating of fine nodules, about 0.5 micron to 5 microns across, was located either on

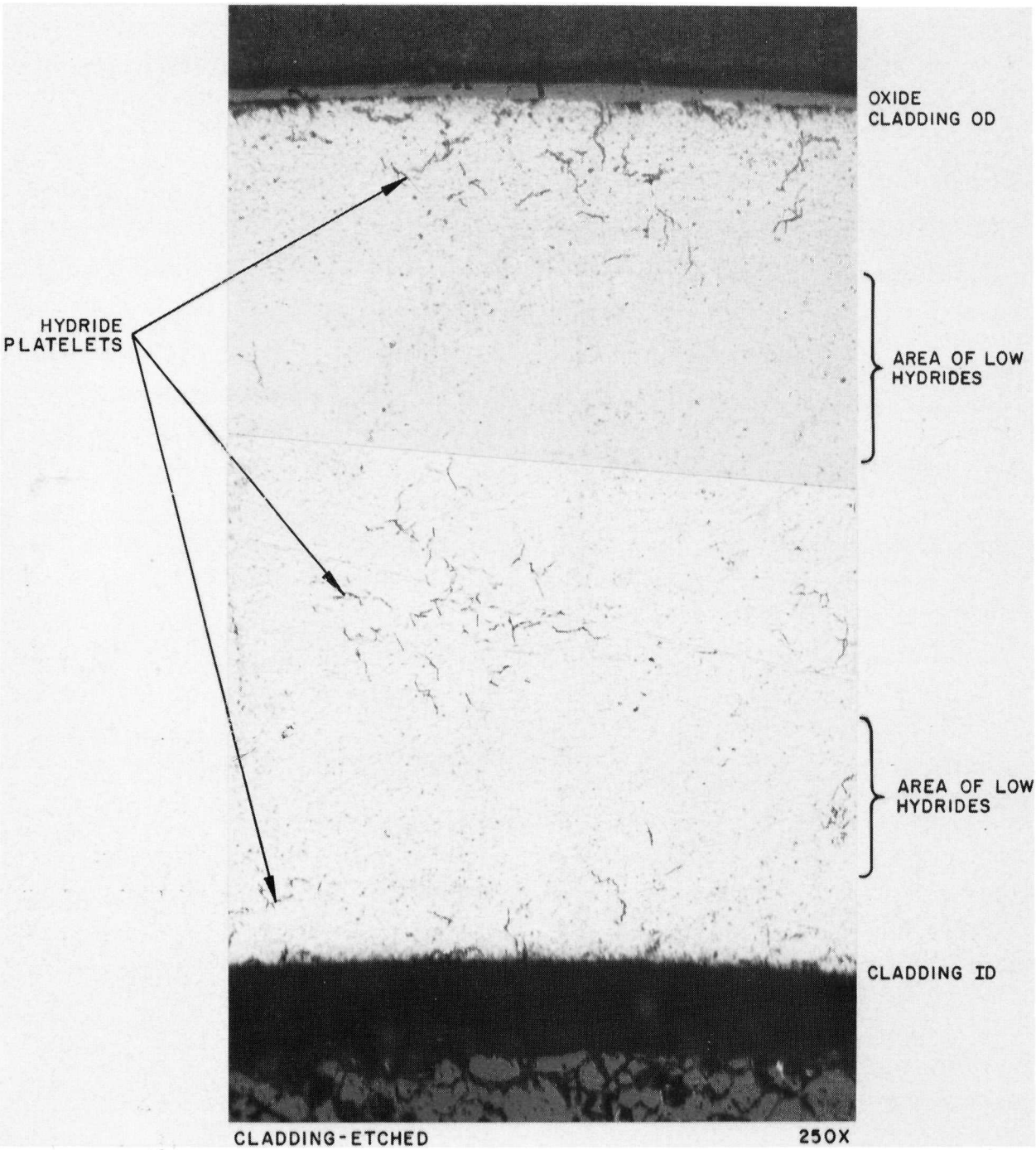

Figure 47. Unusual Hydride Distribution in Zircaloy-4 Cladding from Seed Rod 0205071

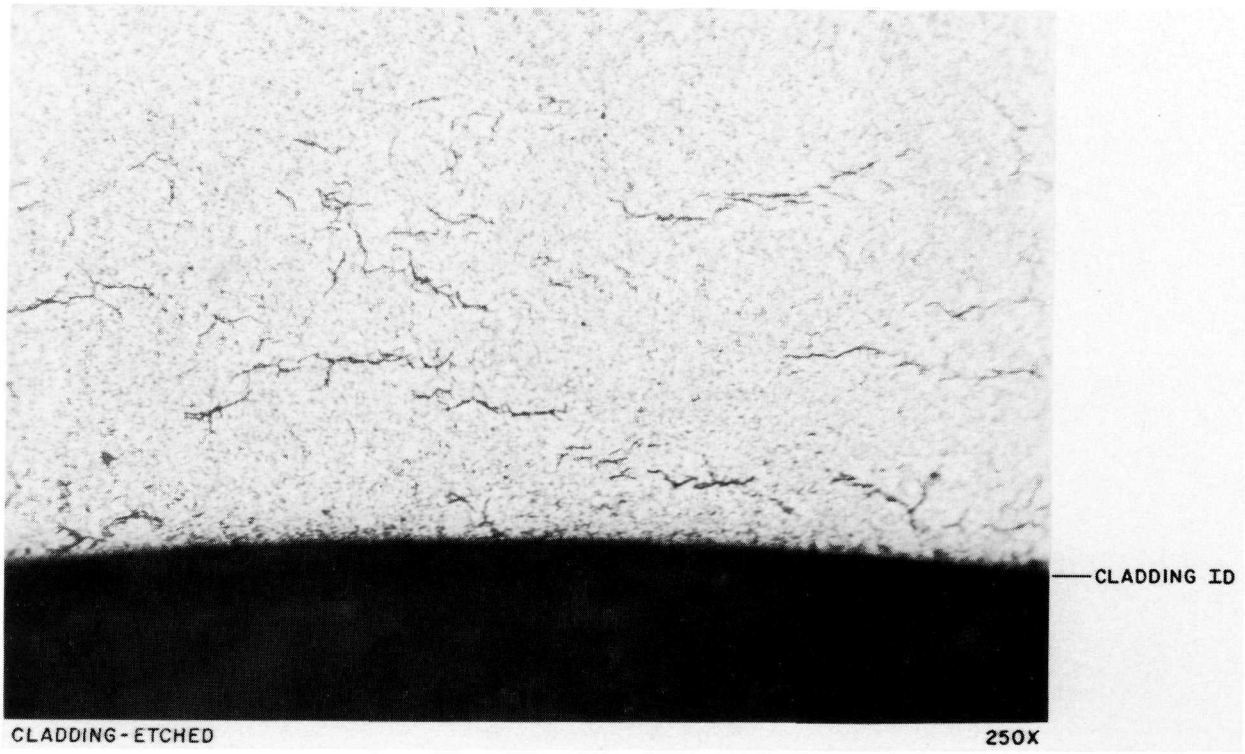

Figure 48. Circumferentially Oriented Hydrides in Transverse Section of Zircaloy-4 Cladding

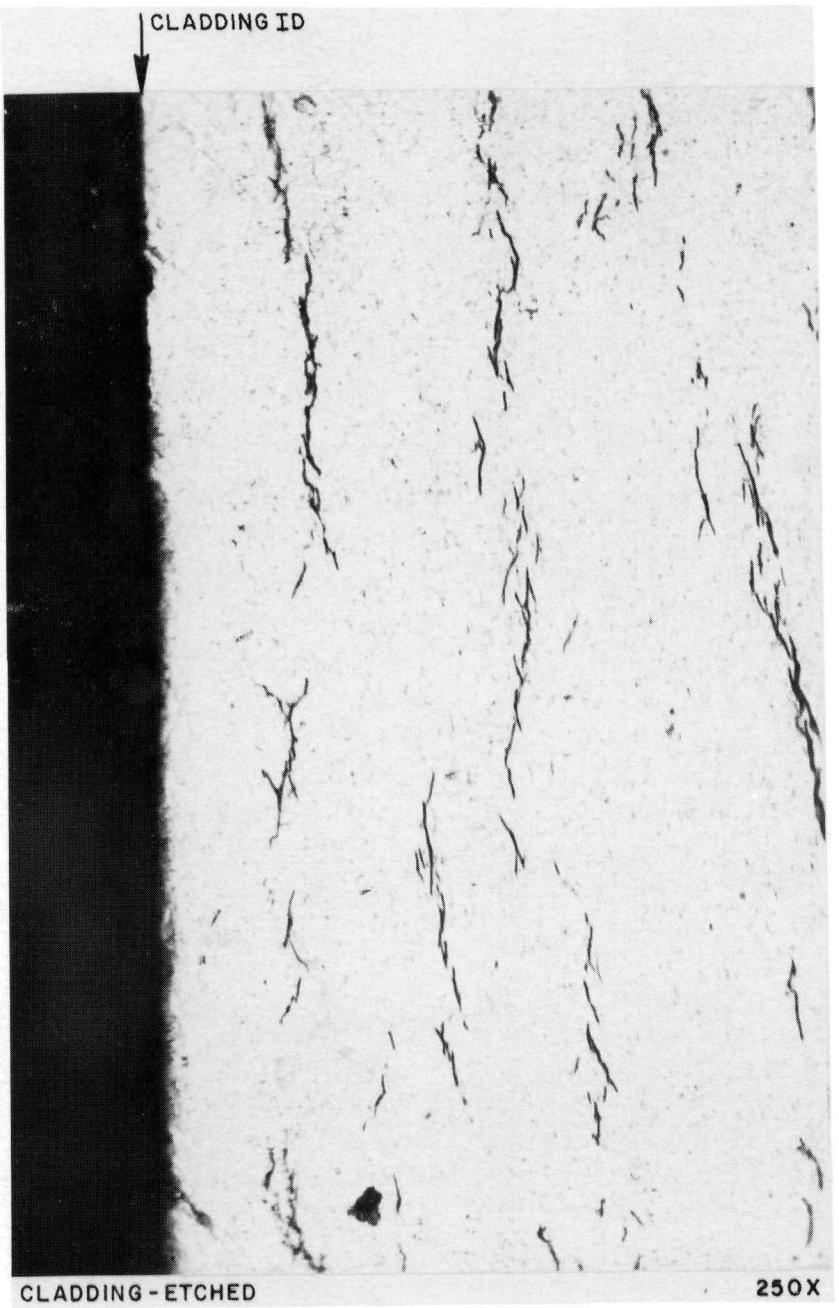

Figure 49. Circumferentially Oriented Hydrides in Longitudinal Section of Zircaloy-4 Cladding of Seed Rod

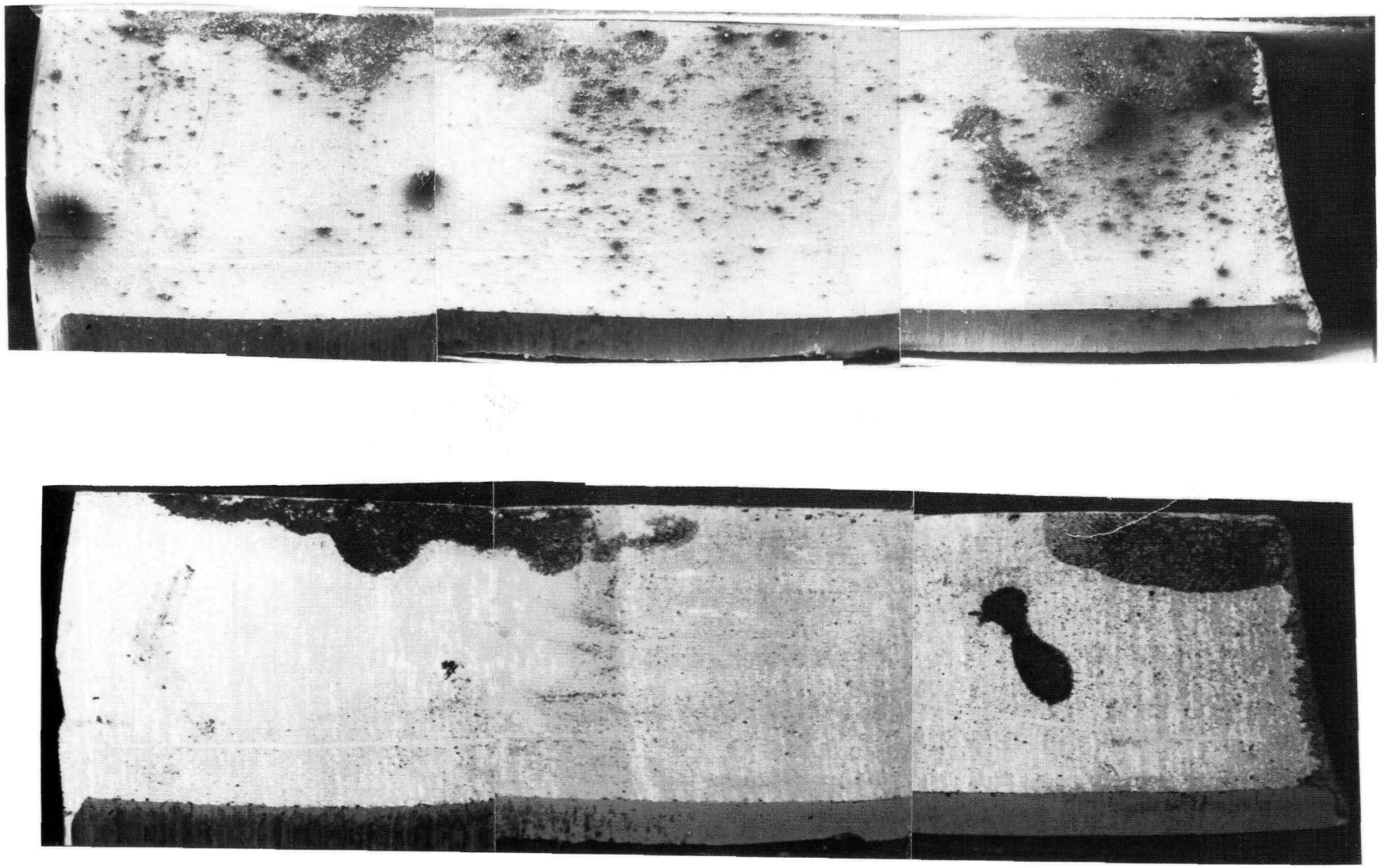

Figure 50. SEM Images of Cladding I.D. Surface from Standard Blanket Rod 1606710 (8X)
(Top, Secondary Electron Image; Bottom, Back-Scattered Electron Image)

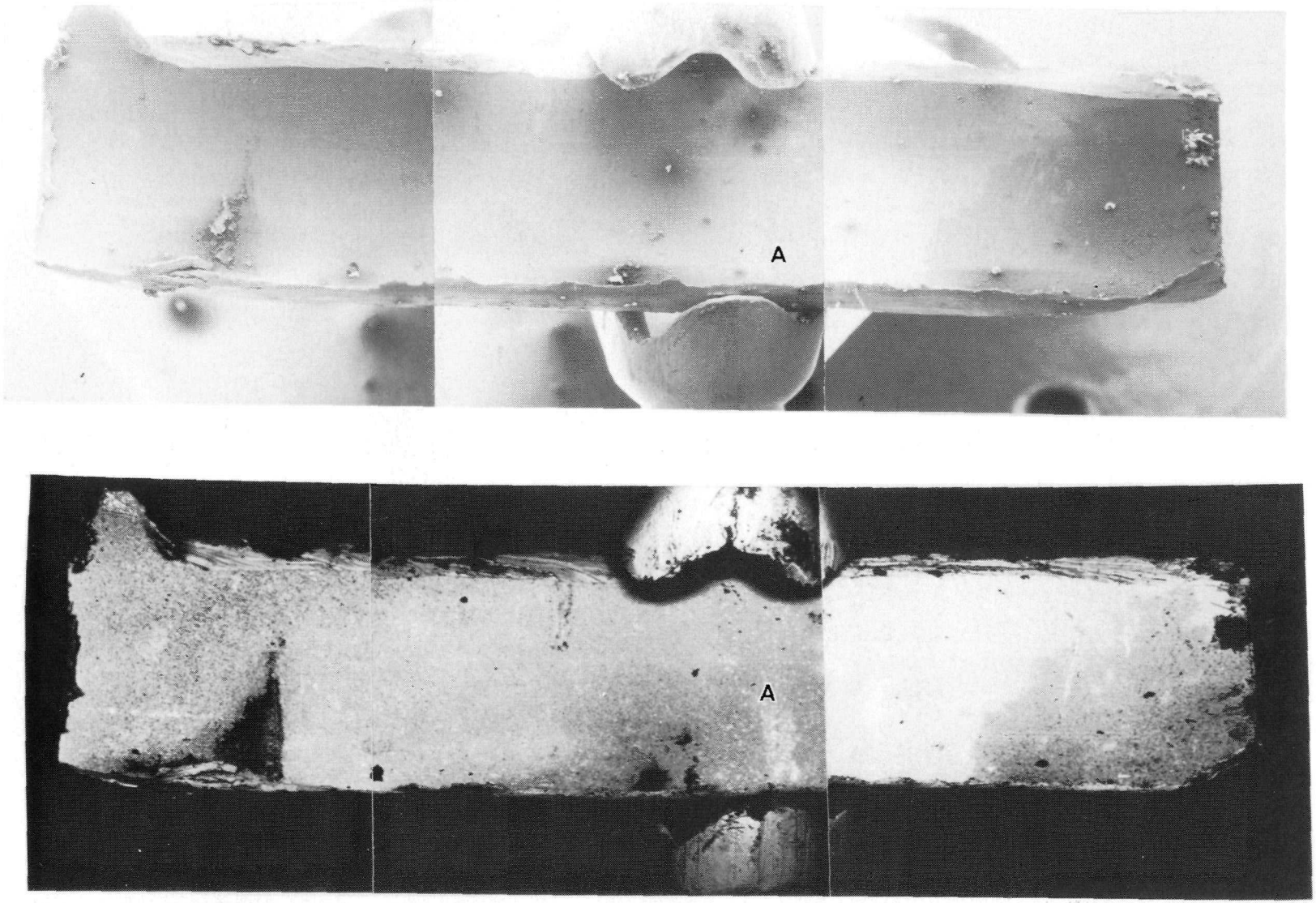

Figure 51. SEM Images of Cladding I.D. Surface from Seed Rod 0205071 (13X) (Top, Secondary Electron Image; Bottom, Back-Scattered Electron Image

the thin film or was joined by the film. The coating and nodules are shown in Figure 52 for the blanket cladding and in Figure 53 for the seed cladding. EDX analysis identified the composition of the nodules as thorium (at least 50 weight percent) and zirconium (balance). Penetration of the nodules by the electron beam, however, could have excited the Zircaloy-4 substrate, causing the observed zirconium level to be artificially high.

Course surface marks (pits and tubing drawing marks), such as those shown in Figure 54 (top) for blanket rod 1606710 were observed underneath the nodule layer. Finer tubing features, however, were concealed. The pits and tubing drawings marks were clearly visible on the unirradiated tubing (see Figure 54, bottom). In the seed samples the nodules were typically joined together to form features which often outlined the cladding pits and drawing marks (Figure 55).

The irradiated blanket cladding I.D. had circumferential rings, as shown in the B.S.E. image in Figures 50 and 56. The white rings contained high atomic number material, principally thorium. This is not unexpected since the nonfreestanding blanket cladding experienced creepdown onto the fuel pellet during core operation. Only isolated patches, rather than circumferential rings, were observed on the seed samples (for example, at location A in Figure 51). The particles in these rings or patches appeared to be fuel -- either whole grains or clusters of grains as shown in Figure 57 for seed cladding, or fragments of fuel grains as shown in Figure 58 for blanket cladding.

4.2.3 - Zircaloy-4 End Stems and Weld Region

As discussed in Section 2.5, nickel is transferred from the Inconel-600 baseplate to the contacting surface of Zircaloy-4 nuts during assembly of the fasteners due to the relative circumferential and radial movement of these components. In the case of the end stem and Inconel-600 baseplate contact regions (Figure 13), no radial motion normally occurs during assembly. Because fuel rods passed through the grids before the end stems contacted the Inconel-600 baseplate during module assembly, cocking of the rods and rubbing of components should not have occurred in LWBR rod assembly operations.

200X

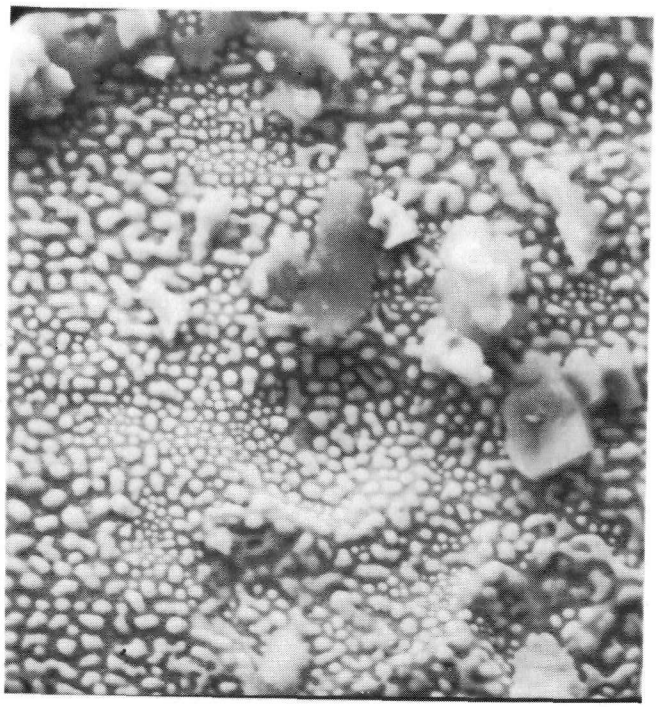

2000X

Figure 52. SEM Secondary Electron Image of the Cladding I.D. Surface from Standard Blanket Rod 1606710 Showing Coating of Fine Nodules

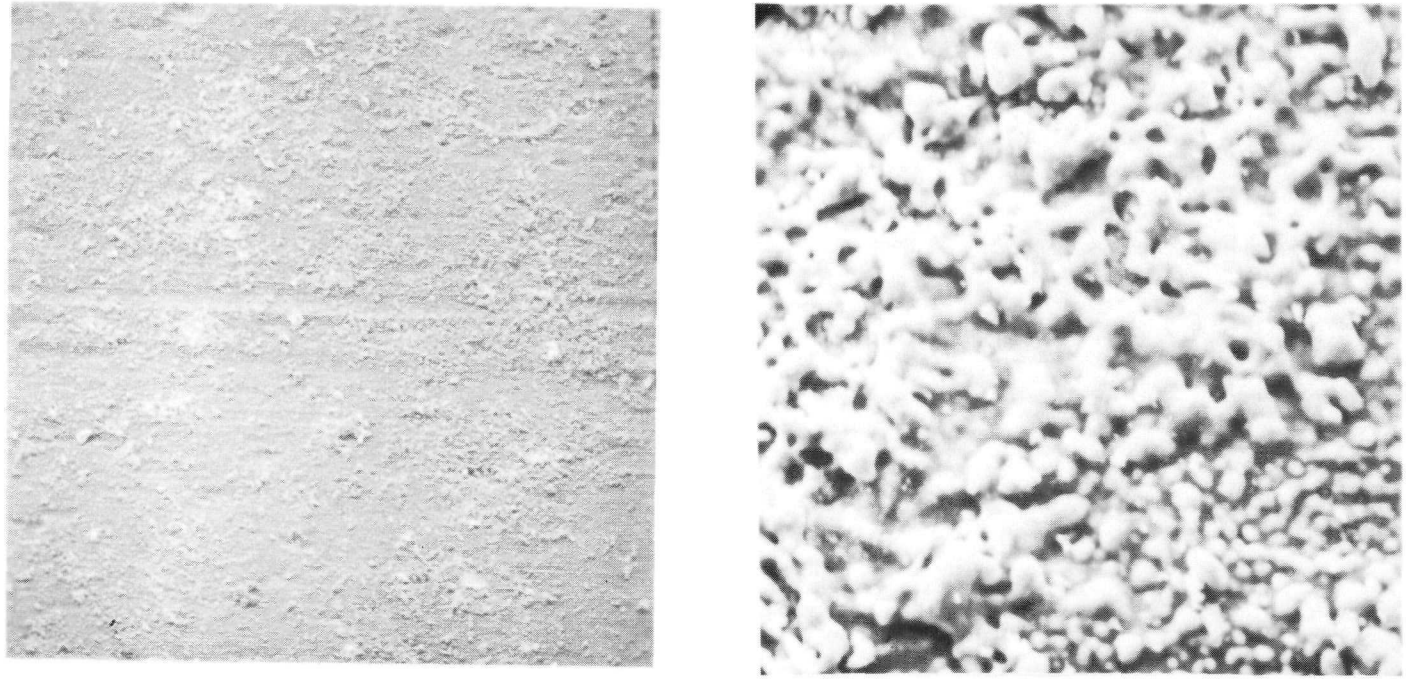

200X 2000X

Figure 53. SEM Secondary Electron Image of the Cladding I.D. Surface from Seed Rod 0205071 Showing Coating of Fine Nodules

IRRADIATED CLADDING I.D. 50 X

UNIRRADIATED TUBING 50 X

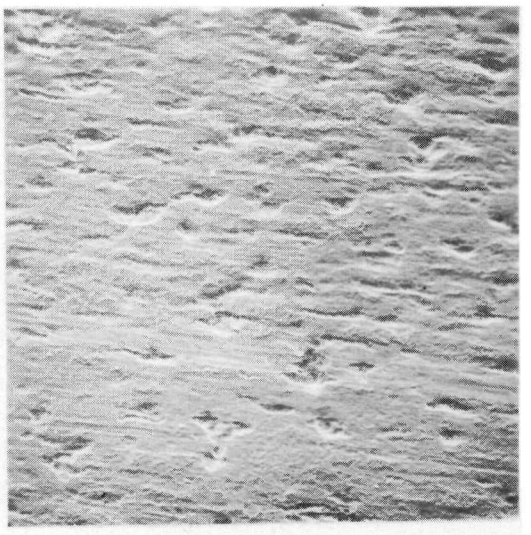

UNIRRADIATED TUBING 200 X

Figure 54. SEM Secondary Electron Image Showing Deposition of Thorium-Rich Material in the Tubing Marks of Blanket Cladding I.D. (Top) and of Tubing Drawing Marks and Pits in Unirradiated Tubing (Bottom)

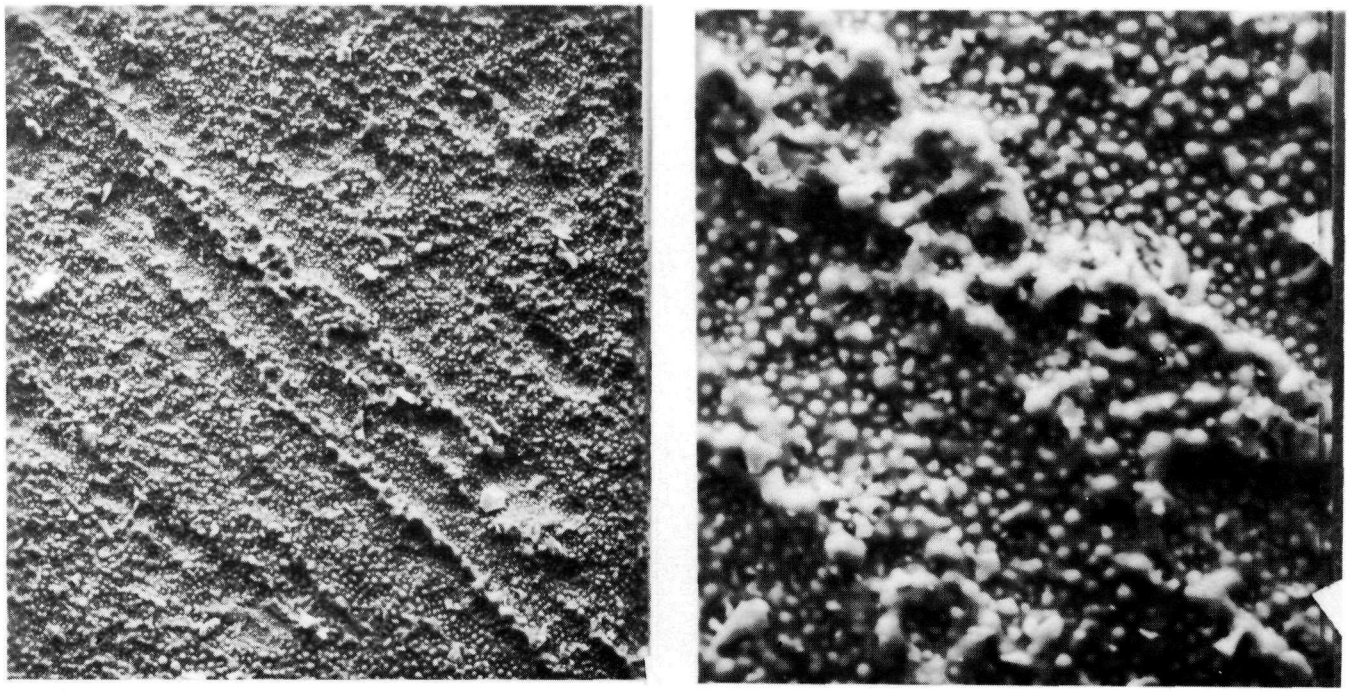

500X 2000X

Figure 55. SEM Secondary Electron Image of Seed Rod Cladding Showing Nodules Extending Longitudinally Along the I.D. Surface

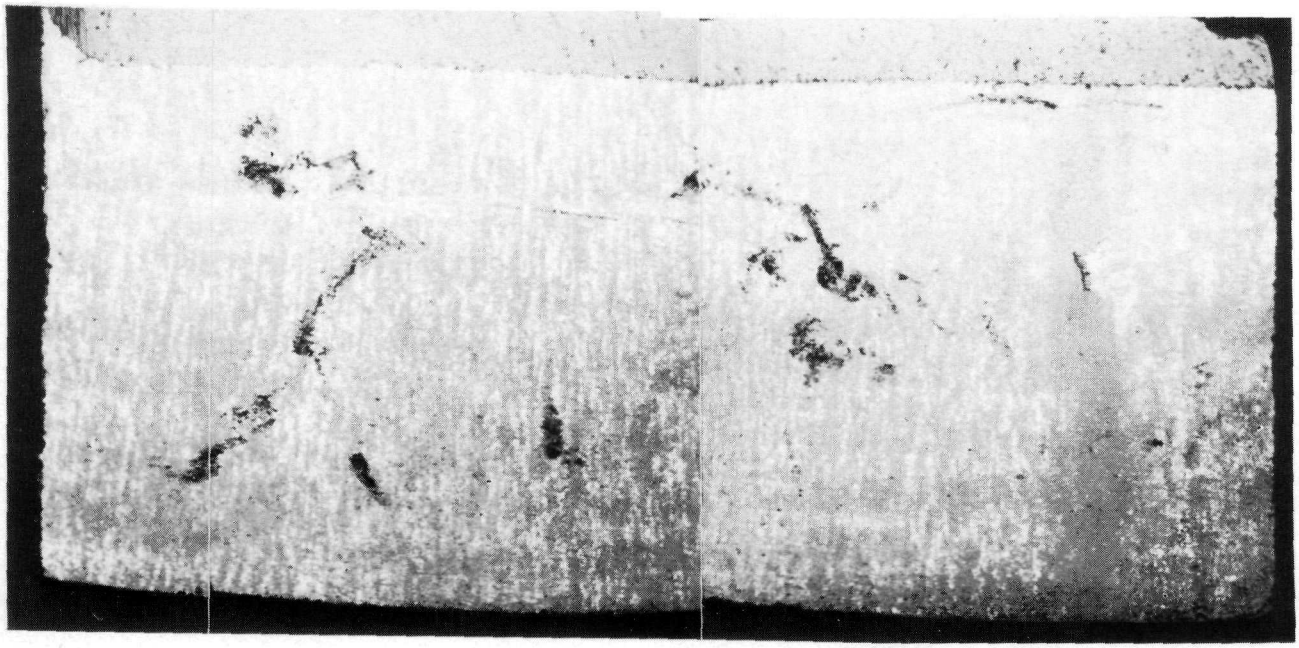

8X

Figure 56. SEM Back-Scattered Electron Image of Blanket Cladding I.D. Surface Showing (White) Circumferential Rings of Deposits

50X

200X

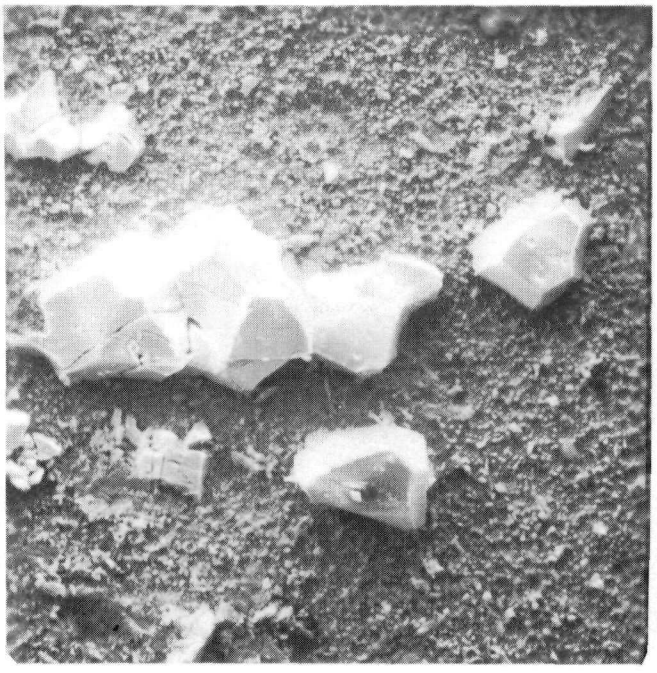

500X

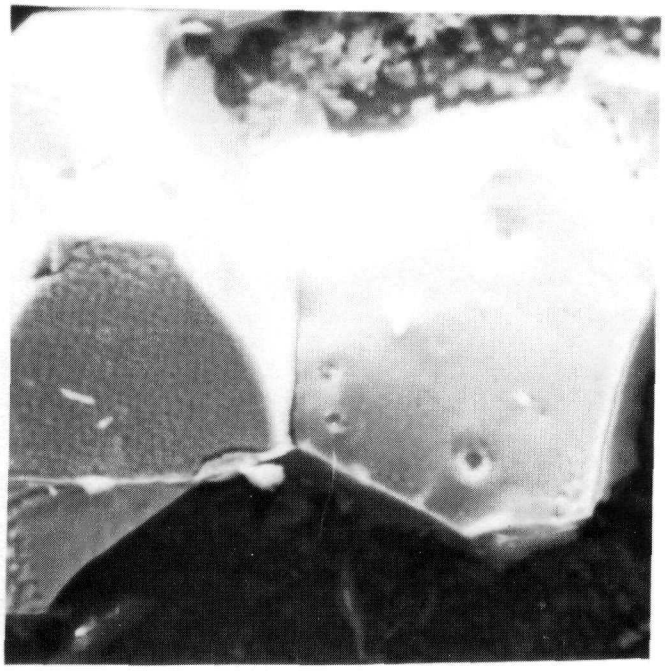

2000X

Figure 57. SEM Secondary Electron Images of Fuel Grains on Cladding I.D. Surface of Seed Rod 0507672

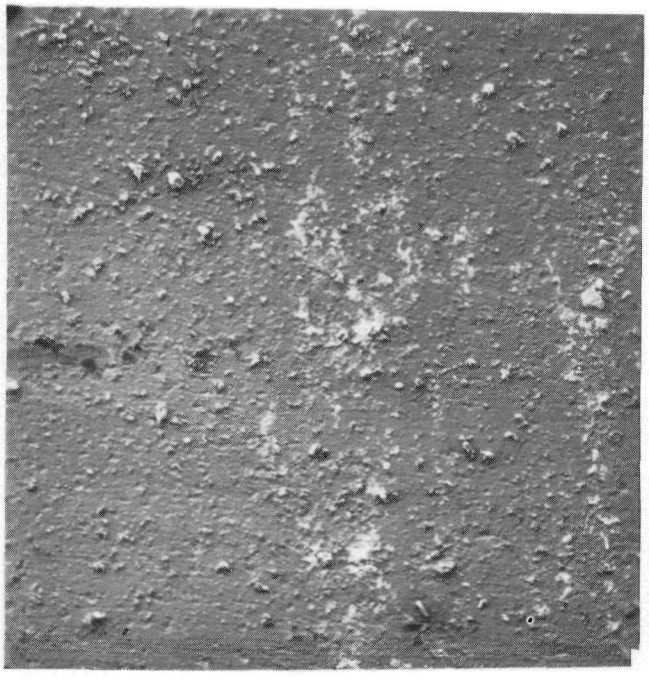

50X

200X

500X

200X

Figure 58. SEM Secondary Electron Images of Fuel Fragments on Cladding I.D. Surface of Standard Blanket Rod 1606710

Such relative motion and nickel transfer, however, did occur inadvertently during assembly of test specimens (Reference (6)). For this reason, the solid Zircaloy-4 end stems and the welds used to attach the end stems to the Zircaloy-4 cladding were examined at end of life. The end stems were examined to determine the degree of hydriding in the region that was in contact with the nickel-bearing Inconel-600 baseplate, and the welds were examined to determine their structural integrity. Longitudinal sections through a seed rod end stem, shown in Figure 59, revealed a low hydride content estimated at 25 to 50 ppm by comparison of micrographs to the visual standards in Reference (11). The contact surfaces were similarly low with no observable hydrogen gradient at the surface. No cracks were noted in this contact region.

Longitudinal sections through the cladding-end stem welds confirmed that the welds remained structurally sound throughout core life. A full penetration weld structure for a seed rod is shown in Figure 60. Although a few small holes are noticeable at the tip of the cladding-end stem weld, no cracks or structural weakness were found. These results confirmed that the LWBR fuel element end stem and weld design was satisfactory in maintaining the fuel within the cladding.

4.2.4 - Plenum Spring and Sleeve

The Inconel X-750 plenum springs were initially visually examined at low power magnification (1X and 3X) prior to metallographic examination. Only minor surface marks indicating contact of the spring coils with either the cladding I.D. (seed) or plenum sleeve I.D. (blanket and reflector) were observed. A plenum spring from the reflector fuel rod is shown in Figure 61.

In one spring, the gap between adjacent coils was approximately 0.020 inch wider than usual (in the free condition), Figure 62. This condition was considered to have been present in the as-built spring. In the unrestrained condition at end of life, a slight bend in the central axis was

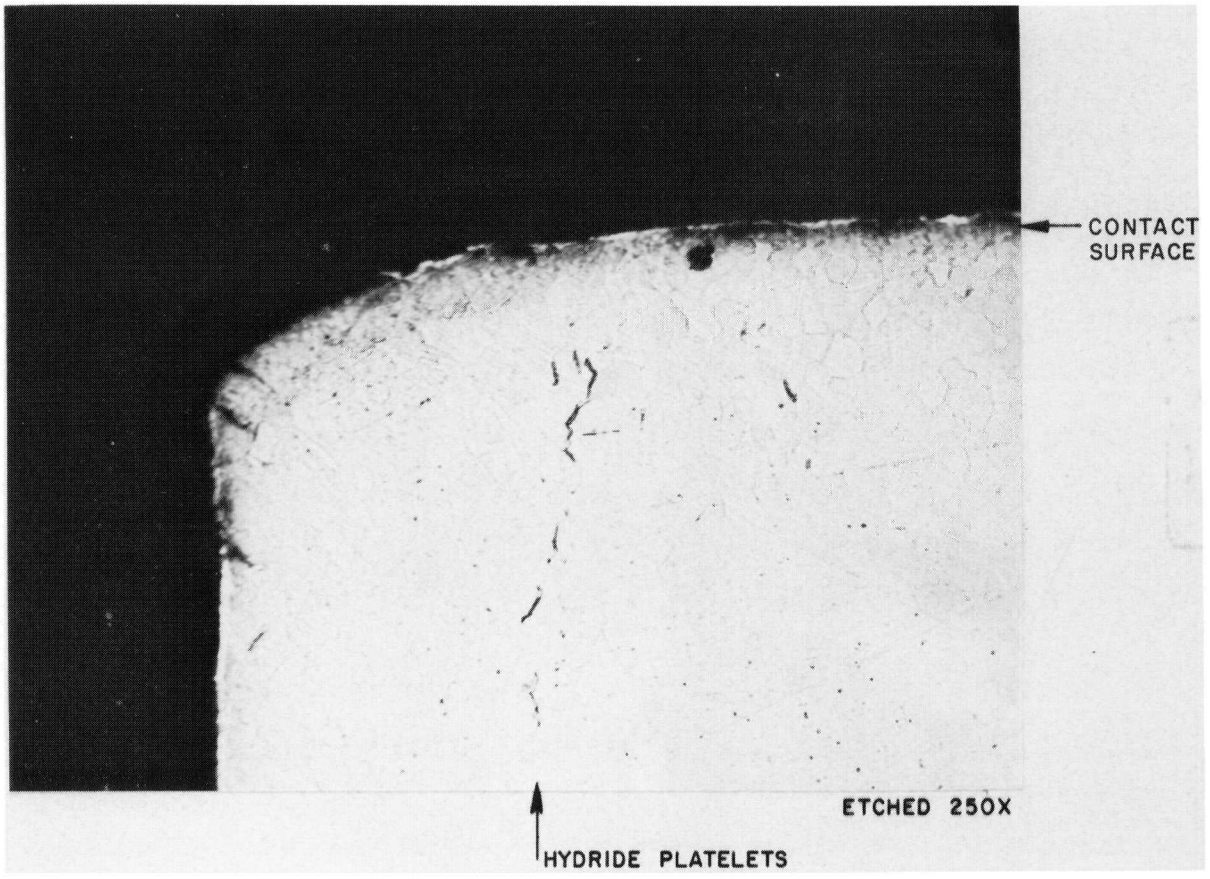

Figure 59. Longitudinal Section Through a Seed End Stem Showing Low Hydride Content at the Contact Surface

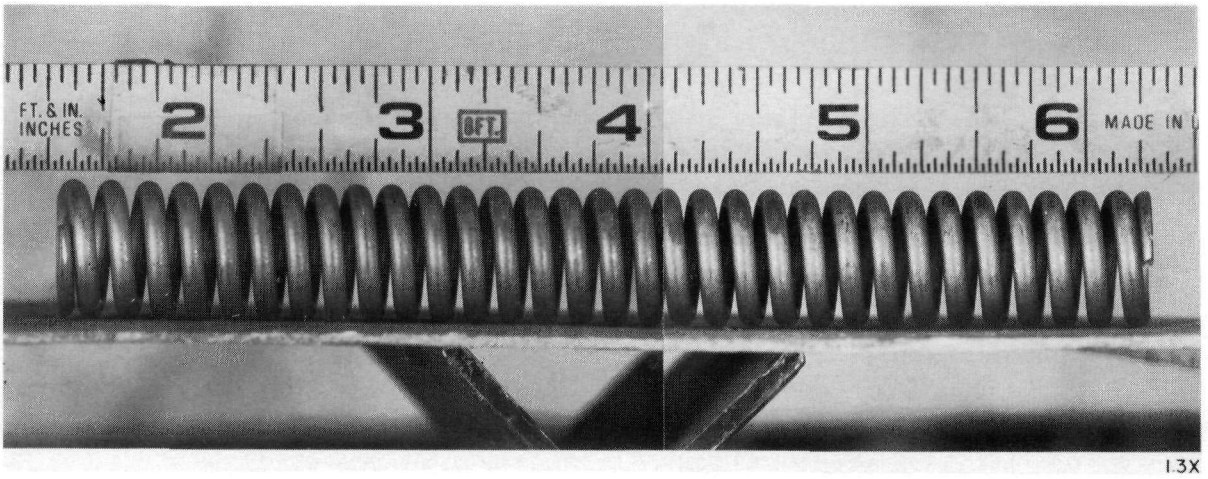

Figure 61. LWBR Reflector Fuel Rod Plenum Spring at End of Life

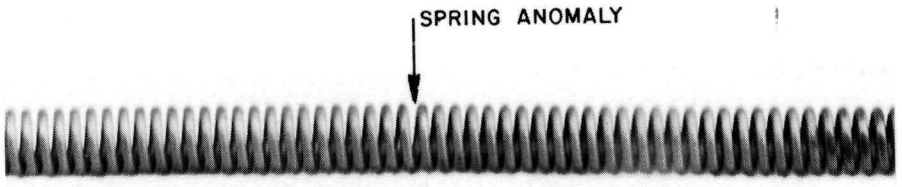

Figure 62. Plenum Spring from Blanket Rod 1504272 Showing Slight As-Built Anomaly in the Coil Spacing

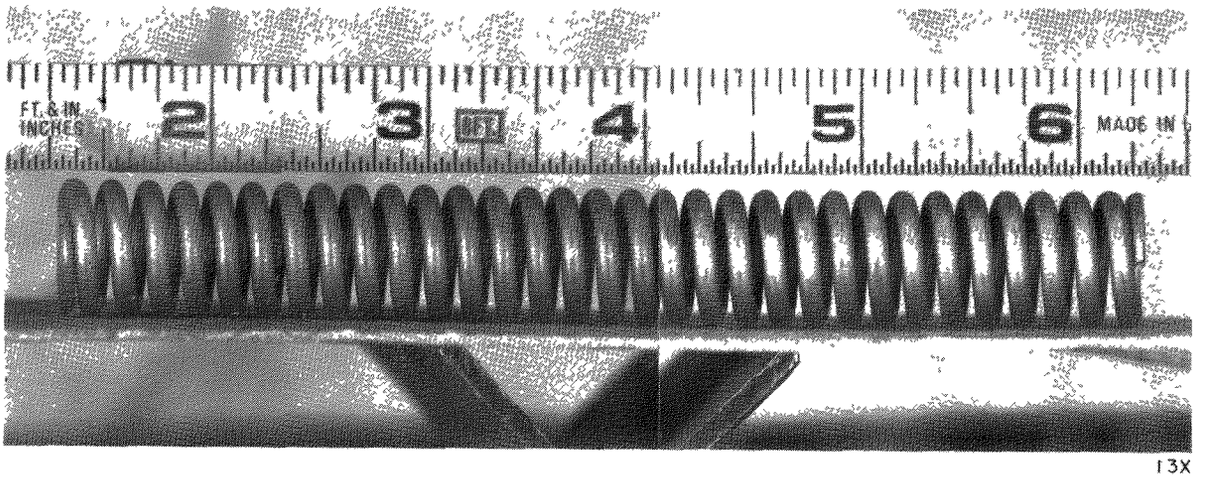

Figure 61. LWBR Reflector Fuel Rod Plenum Spring at End of Life

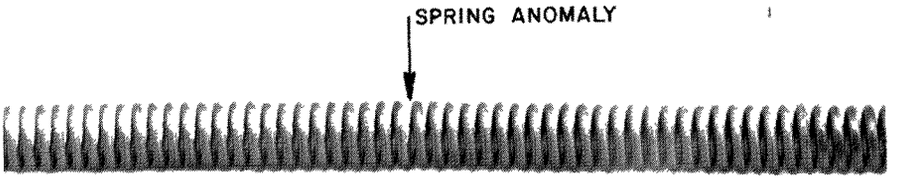

Figure 62. Plenum Spring from Blanket Rod 1504272 Showing Slight As-Built Anomaly in the Coil Spacing

apparent at the point of the larger coil to coil gap. This as-built condition had no effect on spring performance.

Some permanent set of the spring length was encountered as noted in Table 13. The set is primarily the result of stress relaxation in the hot, neutron flux environment since the plenum length increased slightly in the standard blanket and reflector fuel rods and was the same as the beginning-of-life length (see Table 4) in the power flattening blanket fuel rods. Based on comparison of the plenum length and the spring free length at end of life (Table 13), a positive force was maintained on the fuel stack throughout core life. The spring force was sufficient to withstand postulated worst-case shock loads on the fuel rods.

Table 13 - Fuel Rod Plenum Spring Length Measurements

Spring Data	Seed Rod 0606773	Standard Blanket Rod 1105717	Power Flattening Blanket Rod 2610746	Reflector Rod 3102657
BOL free length, in.	12.62	13.41	13.40	5.10
EOL free length, in.	12.12	13.06	13.18	4.98
Permanet set, in.	0.50	0.35	0.22	0.12
EOL plenum length, in.(1)	9.70	9.93	9.90	4.32
Compression at EOL, in.(2)	2.42	3.13	3.28	0.66
Nominal spring load rate, lb/in.	3.06	6.96	5.85	46.8
EOL load (cold), lb	7.41	21.78	19.19	30.89
EOL load (hot), lb	8.66	24.43	21.94	38.64
EOL load (hot), g's	3.6	2.6	2.8	2.3
Spring force required for shock load, g's*	1.4	1.0	1.3	1.3

(1) Measured from neutron radiographs of the fuel rod
(2) Compression = EOL free length - EOL plenum length
* Reference (15)

No oxide, corrosion, erosion, or cracks were evident on the spring coil surfaces of transverse sections that were examined metallographically as shown by the lack of these characteristics in a typical spring in Figure 63. Adequacy of the LWBR spring design and material (Inconel X-750, Condition BH), therefore, was confirmed by the end-of-life visual and metallographic examinations.

No apparent change was observed in the Type 348 stainless steel plenum sleeves examined after core operation. These tubular units, which served to support the nonfreestanding cladding in the plenum region of the blanket and reflector fuel rods, remained structurally sound. The sleeves functioned as designed.

4.2.5 - Fuel Rod Fasteners

Zircaloy-4 fasteners used to attach the fuel rods to the Inconel 600 structural baseplates were examined to determine the extent of hydriding, particularly at the bearing surface of the fastener against the baseplate (Figure 13). Ten fasteners from the seed region and three fasteners from the reflector region were examined. Because the joint between blanket region fasteners and Inconel 600 baseplates contained chromium-plated 17-4 PH washers, the concern for accelerated hydriding did not exist. Three fasteners and washers from the blanket region were examined to confirm the expected behavior.

For the seed fasteners, the bearing surface hydrogen contents were estimated from photomicrographs to be 500-1000 ppm for three fuel rod nuts, 150-400 ppm for three nuts, and 50-100 ppm for three nuts. (The bearing surface hydrogen content for the tenth fastener was not measured.) For the reflector samples, the fastener hydrogen level was of the order of 400 ppm. The measured hydrogen levels in the examined fasteners are listed in Table 14.

The amount of hydrogen present (as zirconium hydroxide) in the bearing region and throughout the examined cross sections of blanket fuel rod fasteners was estimated to be 20 ppm or less. A similar amount of hydride was present in the as-fabricated Zircaloy fasteners. This observation indicated that the blanket fuel rod fasteners were protected from further increase in

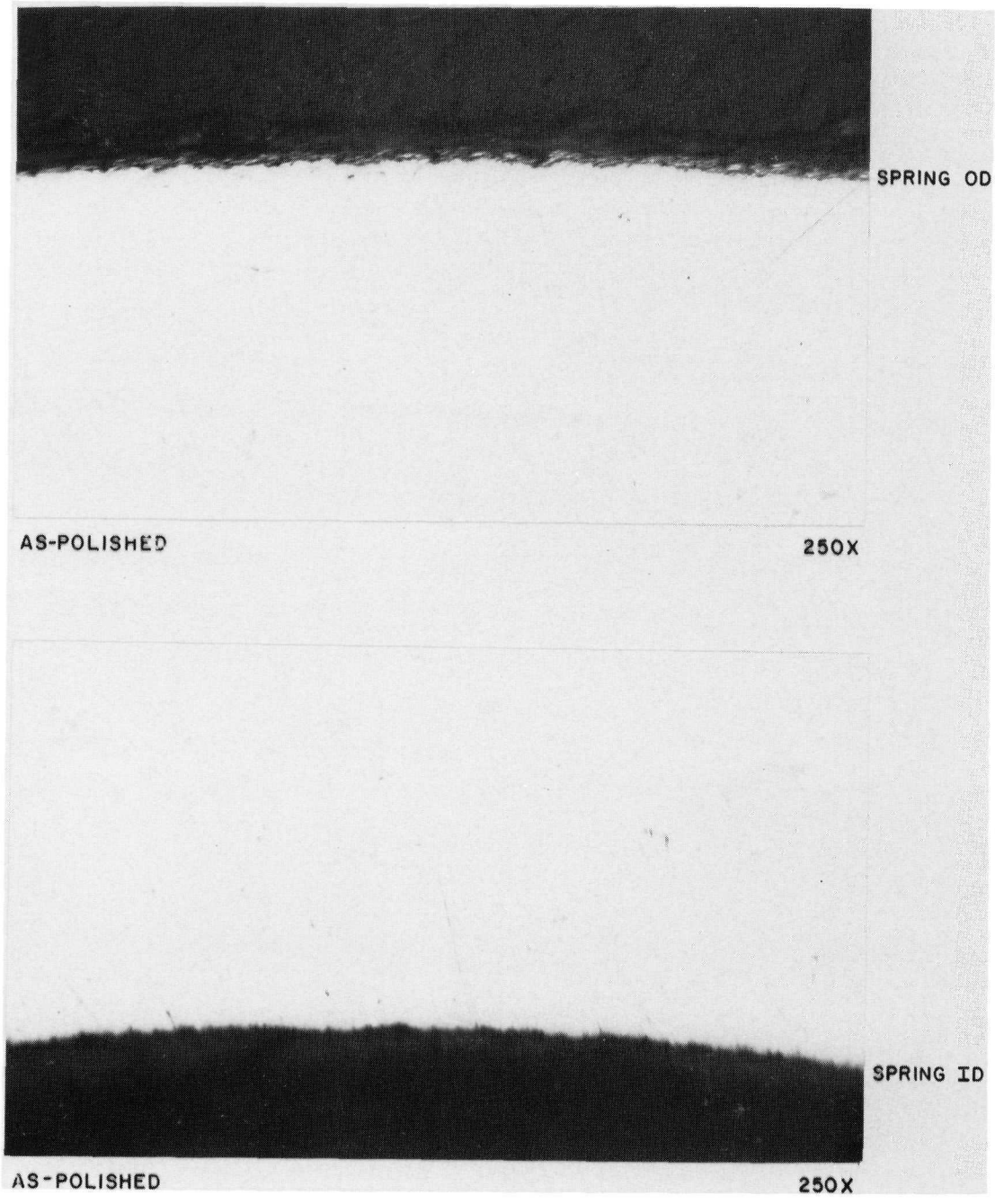

Figure 63. Transverse Section through Plenum Spring from Seed Rod 0606773 Showing O.D. and I.D. Surfaces Were Not Oxidized or Otherwise Attacked

Table 14 - Hydrogen Content (PPM) in Seed and Reflector Fuel Rod Fasteners at End of Life

SEED FASTENERS

Transverse Sections

Depth Below Contact Surface (mils)	Fastener Identification Number									
	9667	9668	9669	9670	9671	9672	9673	9674	9675	9676
1	N.M.	80	220	200	500	1000 to 100	550 to 50	100	50	400
5			550							
8				250		500				
10							100	150		
15	150	150								
18									80	

Longitudinal Sections

1					220 to 150					150 to 100
375					150					150
750					150 to 50					150 to 100

REFLECTOR FASTENERS

Transverse Sections

Depth Below Contact Surface (mils)	Fastener Identification Number		
	9449	9450	9493
3	400	400 to 250	400
15	400	330	400
52	400	330	400

N.M. Not Measured

hydride content during reactor service by the presence of the chromium-plated 17-4 PH washers. Micrographs depicting the low hydride content in blanket fuel rod fasteners are shown in Figures 64 (transverse section) and 65 (longitudinal section).

Typical hydride contents at the bearing surfaces of the seed and reflector fasteners are shown in Figures 66 through 68. Figure 69 shows bands of higher and lower hydride formation in a seed fastener; the bands indicate some cold working of the fastener occurred during the installation torquing operation. In the higher hydride band, the hydride content was estimated (by comparison to visual standards in Reference (11)) to be 550 ppm, whereas the hydride content in the lower hydride band was estimated to be only 100 ppm.

Serial grinding below the bearing surface indicated that in the three seed fasteners with the higher hydride contents (500 ppm to 1000 ppm) at the bearing surface, the hydride content decreased to the background level within approximately 0.010 inch which indicates that a steep hydrogen gradient existed for these fasteners. Two seed fasteners were remounted to permit a view of a longitudinal section and showed no discernible hydrogen gradient throughout the 0.75-inch length of the sample. Again, the background hydride level for both longitudinal sections was estimated to be 150 ppm.

A thin layer of Zirconium oxide was observed on both the outer diameter (waterside) and the inner diameter of all examined fasteners. Thickness typically measured 0.2 mil or less and was uniform over all outside surfaces, as shown in Figure 70.

The localized and erratic hydride contents at the bearing surfaces and the absence of solid hydride rimming are in agreement with the results of an out-of-pile LWBR flow test (REM-3) and some of the in-pile LWBR irradiation tests. Eight REM-3 seed and ten REM-3 reflector fasteners were flow tested for 1320 hours at 530°F and 920 hours at 150-200°F in pH 10.2 (NH_4OH) coolant containing 40-70 cc H_2/kg water. Appreciable amounts of hydride were detected in the bearing surface region. Within 1-3 mils of the contact surface, two seed fasteners had localized areas of heavy hydride (3200-10,500 ppm), three fasteners had areas of accelerated hydride (1200-2300 ppm), and two fasteners

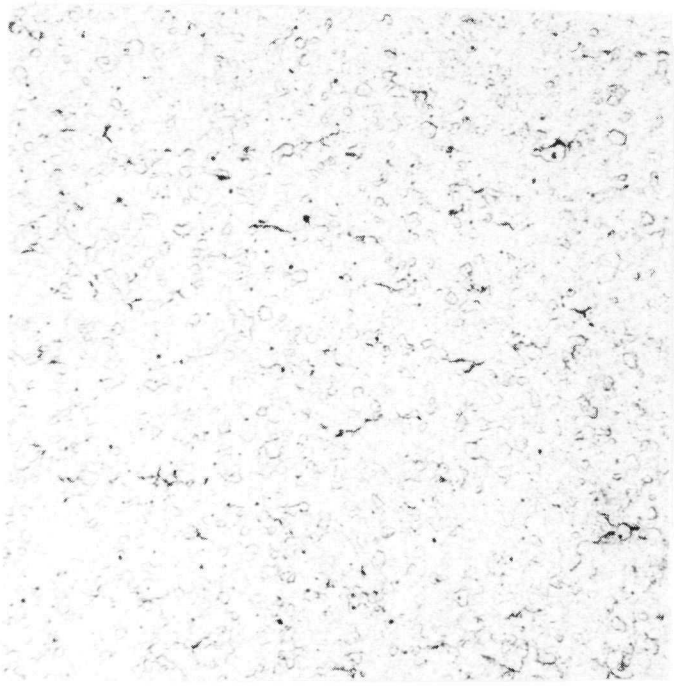

100X

250X

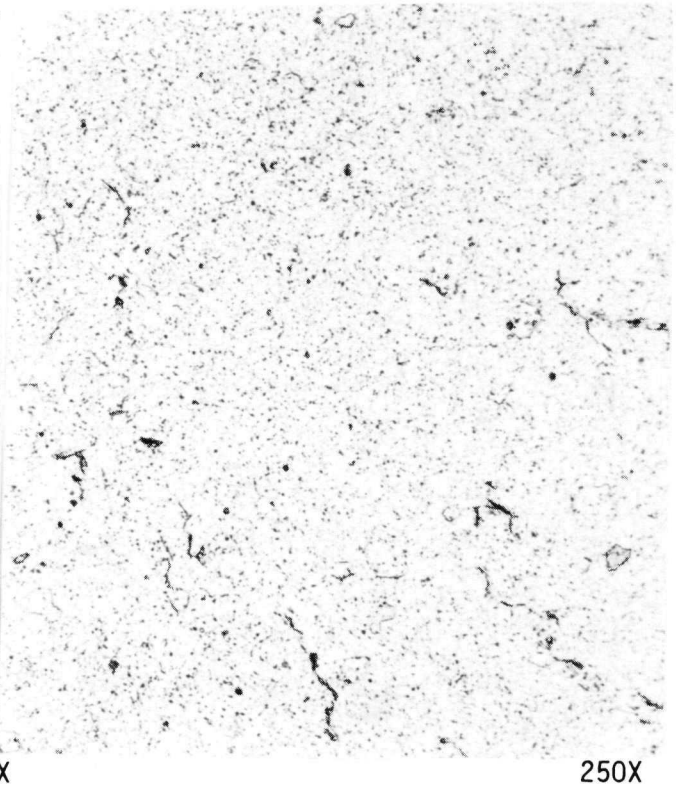

250X

Figure 64. Transverse Section Through Blanket Fuel Rod Fastener Taken About 2 Mils Into the Bearing Surface Hydride Levels are Low at 15 ppm (Etched)

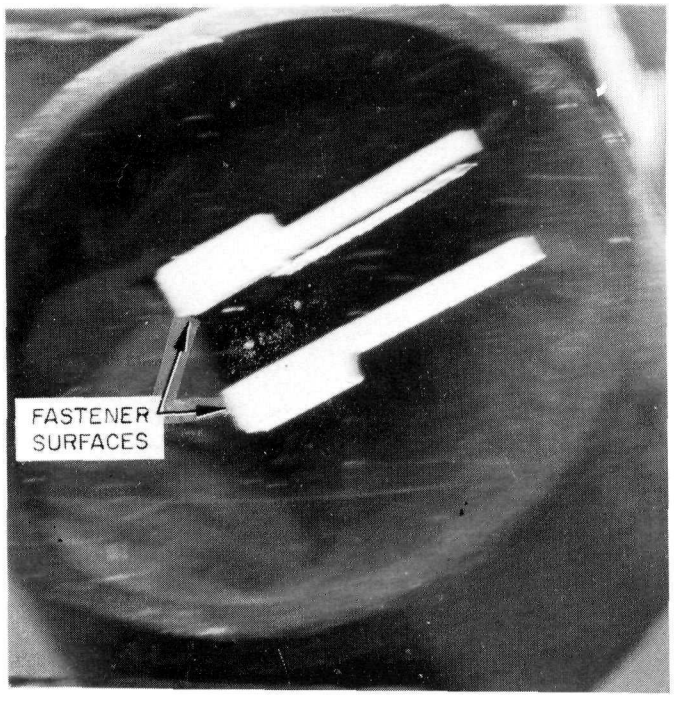

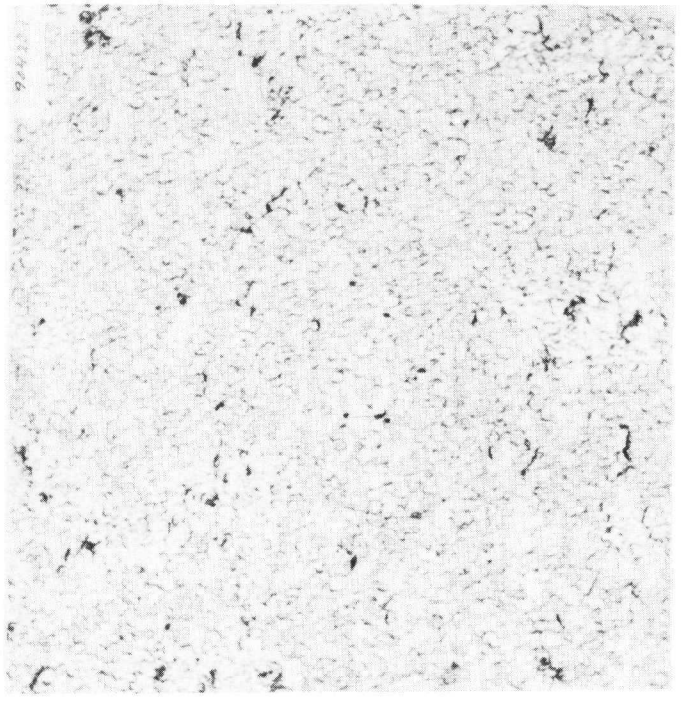

100X

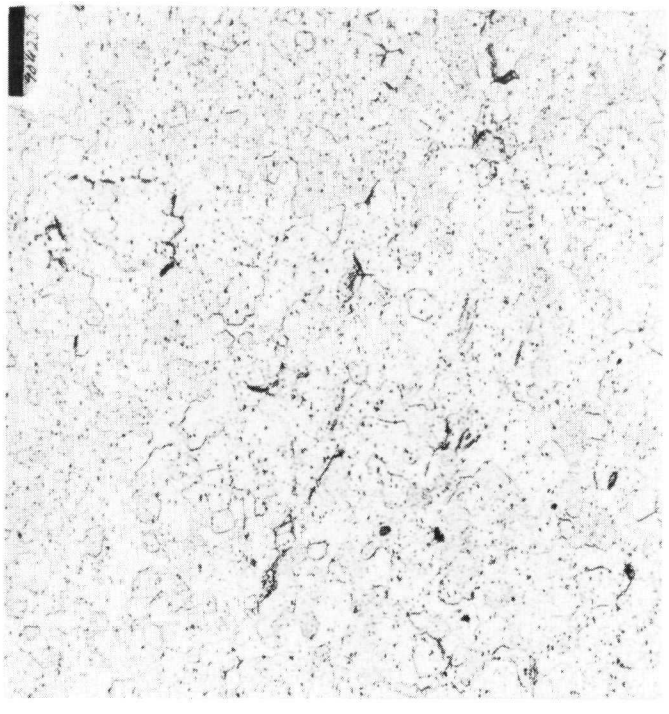

250X

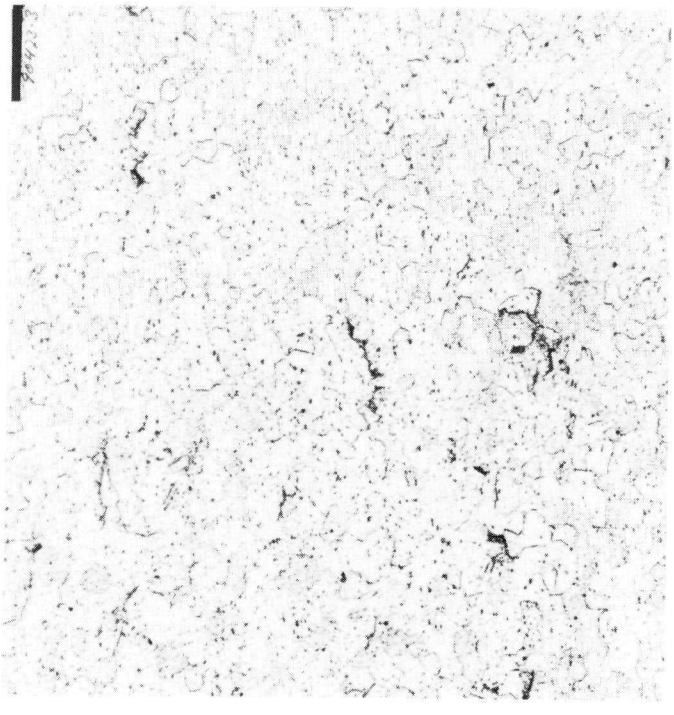

250X

Figure 65. Longitudinal Section Through Blanket Fuel Rod Fasteners Hydrogen Content is Between 10 and 20 ppm Both at the Bearing Surface and Deeper Into the Nut (Etched)

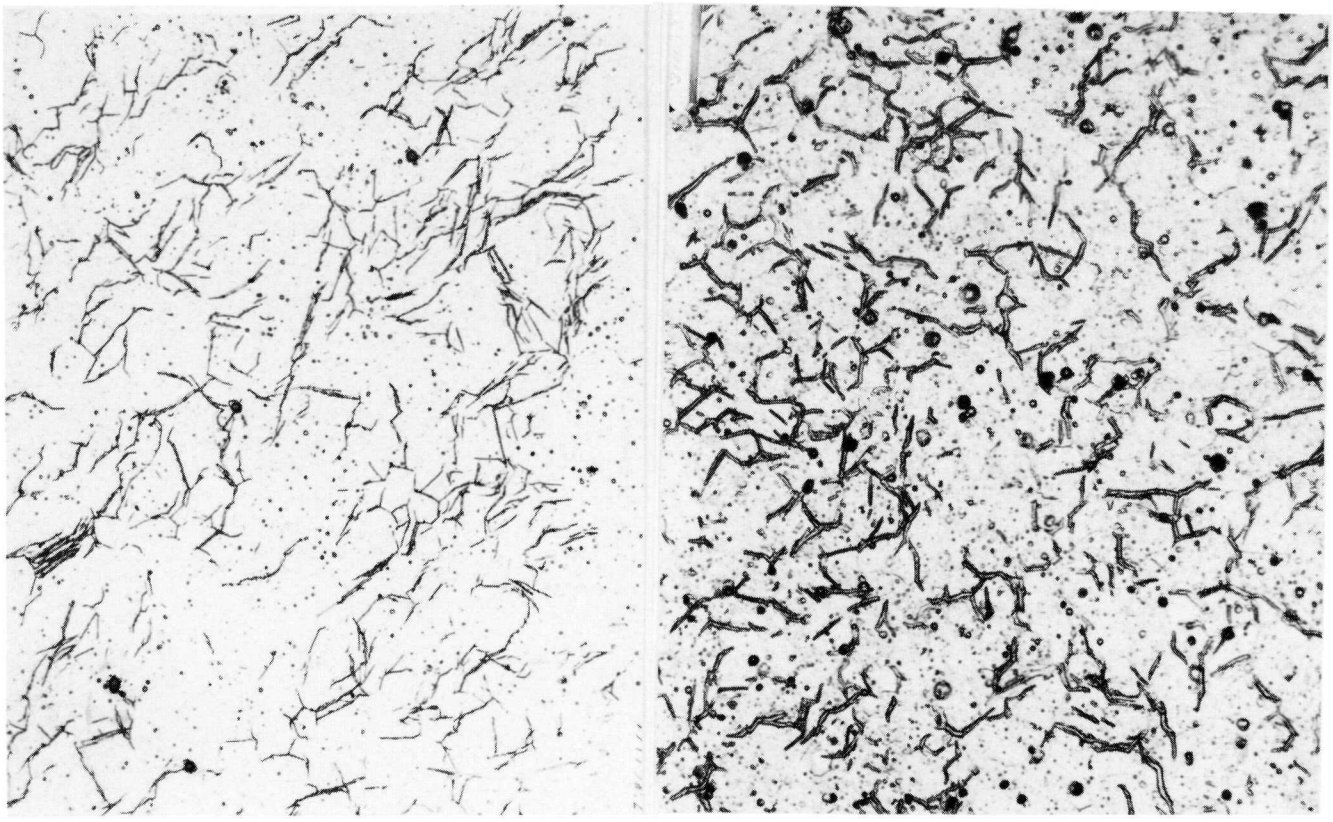

150-200 ppm 250X 330 ppm 250X

SEED REFLECTOR

Figure 66. Typical Hydride Formation in Seed and Reflector Fuel Rod Fasteners (Zircaloy-Etched)

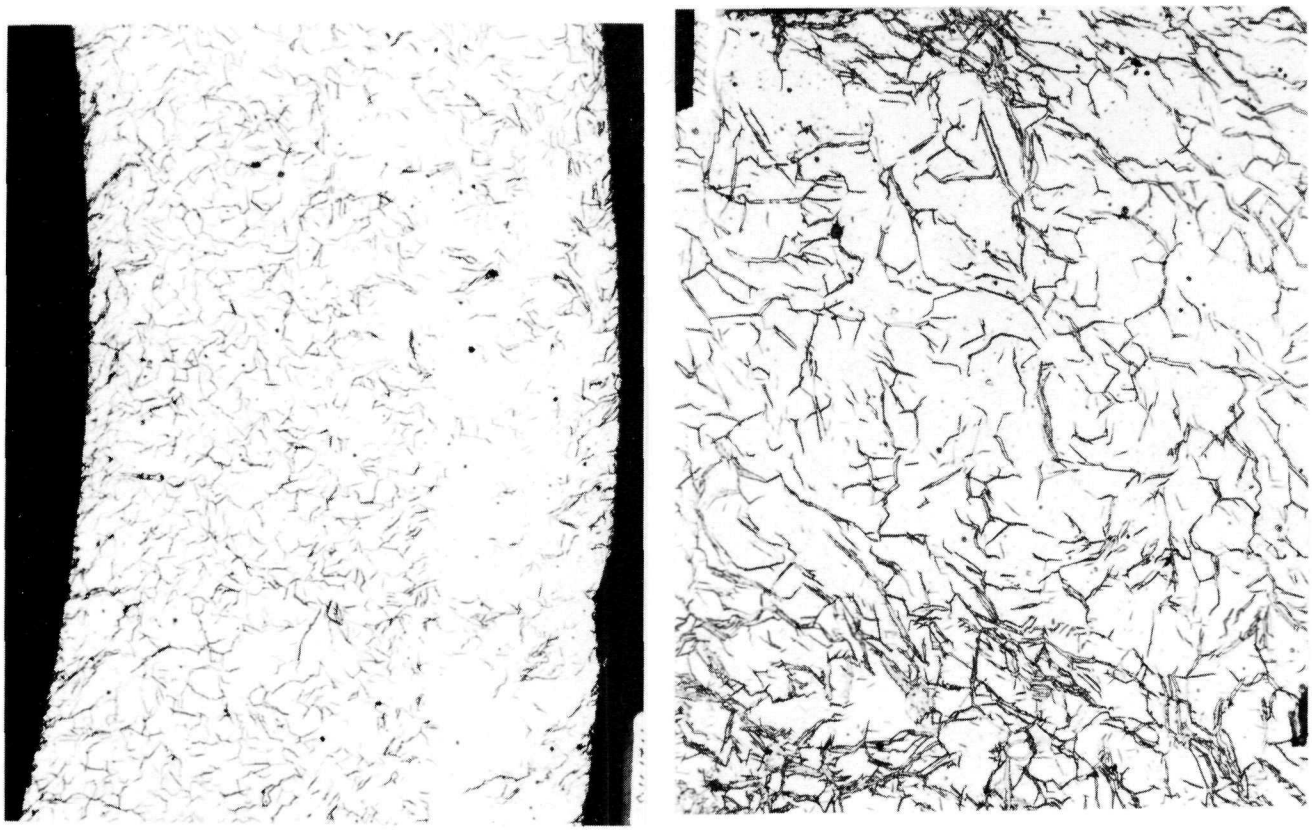

100X 250X

Figure 67. Hydride Formation at Contact Surface of a Seed Fuel Rod Fastener with Relatively High Hydrogen Content (500 to possibly 1000 ppm) (Zircaloy-Etched)

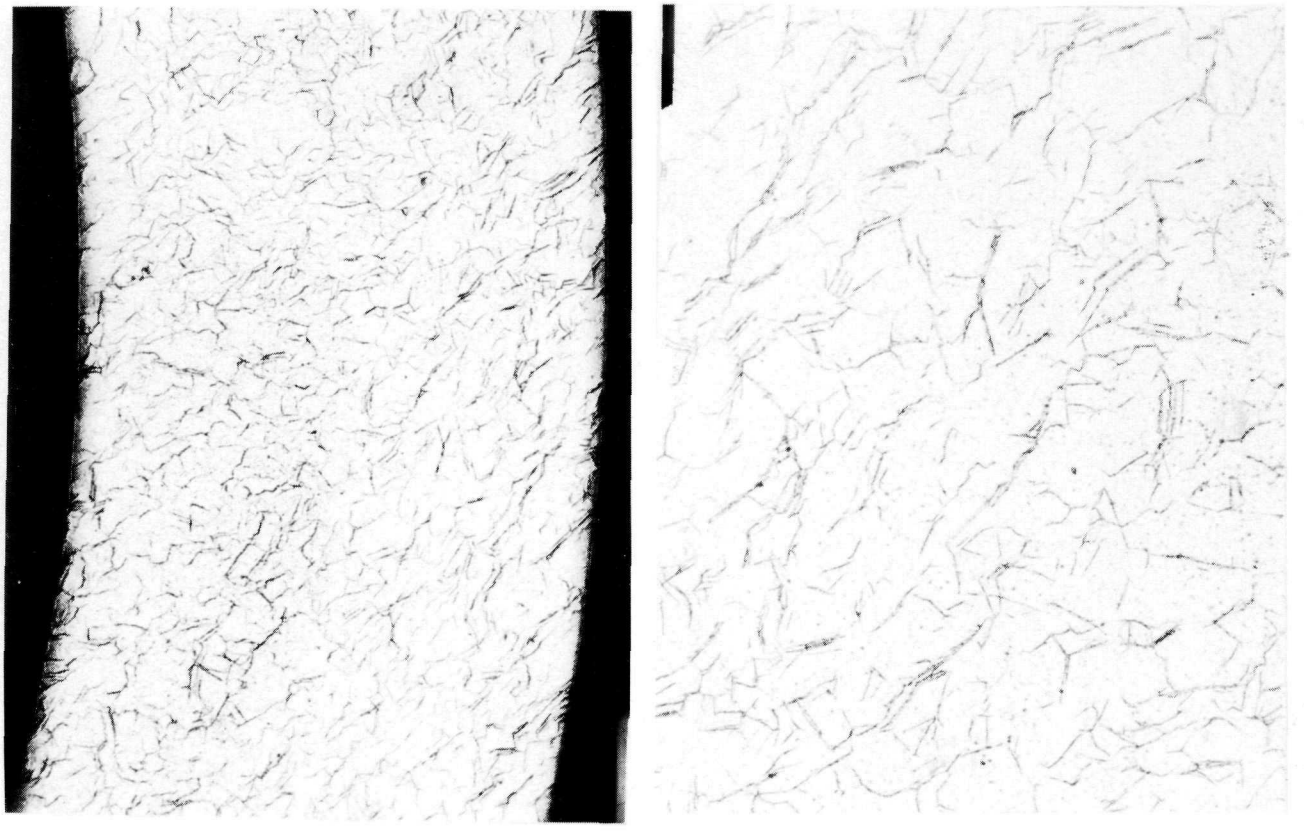

100X 250X

Figure 68. Hydride Distribution at 9 Mils Below the Contact Surface of a Seed Fuel Rod Fastener (500 ppm) (Zircaloy-Etched)

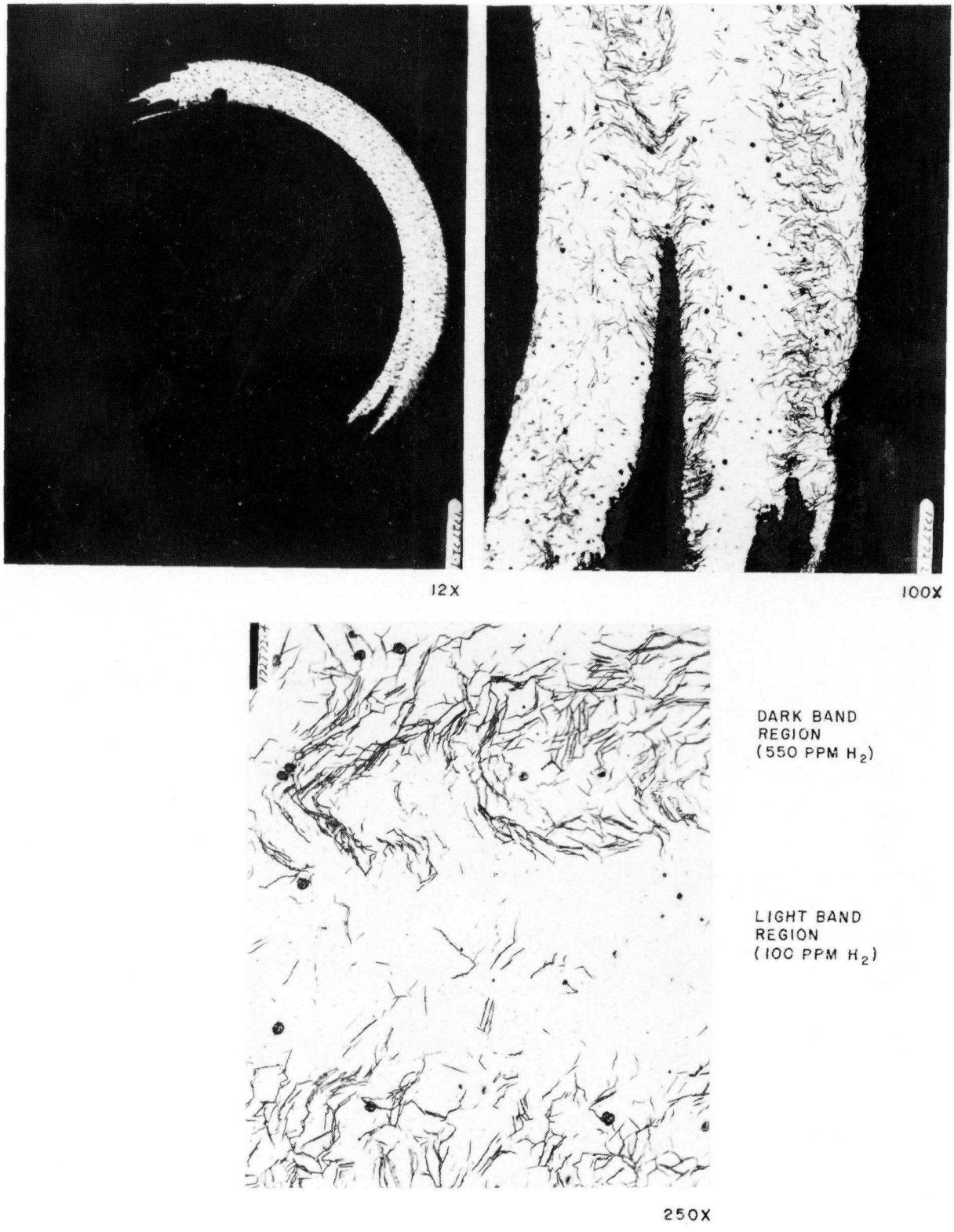

Figure 69. Seed Fuel Rod Fastener Depicting Cold-Worked (Dark-Band) Region of Higher Hydride Content at Bearing Surface (Zircaloy-Etched) NOTE: Grinding of the metallographic mount was terminated when the fuel rod fastener first became visible.

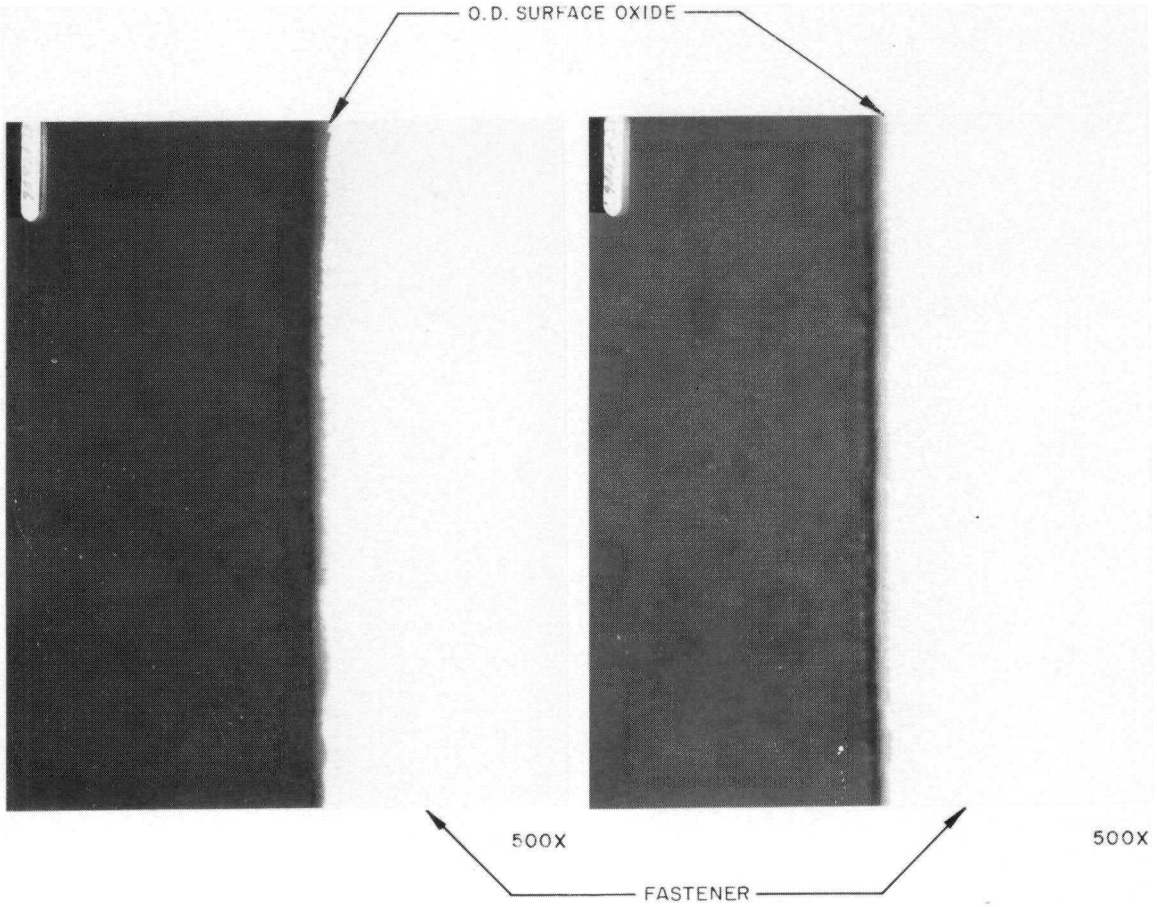

Figure 70. O.D. Surface Oxide, Typically 0.2 Mil or Less in Thickness on LWBR Fuel Rod Fasteners (As-Polished)

had lesser amounts (400 ppm). The remaining seed fasteners had only 75 ppm hydride. Within 1-4 mils of the bearing surface, three reflector fasteners had localized areas of heavy hydride (4500-12,000 ppm), three fasteners had areas of accelerated hydride (1000-3500 ppm), and the remaining four fasteners had lesser amounts (300-700 ppm).

In the LWBR irradiation tests, various degrees of accelerated hydriding were observed at the bearing ends of Zircaloy-4 fasteners. Of 21 fasteners examined metallographically, six were found to contain lower hydride contents (25-100 ppm) uniformly distributed and 15 had accelerated hydriding with two types of hydride distributions. The first type was characterized by localized hydride rims (diffuse and solid) found in three fasteners after 340 hours exposure and in nine fasteners after 1980 hours exposure. Reactor coolant conditions for these tests were pH 10.0 (NH_4OH) at 500-600°F with maximum hydrogen contents of 60-70 cc H_2/kg water. Hydrogen concentrations in the diffuse rims ranged from several hundred to several thousand ppm. The solid hydride rims were estimated to have hydrogen contents of 15,000-16,000 ppm.

The second type of accelerated hydride distribution was characterized by average hydrogen contents of 200-1250 ppm, uniformly distributed with no hydride rims, which was found in three test fasteners after relatively long-time exposure (17,900 hours) under reactor coolant conditions similar to the other tests. Uniform hydride distributions were also found in intermediate exposure (6490 hours) fasteners, but the hydrogen contents were lower (25-100 ppm).

The higher hydride contents in the REM-3 and LWBR irradiation test fasteners compared with the LWBR core fasteners could be due in part to their assembly conditions (greater angle of rotation and total assembly torque for the REM-3 test) and the absence of graphite lubricant for the irradiation tests.

4.3 - FUEL BURNUP

Results of the fuel depletion and burnup determination for the two seed and two blanket fuel pellets are presented in Table 15. Depletion and burnup measurements at end of life were based on separation of stable fission product

^{139}La and ^{148}Nd from the fuel and other fission products and use of these isotopes as burnup monitors. Comparison of measured and calculated depletion and burnup values, based separately on the two monitors, is also given in Table 15.

Table 15 - Comparison of Measured and Calculated Fuel Depletion and Burnup

Rod S/N	Type Fuel	Measured at End of Life: Depletion (10^{20} f/cc)	Measured at End of Life: Burnup (MWD/MT)	Calculated: Depletion (10^{20} f/cc)	Calculated: Burnup (MWD/MT)
Based on ^{139}La					
0205071	Thoria	3.85	17,720	4.27	19,670
	Binary	10.39	48,630	11.56	54,090
1606710	Thoria	0.13	560	0.14	630
	Binary	0.83	3,670	0.86	3,780
Based on ^{148}Nd					
0205071	Thoria	4.04	18,610	4.27	19,670
	Binary	10.55	49,390	11.56	54,090
1606710	Thoria	0.13	580	0.14	630
	Binary	0.86	3,640	0.86	3,780

Measured depletion and burnup values were consistently lower than calculated values. The difference between measured and calculated burnup values typically was on the order of 10 percent or less. Some difference could be attributed to the fact that the calculated values were averaged over a 3.5-inch length of the rod whereas the measured values were obtained on a single pellet length of approximately 0.5 inch. In general, the measured values determined from the ^{148}Nd monitor were closer to the calculated burnup values than those based on the ^{139}La monitor even though the ^{139}La monitor was considered to be more reliable because of the greater fission yield.

4.4 - IODINE AND CESIUM CONTENT IN THE FUEL AND CLADDING

Investigation to determine the presence of iodine and cesium in the fuel-cladding gap was performed by chemical analyses of solutions used to wash the cladding I.D. and, separately, the fuel pellet surface. Two sample locations from two seed rods and two sample locations from two blanket rods were analyzed. The results are tabulated in Tables 16 and 17. Backup samples, identified as "B" in the tables, were analyzed for three of the eight sample locations. One cladding wash solution and three fuel wash solutions contained minute quantities of ^{129}I. Analysis of the backup sample (No. 1B from rod 1606710), however, did not indicate the presence of iodine in the cladding wash. Small quantities of ^{137}Cs were found in the wash solutions from both the cladding I.D. and fuel pellet O.D. surfaces.

Table 16 - Concentration of ^{129}I in LWBR Fuel Rod Cladding and Fuel Pellets (μg/g)

Rod S/N	Type Fuel	Sample No.*	Cladding Wash	Fuel Wash	In Cladding	In Fuel
Seed Region Fuel						
0205071	Thoria	1A	N.D.	N.D.	N.D.	123.2
		1B	N.D.	N.D.	N.D.	135.7
	Binary	2A	N.D.	0.1	N.D.	309.3
		2B	N.D.	0.2	N.D.	317.9
0507672	Binary	1	N.D.	N.D.	N.D.	261.9
	Binary	2	N.D.	N.D.	N.D.	335.4
Blanket Region Fuel						
1606710	Binary	1A	0.4	0.2	N.D.	130.4
		1B	N.D.	N.D.	N.D.	153.3
	Binary	2	N.D.	N.D.	N.D.	136.0
1105717	Thoria	1	N.D.	N.D.	N.D.	112.8
	Binary	2	N.D.	N.D.	N.D.	149.3

* A and B samples were obtained from adjacent fuel rod sections.
N.D. = Not Detected

Table 17 - Concentration of ^{137}Cs in LWBR Fuel Rod Cladding and Fuel Pellets (μg/g)

Rod S/N	Type Fuel	Sample No.*	Cladding Wash	Fuel Wash	In Cladding	In Fuel
Seed Region Fuel						
0205071	Thoria	1A	0.1	1.8	2.8	1609.8
		1B	0.1	3.0	3.1	527.8
	Binary	2A	0.2	4.3	5.9	1261.5
		2B	0.2	4.4	6.5	294.0
0507672	Binary	1	0.2	2.4	5.8	1355.2
	Binary	2	**	**	6.2	1317.0
Blanket Region Fuel						
1606710	Binary	1A	0.6	0.4	2.8	622.1
		1B	0.1	0.6	N.M.	812.7
	Binary	2	0.1	0.4	2.9	571.6
1105717	Thoria	1	1.9	0.4	1.5	234.5
	Binary	2	0.1	0.7	1.8	622.0

* A and B samples were obtained from adjacent fuel rod sections.
** 0.2 μg/g was recorded for a combined cladding and fuel wash solution.
N.M. = Not Measured

Subsequent analyses of the cladding and fuel samples following dissolution confirmed that all of the iodine was contained within the fuel except for the minute quantity of iodine found in four of the 22 wash solutions. No iodine was detected in the cladding. Cesium was found to be primarily dissolved in the fuel, although small quantities were also found in the cladding.

These results indicate that, although the thoria and thoria-urania fuel used in LWBR produced iodine as a product of fission, the iodine remained within the fuel. Migration and diffusion of the iodine to the cladding-fuel gap did not occur to any appreciable extent. Because iodine essentially was not observed either within or on the surface of the cladding, the potential for iodine-induced stress corrosion cracking of the cladding was not significant.

These findings were corroborated by electron microprobe (EMP) studies of separate cladding samples from three of the same four fuel rods. (The surface of one of the two seed cladding samples was inadvertently contaminated by a too generous application of silver epoxy mounting and was not examined.) The objective of the EMP studies was to determine the distribution of iodine and cesium as a function of distance in the axial (longitudinal) direction of the Zircaloy-4 cladding I.D. surfaces. Cesium was observed to be uniformly present in all three samples at about 0.1 weight percent along the longitudinal traverse. In the longitudinal traverse for iodine, the iodine X-ray signal was nearly indistinguishable from background levels. Again, the lack of iodine on the cladding I.D. surface indicated that iodine-induced stress corrosion cracking of the Zircaloy-4 cladding was not a problem in LWBR.

4.5 - MECHANICAL PROPERTIES OF THE IRRADIATED CLADDING

The results of tensile testing of the irradiated fuel rods at end of life and of unirradiated Zircaloy-4 tubing from similar tubing lots are tabulated in Table 18. As expected, yield and tensile strengths for both RXA and SRA cladding were significantly higher at end of life than at beginning of life (unirradiated). The results confirmed that the LWBR cladding mechanical properties were adequate throughout core life.

Comparison of results for SRA cladding and RXA cladding at the two test temperatures is shown in Figure 71 for the 0.2 percent offset yield strength and ultimate tensile strength. The SRA (70 percent cold worked and stress relief annealed) cladding was designed to provide tubing with higher strength at beginning of life than the RXA (fully recrystallization annealed) cladding. Room temperature tensile test results of the unirradiated tubing pulled at the same time as the irradiated fuel rod cladding also showed higher strength for SRA cladding. The unirradiated tubing tensile test results were in agreement with the average as-built tubing tensile strengths reported in Table 2.

As shown in Figure 71, both yield and tensile strengths of the irradiated cladding increased with increasing neutron fluence. Test samples for the SRA cladding were limited to low fluence levels because pellet-cladding contact prevented separation of the cladding from the pellets at higher fluence

Table 18 - Results of EOL Tensile Tests of LWBR Irradiated Fuel Rods and Unirradiated Tubing

Test Number	Serial Number	Cell Number	Sample Location[4] (in from end stem shoulder)	Heat Treatment	Calculated Fast Neutron Fluence (n/cm^2)	Test Temperature (°F)	0.2% Yield Stress (YS) (PSI)	Ultimate Tensile Strength (UTS) (PSI)	Ratio UTS/YS	Elongation[1] (%)	Reduction in Area (%)	Outside Diameter (in)	Lot Number
Seed Tubing													
1[2]	04689	--	--	RXA	0	77	66,458	85,143	1.28	23.8	--	0.310	0-08
2[3]	04689	--	--	RXA	0	77	53,410	80,973	1.52	30.5	53.9	0.310	0-08
3	04689	--	--	RXA	0	77	53,982	80,305	1.49	30.7	57.2	0.310	0-08
4	04689	--	--	RXA	0	500	17,167	36,910	2.15	29.8	76.1	0.310	0-08
5	04689	--	--	RXA	0	500	17,644	34,049	1.93	26.5	74.1	0.310	0-08
6	0606773	6B4	54	RXA	91×10^{20}	77	101,097	126,848	1.25	6.1	32.6		0-08
7	0507672	5L31	15.5	RXA	31×10^{20}	500	61,039	73,438	1.20	6.5	54.9		0-10
8	0606773	6B4	69	RXA	96×10^{20}	500	71,531	90,510	1.26	5.5	23.6		0-08
9	0507672	5L31	102.5	RXA	5×10^{20}	77	80,114	100,620	1.26	5.6	40.3		0-10
10	0507672	5L31	93.75	RXA	38×10^{20}	500	63,901	78,588	1.23	5.0	13.5		0-10
11	0606773	6B4	76.25	RXA	92×10^{20}	77	101,097	126,752	1.25	5.6	20.6		0-08
Standard Blanket Tubing													
12	06689	--	--	SRA	0	77	78,550	115,541	1.47	20.0	35.7	0.576	1-78
13	1208823	12A12	13.25	SRA	0.9×10^{20}	77	91,336	123,305	1.35	13.9	42.8		1-87
Reflector Tubing													
14	3102657	1A1	41.5	SRA	9×10^{20}	500	81,010	93,376	1.15	7.9	12.4		3-89
15	--	--	--	SRA	0	500	52,444	69,925	1.33	17.4	46.3	0.835	Unknown
16	--	--	--	SRA	0	77	76,746	110,004	1.43	24.9	36.3	0.835	Unknown
17	3102657	1A1	78.25	SRA	19×10^{20}	77	115,121	139,851	1.21	10.8	19.6		3-89

(1) Two-inch gauge length
(2) Strain rate = 0.080 in/in/min
(3) Strain rate = 0.058 in/in/min for remaining tests
(4) Location is the center of the sample; samples were approximately 7-8 in long

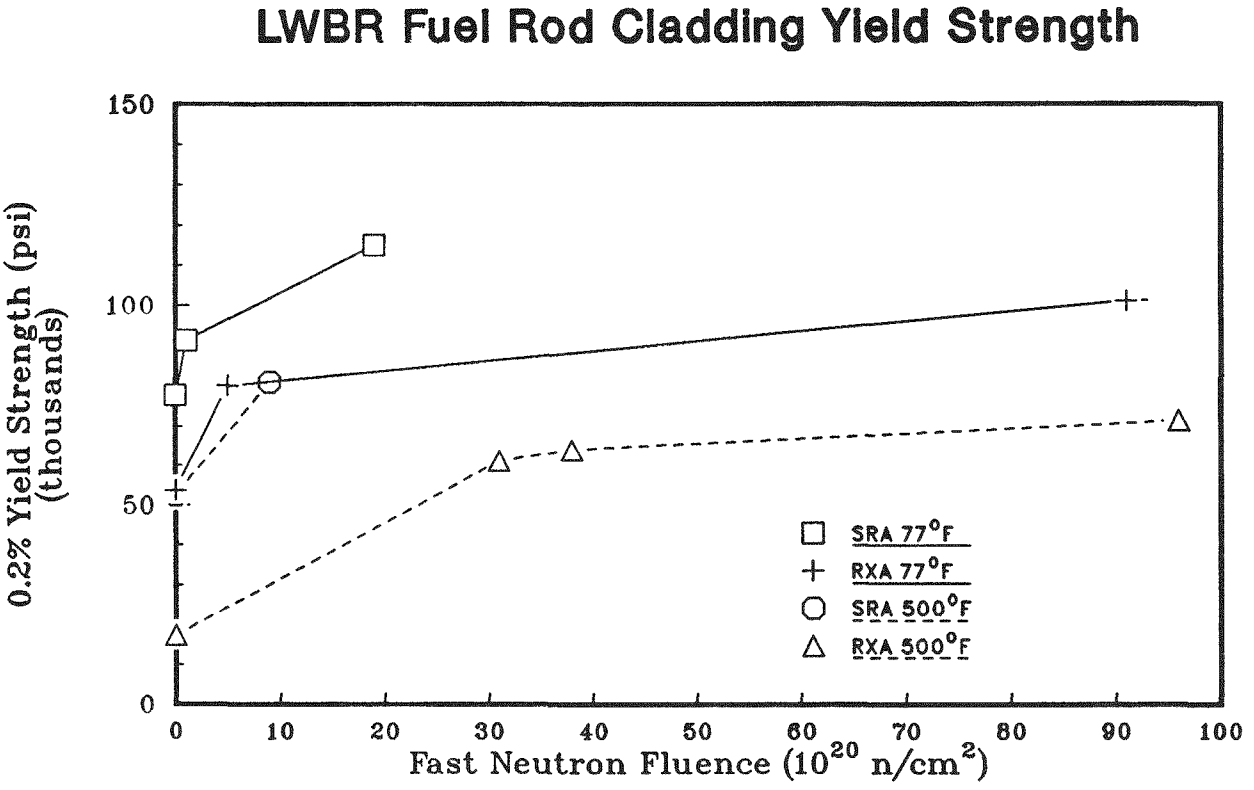

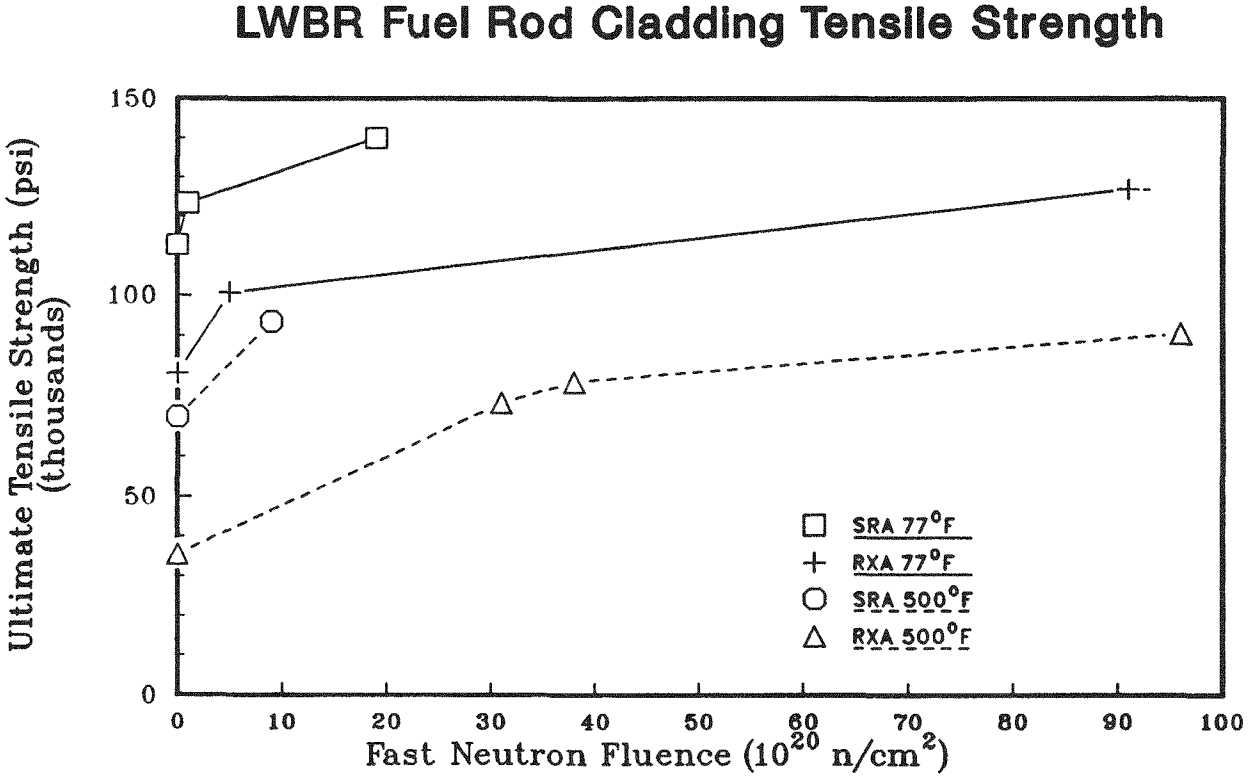

Figure 71. LWBR Fuel Rod Cladding Yield and Tensile Strength Versus Fast Neutron Fluence

levels without slitting the cladding. SRA cladding tensile test samples had to be obtained from cooler, lower fluence regions of the core at top and bottom rod locations which experienced less pellet-cladding contact.

Compared to RXA cladding, SRA cladding was higher in strength at beginning of life and remained higher (at comparable neutron fluence levels) throughout core life. Although significant reductions in ductility occurred, as measured by elongation in the 2-inch gage length, sufficient ductility (about 5 to 6 percent for RXA cladding and 8 to 14 percent for SRA cladding) remained at end of life to prevent brittle behavior.

Photographs of selected samples before and after tensile testing are shown in Figures 72 to 79. A dark colored dye was used to highlight the center and ends of the gage length. Dulled knife edges set in a jig were used to remove the dye to establish the gage length marks. Changes in surface appearance, ranging from dulling of the surface finish (Figure 78) to localized slip bands (Figure 74), were observed for most samples. Most samples broke within the 2-inch gage length; only three of the 17 samples broke at or outside the gage marks.

The tensile test results for irradiated cladding were adequately predicted by design equations. The design equations used to predict cladding yield strength during irradiation, shown in Table 19, were derived empirically from irradiaton test data. Table 20 and Figure 80 show calculated (predicted) and measured cladding yield strengths. A correction was applied to the reference values for irradiated samples to account for in-reactor thermal annealing (based on an assumption that the cladding temperature was 600°F at its midplane at power throughout lifetime). All yield strengths of irradiated samples were adequately predicted.

Two of the unirradiated RXA (seed) cladding tested at 500°F, however, were unexpectedly below the minimum predicted values (by 13 percent). As noted in Table 20, the measured yield strengths for these two samples (Numbers 4 and 5) were also lower than the 700°F values reported for unirradiated tubing of the same lot number. The measured value for the one unirradiated SRA tubing tested at 500°F, however, was above the predicted value.

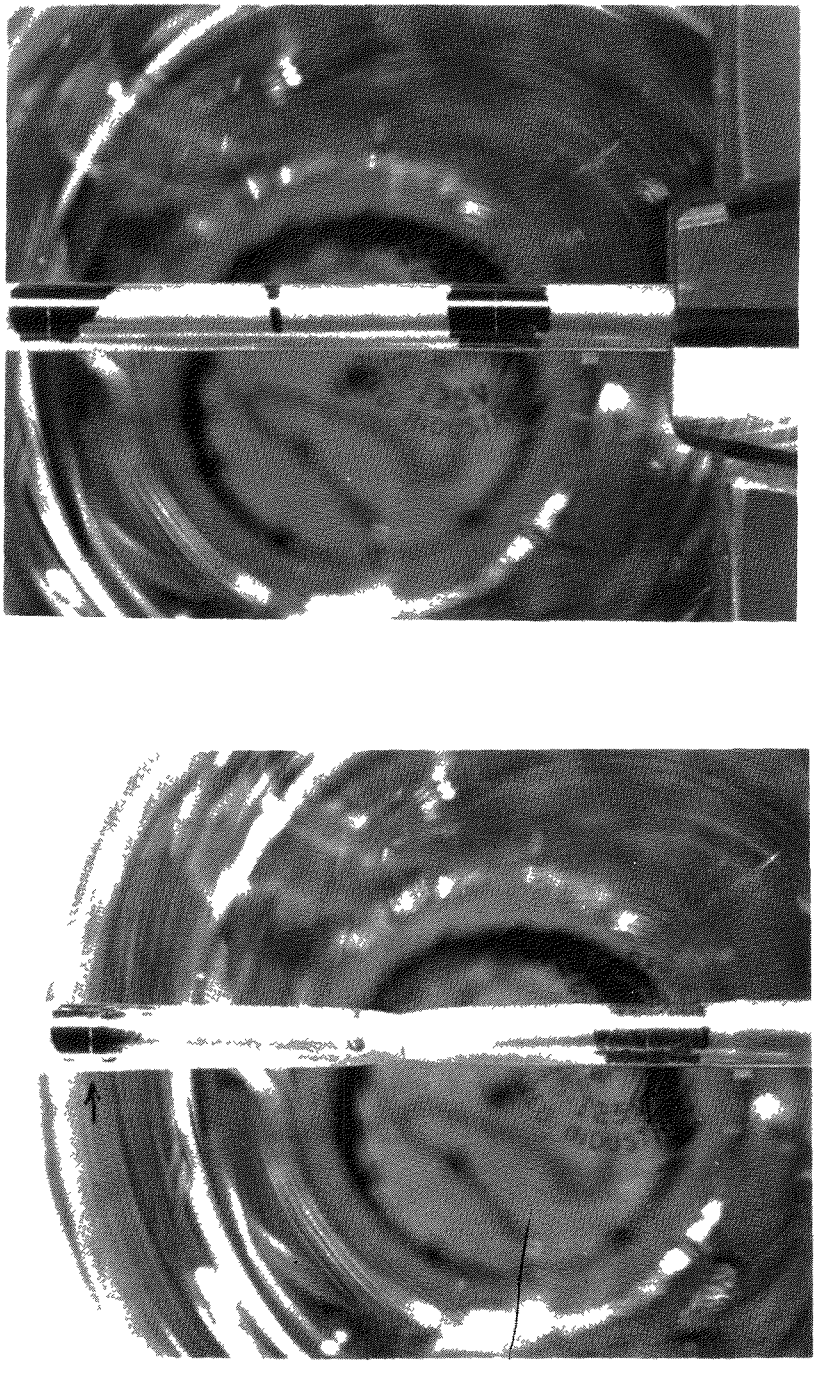

Figure 72. Typical Appearance of Unirradiated Seed Tubing Tensile Test Results (Before and After) Showing Necking and Fracture at Room Temperature (1.228X)

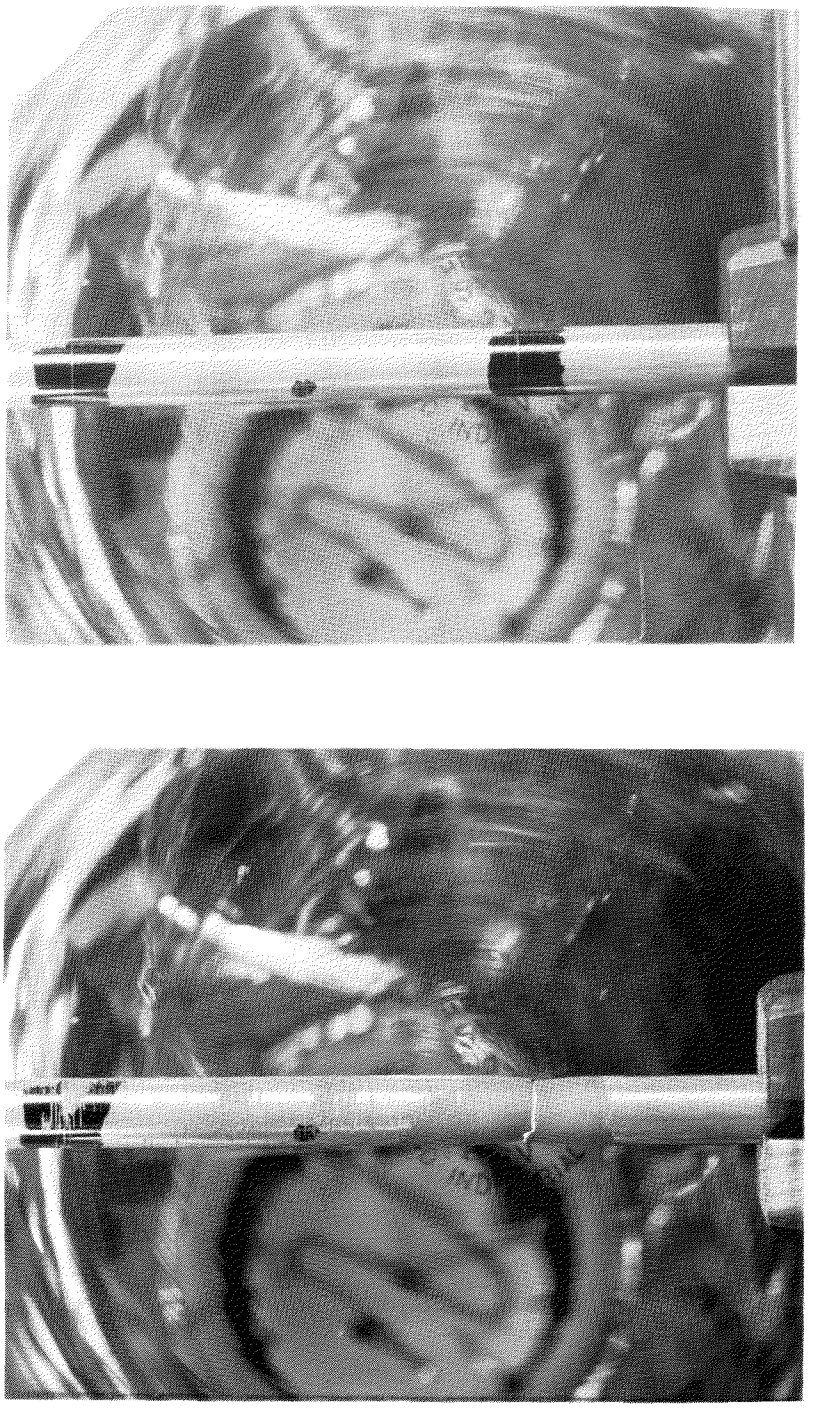

Figure 73. Appearance of Irradiated Seed 0606773 Tensile Test Results (Fast Fluence of 91 x 10^{20} n/cm^2, Room Temperature) Showing Bands (Perpendicular to the Tube Length) and Fracture (1.230X)

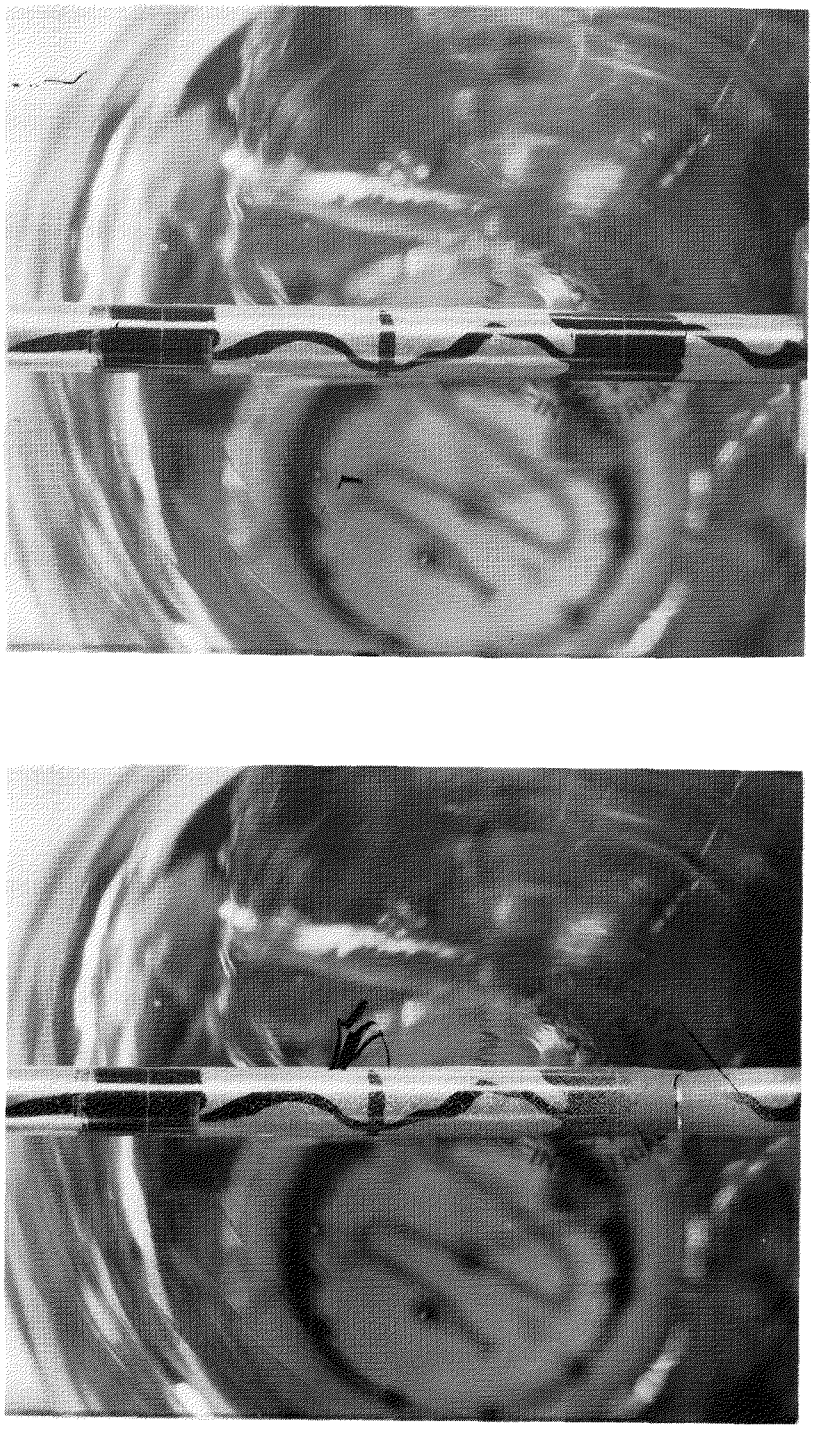

Figure 74. Appearance of Irradiated Seed 0606773 Tensile Test Results (Fast Fluence of 92×10^{20} n/cm^2, Room Temperature) Showing Intersecting Bands at 45 Degrees and Fracture (1.223X)

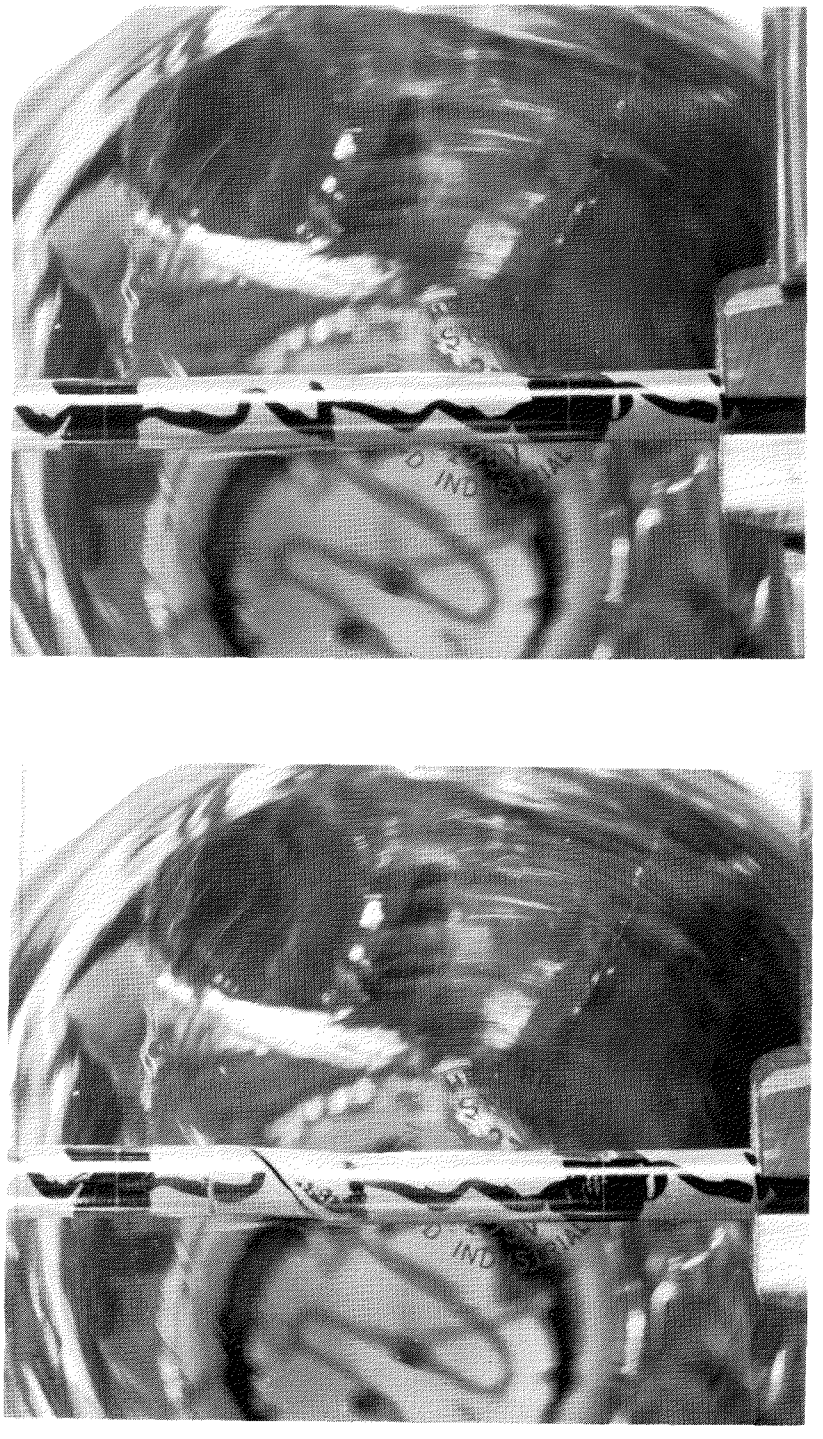

Figure 75. Appearance of Irradiated Seed 0606773 Tensile Test Results (Fast Fluence of 96 x 10^{20} n/cm^2, 500°F) Showing Intersecting Bands and Fracture at 45 Degrees (1.238X)

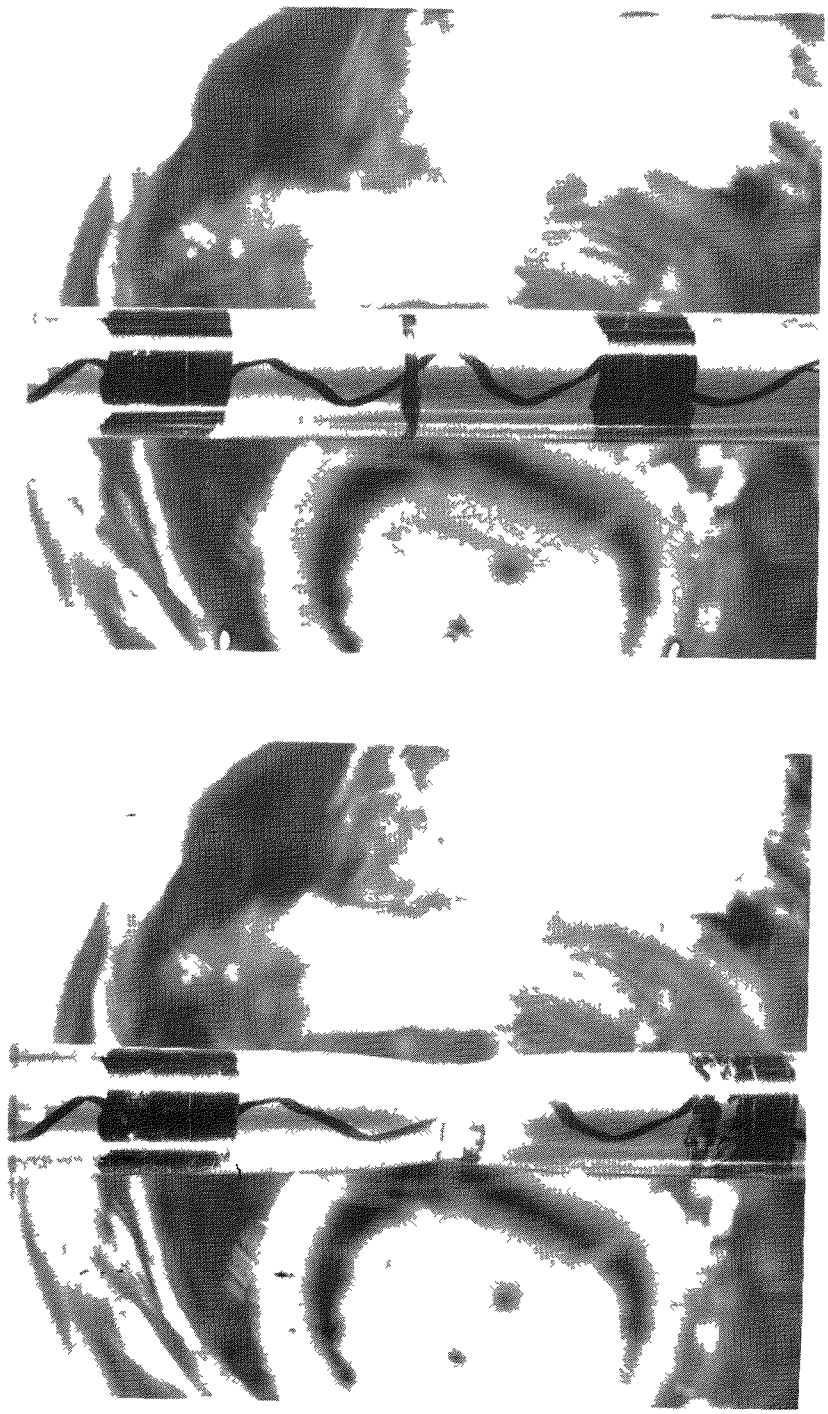

Figure 76. Typical Appearance of Unirradiated Standard Blanket Tubing Tensile Test Results (Before and After) Showing Necking and Fracture at Room Temperature (1.225X)

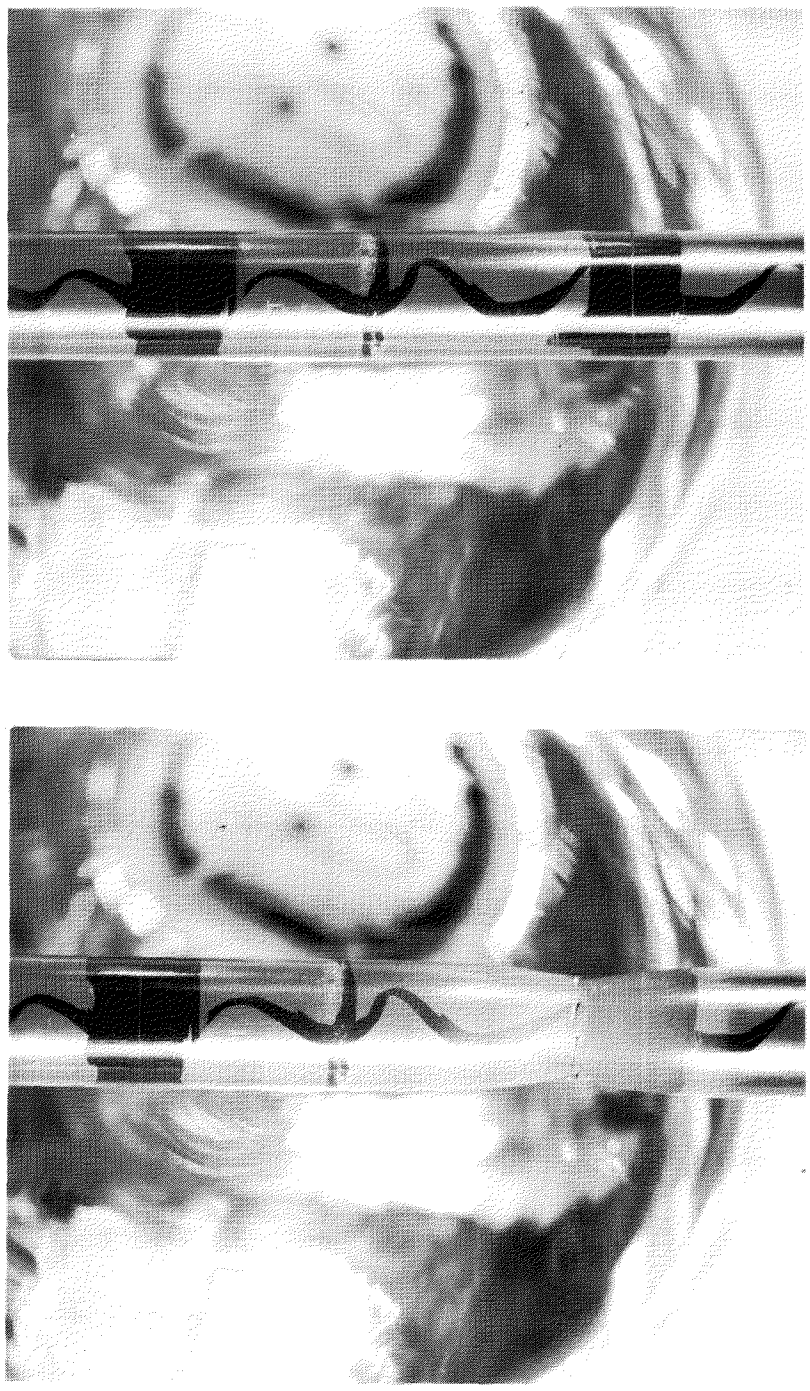

Figure 77. Appearance of Irradiated Standard Blanket 1208823 Tensile Test Results (Fast Fluence of 1×10^{20} n/cm^2) Showing Necking, Dulled Surface Finish, and Fracture at Room Temperature (1.220X)

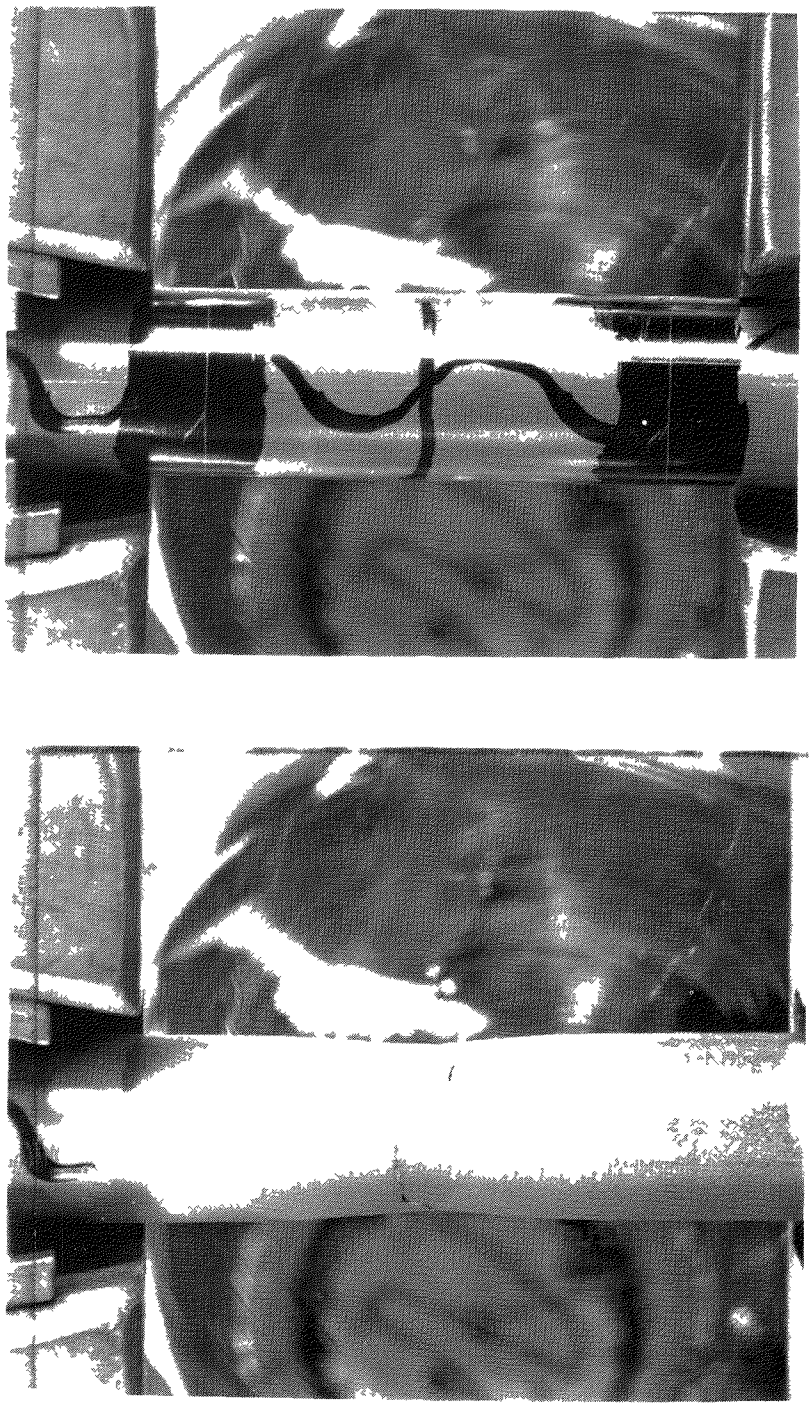

Figure 78. Appearance of Irradiated Reflector 3102657 Tensile Test Results (Fast Fluence of 19 x 10^{20} n/cm^2, Room Temperature) Showing Necking, Very Fine Bands at 45 Degrees, and Fracture (1.233X)

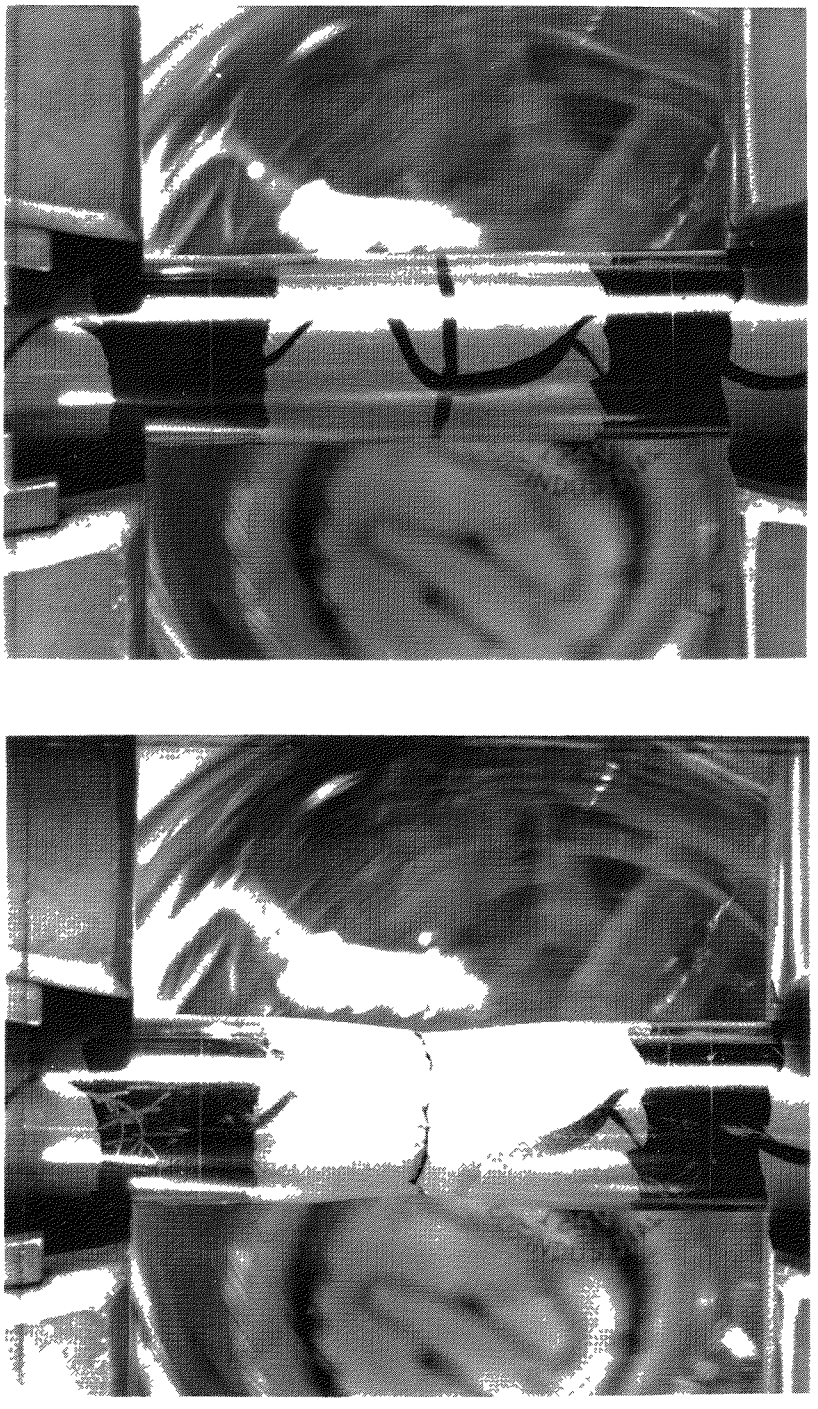

Figure 79. Appearance of Irradiated Reflector 3102657 Tensile Test Results (Fast Fluence of 9×10^{20} n/cm^2, 500°F) Showing Necking, Dulled Surface Finish, and Fracture (1.233X)

Table 19 - Design Equations Used to Calculate Reference Yield Strength of LWBR Tubing[1]

A. Unirradiated Tubing (Fast Fluence of $< 10^{18}$ n/cm^2)

Tensile Test Temp (°F)	Yield Stress (PSI) RXA	SRA
70	35,000	55,750
700	16,500	42,500

B. Irradiated Tubing (Fast Fluence of $> 10^{18}$ n/cm^2)

Tensile Test Temp (°F)	RXA	SRA
70	$\sigma_R = 10^{2.7681} (nvt)^{0.0987}$	$\sigma_R = 10^{3.6052} (nvt)^{0.0634}$
700	$\sigma_R = 10^{1.4345} (nvt)^{0.1546}$	$\sigma_R = 10^{3.593} (nvt)^{0.0575}$

σ_R = Reference Yield Stress (PSI)
nvt = Fast Neutron Fluence (n/cm^2)
RXA = Recrystallized Annealed (Seed)
SRA = Stress Relief Annealed (Blanket and Reflector)

(1) Equations determined empirically from irradiation test data to provide a base value (a conservative lower bound) of the tubing yield strength from which additional adjustments are made for such factors as annealing of the cladding at in-core temeratures.

Table 20 - Calculated and Measured Cladding Yield Strengths (YS)

Tensile Test[1] Number	Fast Neutron Fluence[1] 10^{20} (n/cm^2)	Test[1] Temperature (°F)	Calculated Minimum Expected YS (psi) at Test Temp[2]	Measured Tensile Test YS[1] (psi)
Seed (RXA)				
1-3	0	77	31,080	≥ 53,410
4	0	500	19,810[3]	17,167
5	0	500	19,810[3]	17,644
6	91	77	75,320	101,097
7	31	500	54,270	61,039
8	96	500	64,360	71,531
9	5	77	49,940	80,114
10	38	500	56,350	63,901
11	92	77	75,390	101,097
Standard Blanket (SRA)				
12	0	77	49,210	78,550
13	0.9	77	58,600	91,336
Reflector (SRA)				
14	9	500	56,570	81,010
15	0	500	41,310	52,444
16	0	77	49,210	76,746
17	19	77	75,860	115,121

(1) From Table 18
(2) Calculated from design equations, including adjustments for thermal annealing at 600°F average cladding temperature in-core and 5 percent engineering allowance
(3) Overpredicted YS

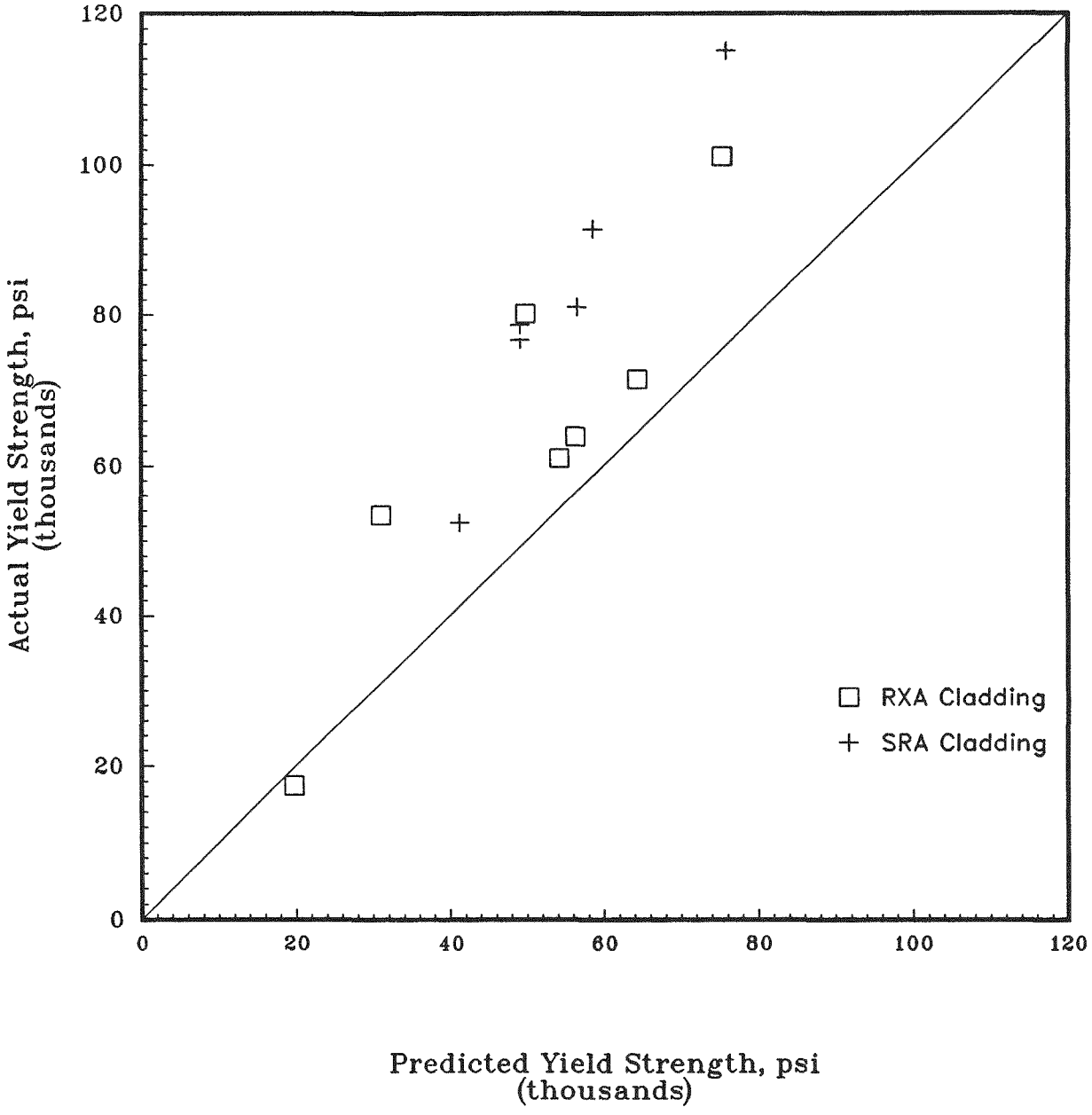

Figure 80. Comparison of Design Predictions with Results of End-of-Life Cladding Tensile Tests

These results confirmed that LWBR cladding, both RXA and SRA, behaved as expected and that the mechanical properties were adequate throughout core life.

SECTION 5 - SUMMARY AND CONCLUSIONS

Performance of the LWBR Zircaloy-4 clad thorium oxide/uranium-233 oxide fuel rods during core life to 29,047 EFPH was excellent. No evidence of fuel rod failure was observed during operation and the fuel operating temperature was low, below the boundary temperature (2580°F) at which an increased percentage of fission gas is released. The possibility of cladding defects in two seed modules was noted during preparation for final disposition at Idaho. Specific conclusions are summarized below:

1. Fission gas (xenon and krypton) release from LWBR fuel to the plenum region was very small, less than 0.2 percent of total gas generated, and within best estimate predictions. LWBR fuel rods, therefore, operated at low fuel temperatures, below 2580°F. Microstructural features, such as fuel grain size and porosity, confirmed this observation.

2. Fuel pellets remained cylindrical and essentially intact within the rods. Axial and circumferential cracks were observed in the fuel pellets, but the basic shape was maintained. The extent of cracking was limited. Fuel chips were not observed, and pellet fragments were not dislocated axially as observed in some irradiation test rods. Hence, pellet-cladding interaction due to dislodged fuel sections or chips was minimized.

3. Axial expansion of the pellet ends into the end dishes did not occur to any measurable extent. End dishes were observed in neutron radiographs of all rod types. Longitudinal cross sections through the end-dish regions confirmed that the dish depth had not changed measurably from as-built dimensions. Pellet-cladding interaction (PCI) and cladding ridging (diametral expansion) at pellet ends, therefore, were minimized by this low axial expansion.

4. Fuel porosity remained small in size in the binary fuel pellets at burnups below 20,000 MWD/MT. Fission gas bubbles (porosity) became more evident in the grain boundaries at higher depletions.

5. Central coring of the fuel was not observed.

6. Large grained fuel was not observed. The reported ASTM grain size varied from 2.6 to 6.0. Grain size was larger at the edge of the blanket fuel pellets by an average of 1.15 ASTM grain size but was larger in the center of the seed fuel pellets by an average of 0.5 ASTM grain size. Lack of significant grain growth confirmed that the LWBR fuel operated at low temperatures (below 2580°F) and was stable.

7. Cladding in the seed region remained freestanding (separated from contact with the fuel) as designed. The pellets were free to slide inside the cladding. PCI was not significant in the seed fuel rods; cladding strains due to PCI, therefore, were low.

8. Cladding in the blanket region was in tight contact with the cladding and was not free to slide. This was expected since the cladding was designed to be nonfreestanding and significant grooving was observed in nondestructive fuel rod diameter measurements in the blanket region. This indicated that high local cladding strains due to axial expansion (ridging) at pellet ends were not realized.

9. Cladding in the one examined reflector region rod (which contained thoria fuel) was separated from the fuel by a small gap of one to two mils.

10. The hydrogen content in the Zircaloy-4 cladding increased moderately from the as-fabricated level of 45 ppm maximum to approximately 100 ppm in the seed and blanket fuel rods. Hydrogen pickup in the reflector cladding was very small with an average measured hydrogen content of 34 ppm. Measured values were well below predicted levels for all rods examined.

11. The zirconium hydrides in the cladding were oriented in the preferred circumferential direction parallel to the rod surface, which minimized the potential for surface cracks. No massive hydrides were observed. Lack of hydrogen embrittlement was beneficial to fuel rod performance.

12. A cladding oxide layer of varying thickness was observed on the waterside surface of all fuel rods examined. The oxide thickness ranged from approximately 0.05 mil for cladding with the thinnest oxide layer to 1.75 mils for cladding with the thickest oxide layer. For fast neutron fluences to approximately 40 x 10^{20} n/cm^2, oxide thickness for the RXA seed cladding and the SRA blanket cladding (over binary fuel) was comparable. Above this fluence level the SRA cladding experienced greater oxide thickness than RXA cladding. The results for the maximum measured oxide thickness are in reasonable agreement with the CHORT model predictions.

13. No oxide was observed on the cladding I.D. (fuel side) surface. Corrosion of the cladding I.D. in LWBR fuel rods was not a concern.

14. The potential for iodine-induced stress corrosion cracking of the Zircaloy-4 cladding in LWBR fuel rods was not significant. Essentially no iodine was detected in the fuel-cladding gap or on the cladding inner surface. Only iodine dissolved in the fuel was detected.

15. Low levels of the fission product ^{137}Cs were observed on the cladding I.D., at about 0.1 weight percent.

16. The inner (fuel-side) surface of seed and blanket cladding was covered with a thin film and a coating of fine nodules (about 0.5 micron to 5 microns across). Both the film and nodules consisted primarily of thorium and zirconium. The inner surface of the nonfreestanding blanket cladding had circumferential rings consisting of fuel particles; only isolated patches of fuel particles were observed on the freestanding seed cladding.

17. Mechanical strength of the LWBR Zircaloy-4 cladding at end of life was adequate and behaved as expected. Both the SRA and RXA cladding increased in strength as a function of neutron fluence. SRA cladding, having higher yield and ultimate strength than RXA cladding at beginning of life, remained higher in strength throughout the core life.

18. Inconel X-750 plenum springs and Type 348 stainless steel plenum sleeves remained structurally sound during core life. Some relaxation of spring free lengths from beginning of life was experienced, but positive spring force was maintained throughout core operation based on comparison of spring free lengths with plenum lengths under load. No cracks or other degradated conditions were observed.

19. The fuel rod cladding-to-end stem weld remained structurally sound with no evidence of cracking or hydriding.

20. The solid Zircaloy-4 end stem components which were in contact with the nickel-bearing Alloy 600 baseplates in the seed and reflector regions did not show evidence of embrittlement due to high hydrogen content; the hydrogen content was very low, 25 to 50 ppm.

21. Performance of the Zircaloy-4 fuel rod fasteners which attached the fuel rods to either top or bottom baseplates was good. The hydride content of 150 to 200 ppm in the seed region and 350 to 400 ppm in the reflector region was higher than in the cladding, as expected. Local regions of higher hydride (to 1000 ppm) were observed in several seed fasteners at locations of apparently greater contact pressure with the Inconel-600 baseplate. The low (20 ppm) hydride content in the blanket region indicated that the presence of the chromium-plated washers performed as designed by inhibiting hydrogen pickup in the Zircaloy fasteners at the bearing surface. Hydride content in the blanket region rod fasteners did not increase above as-fabricated levels. All fasteners performed as designed.

SECTION 6 - ACKNOWLEDGMENTS

The authors acknowledge the following persons whose efforts contributed to the successful examination and reporting of these fuel rod destructive examinations:

Messrs. R. S. Wisner, G. C. McClellan, R. Villarreal, and B. G. Carlson of Argonne National Laboratory, Argonne - West, for their fine efforts in obtaining fission gas analyses, chemical analyses of the fuel and cladding, and metallography of the fuel rod fasteners, as well as for the initial sectioning of the fuel rods.

Mr. L. A. Neimark and Dr. D. G. Graczyk of Argonne National Laboratory, Argonne-East for their significant efforts in obtaining examination specimens from the fuel rods, and in performing much of the destructive examinations.

Mr. P. E. Ireland of the Expended Core Facility in Idaho for his coordination of the contract effort with Argonne National Laboratory.

Ms. M. O. Malinchak and D. M. Bailey for their help in preparing the manuscript.

The authors are also indebted to Messrs. W. J. Babyak, D. S. Duncan, and M. D. Novotnak, and Drs. P. L. Pfennigwerth and W. E. Franzen for their careful review and helpful suggestions.

(Intentionally Blank)

SECTION 7 - REFERENCES

1. W. C. Schick, "Proof-of-Breeding of LWBR," WAPD-TM-1612 (October 1987).

2. J. E. Wargo, "End-of-Life LWBR Component Examinations at Shippingport and Module Visual and Dimensional Examinations at ECF," WAPD-TM-1602 (October 1987).

3. D. A. Gorscak, "End-of-Life Nondestructive Examinations of LWBR Fuel Rods," WAPD-TM-1605 (October 1987).

4. D. R. Connors, et al, "Design of the Shippingport Light Water Breeder Reactor," WAPD-TM-1208 (January 1979).

5. J. H. Eyler, "The Characteristics of the Zircaloy-4 Tubing in LWBR Fuel Rods," WAPD-TM-869 (November 1979).

6. J. C. Clayton, "Out-of-Pile Accelerated Hydriding of Zircaloy Fasteners," WAPD-TM-1426 (October 1979).

7. J. C. Clayton, "Out-of-Pile Nickel Alloy-Induced Accelerated Hydriding of Zircaloy Fasteners," in "Zirconium in the Nuclear Industry: Sixth Conference," ASTM-STP 824, 1984, pp. 572-591.

8. J. Belle, and R. M. Berman, Eds., Thorium Dioxide: Properties and Nuclear Applications, U. S. Government Printing Office, Washington, D.C. (1984).

9. J. C. Clayton, T. J. Burke, and C. R. Hutchison, "Preparation, Characterization, and Processing of Thoria-Based Fuels for Light Water Breeder Reactors," Advances in Ceramics (Ceramic Powder Science), 21, 69-89 (1987).

10. W. A. Budd, "Shippingport Operations with the Light Water Breeder Reactor Core," WAPD-TM-1542 (March 1986).

11. B. Z. Hyatt, "Metallographic Standards for Estimating Hydrogen Content of Zircaloy-4 Tubing," WAPD-TM-1431 (February 1982).

12. ASTM Standard E-8-78, "Tension Testing of Metallic Materials" in "ASTM Standard (1978), Part 10, Metals-Physical, Mechanical, Corrosion Testing," pp 160 to 180, American Society for Testing Materials, Philadelphia, Pennsylvania.

13. ASTM Standard E-21-70, "Elevated Temperature Tension Tests of Metallic Materials, Recommended Practice for:" in "ASTM Standard (1978), Part 10, Metals-Physical, Mechanical, Corrosion Testing," pp 225 to 234, American Society for Testing Materials, Philadelphia, Pennsylvania.

14. I. Goldberg, et al., "Fission Gas Release from ThO_2 and ThO_2-UO_2 Fuels," WAPD-TM-1350 (August 1978).

15. W. R. Campbell and J. F. Giovengo, "LWBR Fuel Rod Design and Performance Characteristics," WAPD-TM-1387 (October 1987).

16. F. A. Nichols, "Theory of Grain Growth in Porous Compacts," Journal of Applied Physics, Volume 37, Number 13, December 1966.

17. B. W. Hodges, "Preparation of LWBR Spent Fuel for Shipment to ICPP for Long-Term Storage," WAPD-TM-1601 (October 1987).

18. J. C. Clayton, "Corrosion and Hydriding of Irradiated Zircaloy Fuel Rod Cladding," WAPD-TM-1440 (September 1982).

19. G. P. Marino and R. L. Fischer, "Corrosion of Zircaloy-4 Tubing in 680F Water," WAPD-TM-1322 (December 1978).

20. J. C. Clayton and R. L. Fischer, "Corrosion and Hydriding of Zircaloy Fuel Rod Cladding in 633 K Water and Reactor Environments," pp. 3.1 - 3.16, Proc. ANS Topical Meeting on Light Water Reactor Fuel Performance, Orlando, Florida (1985).

21. J. C. Clayton, "Internal Hydriding in Irradiated Defected Zircaloy Fuel Rods - A Review," WAPD-TM-1604 (September 1987).

*U.S. GOVERNMENT PRINTING OFFICE: 1988-505-001/80231